

HIGH TEMPERATURE COMPRESSIVE CREEP
OF SINTERED NICKEL

BY

WALTER RALPH TARR

A DISSERTATION PRESENTED TO THE GRADUATE COUNCIL OF
THE UNIVERSITY OF FLORIDA IN PARTIAL
FULFILLMENT OF THE REQUIREMENTS FOR THE DEGREE OF
DOCTOR OF PHILOSOPHY

UNIVERSITY OF FLORIDA
1973

DEDICATED TO THE MEMORY OF

FLORENCE LYNNE WILLIAMS

ACKNOWLEDGMENTS

The author wishes to thank Dr. F. N. Rhines, chairman of the supervisory committee, for guidance in this research and in putting it together as a unified concept.

The author wishes to thank Dr. R. T. DeHoff for the large amount of time he expended in discussing this work.

The author is indebted to Dr. E. D. Verink, Jr. for personal and professional guidance.

The author wishes to thank Dr. E. H. Hadlock and Dr. J. F. Burns for serving on his supervisory committee, and Mr. T. M. Slean for assistance in sample preparation and quantitative metallography data.

The author thanks Mrs. R. V. Whitehead for all her help throughout the years.

The financial support for this research by the Atomic Energy Commission was appreciated, and is hereby acknowledged.

TABLE OF CONTENTS

	Page
ACKNOWLEDGMENTS	iii
LIST OF TABLES	vi
LIST OF FIGURES	vii
ABSTRACT	xi
CHAPTER	
1 INTRODUCTION	1
1.1 General Characteristics of the Sintering Process .	1
1.2 Background and Previous Investigations of Sintering	4
1.3 General Characteristics of the Creep Process . . .	8
1.4 Background and Previous Investigations of the Creep Process	9
1.5 Dislocation Modelling	10
1.6 Purpose and Scope of This Research	16
2 MATERIAL SPECIFICATIONS	18
2.1 Material	18
2.2 Particle Sizes Used	18
2.3 Sample Preparation	21
2.4 Experimental Investigation into the Creep of Sintered Nickel	25
2.4.1 Equipment (Creep Apparatus)	25
2.4.2 Test Conditions	31
2.5 Experimental Procedure	31
3 EXPERIMENTAL RESULTS	33
3.1 Densification and Shrinkage in Sintering	33
3.2 Calibrate ΔL in Creep as a Function of Particle Size, Density, Load, Temperature, and Time	43
3.2.1 Particle Size Effect	49
3.2.2 Temperature Effect	49
3.2.3 Effect of Starting Density	49
3.2.4 Stress Effect	55

TABLE OF CONTENTS (Continued)

CHAPTER		Page
3	(Continued)	
3.3	The Quantitative Microscopy of Sintered Nickel Creep Samples	55
3.3.1	Quantitative Microscopy on Polished Surfaces	55
3.3.2	Quantitative Microscopy on Fracture Surfaces	73
4	DISCUSSION OF RESULTS	88
4.1	Description of Physical Aspects of a Sample Undergoing Creep	88
4.2	Sintering Process in Creep	92
4.3	Creep	94
4.3.1	Particle Size Effect	95
4.3.2	Temperature Dependence	96
4.3.3	Density Effect	97
4.3.4	Stress Effect	98
4.4	Specimen Examination	100
4.5	Quantitative Microscopy in the Creep of Sinter Bodies	104
4.6	Summary	115
5	CONCLUSIONS	120
	BIBLIOGRAPHY	122
	BIOGRAPHICAL SKETCH	129

LIST OF TABLES

Table		Page
1.	Chemical analysis of the Sherritt-Gordon nickel powders used in the experimental work	19
2.	Loose stack densification data for -20μ , 30μ , 57μ , and 115μ nickel powders at 1100°C , 1250°C , 1350°C and the corresponding calculated incremental average shrinkage rates	41
3.	Creep data containing before and after densities, loads, temperatures, total creep, total test time, and Andrade constants ϵ_0 , a , and n	45
4.	Quantitative microscopy data of polished sections Creep Samples and Loose Stack Sintered Samples	56
5.	Quantitative metallography of fracture surfaces	79
6.	Calculations of the components of the stress activated sintering model	110

LIST OF FIGURES

Figure		Page
1.	Intraparticle porosity in the nickel powder	20
2.	Scanning electron photomicrographs of -20μ and 30μ nickel powders	22
3.	Scanning electron photomicrographs of 57μ and 115μ nickel powders	23
4.	Creep furnace in operation	27
5.	Molybdenum creep rig with sample in test position	28
6.	Stainless steel plate supporting the molybdenum creep rig	29
7.	Working surface of creep apparatus as in operation	30
8.	Densification curves for the four particle sizes when loose stack sintered at 1100°C	35
9.	Densification curves for the four particle sizes when loose stack sintered at 1250°C	36
10.	Densification curves for the four particle sizes when loose stack sintered at 1350°C	37
11.	Shrinkage rates of -20μ , 30μ , 57μ , and 115μ nickel powder specimens at 1100°C	38
12.	Shrinkage rates of -20μ , 30μ , 57μ , and 115μ nickel powder specimens at 1250°C	39
13.	Shrinkage rates $\Delta L/L$ /hr for -20μ , 30μ , 57μ and 115μ nickel powders at 1350°C	40
14.	The creep of 80% dense nickel samples of four different size fractions versus time at 1100°C and 500 P.S.I.	50
15.	The creep of 80% dense nickel samples of four different size fractions versus time at 900°C and 1000 P.S.I.	51.

LIST OF FIGURES (Continued)

Figure		Page
16a.	The creep of 80% dense nickel samples of four different size fractions versus time at 700°C and 1000 P.S.I.	52
16b.	Creep curves of 100% dense samples made from -20 μ , 30 μ , and 115 μ particle size fractions at 1000 P.S.I. and 900°C	53
17.	The dependence of the creep of 80% dense 115 μ particle size samples on temperature at a constant load of 1000 P.S.I.	54
18.	The effect of starting density on creep of samples made of 115 μ powder and tested at 900°C and 1000 P.S.I.	61
19.	The effect of starting density on creep of samples made from 115 μ powder and tested at 1100°C and 500 P.S.I. . . .	62
20.	The effect of starting density on creep of samples made from 115 μ powder at 1100°C and 250 P.S.I.	63
21.	The effect of starting density on creep of samples made from 115 μ powder and tested at 1100°C and 100 P.S.I. . . .	64
22a.	The effect of stress on 65% dense samples made from 115 μ powder and tested at 1100°C	65
22b.	The effect of stress on 65% dense samples made from 115 μ powder and tested at 1100°C	66
23.	The effect of stress on 70% dense samples made from 115 μ powder and tested at 1100°C	67
24.	The effect of stress on 75% dense samples made from 115 μ powder tested at 1100°C	68
25.	The effect of stress on 80% dense samples made from 115 μ powder tested at 1100°C	69
26.	The effect of stress on 85% dense samples made from 115 μ powder and tested at 1100°C	70
27.	The effect of stress on 80% dense samples made from 115 μ powder and tested at 900°C	71

LIST OF FIGURES (Continued)

Figure		Page
28.	Surface area (S_V) versus volume fraction porosity (V_V) for the 30 μ , 57 μ , and 115 μ nickel powders loose stack sintered to different densities	72
29.	S_V versus V_V for crept 115 μ samples compared to S_V versus V_V for loose stack sintered samples	74
30.	Anisotropy in surface area of crept samples, plotted as a function of the amount of creep	75
31.	Apparatus used to fracture notched, sintered samples for quantitative metallography of fracture surfaces . .	77
32.	The percent fracture area versus percent creep undergone by 63% dense, 115 μ samples at 700°C	78
33.	Number of intersections of fracture outline with test probe per unit length of probe, N_{Lf} , plotted against percent creep undergone by 63% dense, 115 μ samples at 700°C	81
34.	Number of fracture areas per unit area of exposed fracture, N_{Af} , plotted against percent creep undergone by 63% dense, 115 μ samples at 700°C	82
35.	A_{Af} versus percent density for samples of 20 μ , 30 μ , 48 μ , and 115 μ samples	83
36.	Total creep after two hours for five densities at 1100°C with $\sigma_{Af} = 1510$ P.S.I.	84
37.	Total creep after two hours for three densities at 1100°C with $\sigma_{Af} = 3020$ P.S.I.	85
38.	Normalized fracture stress and area fraction of fractured surface plotted against volume fraction porosity for sintered nickel tensile bars	87
39.	Model showing change in state of stress of a sintered pore from the addition of an external compressive load	90

LIST OF FIGURES (Continued)

Figure	Page
40. Density change undergone by 80% dense creep samples at various temperatures and varying amounts of creep . . .	93
41. Creep of -20μ samples at four densities at 1100°C with $\sigma_{Af} = 1500$ P.S.I.	102
42. Creep curves of 100% dense, -20μ and 115μ samples at 1100°C and 1500 P.S.I.	105
43. Model used in the analysis of creep and stress assisted sintering	109
44. Total creep in test versus percent calculated from the model to be stress activated sintering	112
45. Total time of test versus $\% h_{as}$ as calculated from the model	114

Abstract of Dissertation Presented to the
Graduate Council of the University of Florida in Partial
Fulfillment of the Requirements for the Degree of Doctor of Philosophy

HIGH TEMPERATURE COMPRESSIVE CREEP
OF SINTERED NICKEL

By

WALTER RALPH TARR

August, 1973

Chairman: Dr. Frederick N. Rhines
Major Department: Materials Science and Engineering

Compressive creep of sintered nickel was performed under the
following range of conditions.

Temperature	700°C - 900°C
Load	25 P.S.I. - 4000 P.S.I.
Density	60% - 100%
Particle size	-20 μ - 115 μ .

The data show that the creep rate was determined by the load on an
effective cross section of material which was determined to be the
fracture cross section in tension. This cross section called the area
fraction of fracture surface is designated A_{Af} . The effect of sinter-
ing on the creep process was determined to be primarily one of return-
ing the pore shape to isotropy after the pore was deformed in creep.

CHAPTER 1

INTRODUCTION

The powder metallurgy field has been an art throughout much of history. With the application of materials science and quantitative microscopy, the geometric processes through which a loose powder aggregate goes during the sintering process are well established. The fabrication of parts by the use of powder metallurgy techniques and the application of these parts in the severe environments of high temperature, high load, and sometimes high neutron flux demand an understanding of how a porous material acts under severe conditions.

An aggregate of powder possesses more energy than a solid piece of the same material of the same mass because it contains more surface area. This energy, called surface energy, comes from the fact that there is an imbalance of energy associated with atoms situated next to a free surface.

When particles which are in contact with each other are heated to a high temperature, but below their melting point, they weld together and densify into a solid mass which may approach the theoretical bulk density of the material. This densification process is called sintering and is driven by the surface energy possessed by the powder aggregate [1,2,3,4,5,6].

Another phenomenon seen primarily at high temperature is creep, which is the time dependent strain of a material under a stress. The driving force for creep is the stress applied to the part. This time dependent strain of a part in service becomes critical where close tolerances are required for long times under severe operating conditions. An example of severe conditions encountered by porous materials is that of sintered fuel elements for reactors. The sinter body must be reasonably dimensionally stable at high temperatures, high stress, and high neutron flux. Applications such as fuel elements wed the problems of the sintering and creep processes so that a knowledge of how a porous body reacts under load at high temperature and the physical changes that take place in the structure becomes necessary.

1.1 General Characteristics of the Sintering Process

Loose stack sintering is the term applied to the phenomena by which an aggregate of finely divided particles welds together and densifies at high temperature. This densification requires neither melting nor the application of an external load. A reduction in surface area is effected with densification with the attendant reduction of surface energy and thus the total energy of the system. Due to the complexity of the geometric changes taking place during sintering, the topological approach to the evolution of the microstructure of a sinter body developed by Rhines [7] will be used as a basis for description of the changes that take place as a mass of loose powder proceeds from separate parts to a single dense body.

The sintering process is conveniently thought of as possessing three stages [1,8]. The first stage is characterized by the welding and growth of particle contacts and the smoothing of particle surfaces. The topological state, i.e., genus, fixed by the original stacking, remains constant during this process. The particle network is striving for a minimum surface energy for its given topological state. As the surface total force/unit area is greatest at areas of highest curvature, the largest geometric changes take place at weld necks, particle corners, and fine tips in dendritic powder, where this force is the largest. The surface energy expended in rounding the internal surface is wasted as far as densification is concerned as no process which acts solely on the surface can contribute significantly to the densification of the particle compact. The weld necks grow and surface rounding continues until a minimal surface for the given topological state has been effectively achieved. Further reduction in surface area can come about only by reducing the genus, i.e., connectivity of the pore network; i.e., second stage sintering. Second stage sintering is the stage in which the pore network goes from a completely interconnected state to a completely isolated state. As the connections between pores, or channels, are pinched off, a new minimal surface area state prevails corresponding to the new topological state. This direct dependence of minimal surface area on state can be seen in the fact that during second stage sintering, the surface area per unit volume, S_v , decreases linearly with increase in density. Channel closure persists until all porosity is isolated. Particle identity is generally lost during

second stage. Third stage sintering is concerned with what happens to the isolated pores. As time proceeds, conglomeration of the remaining porosity occurs. The large pores grow at the expense of smaller pores, thus the average pore size becomes larger [9]. Some reduction in total porosity also is characteristic of third stage. Total removal of all porosity from the interior of a sinter body rarely, if ever, occurs solely under the action of the sintering force (surface tension) in the finite time of sintering operations. Densification occurs in all three stages of sintering and the three stages overlap in the times in which they occur.

1.2 Background and Previous Investigations of Sintering

Sintering has been used in the manufacture of products from particles of all classes of solids: metals, ceramics, glasses, and organics [1]. Commercial sintering is seldom loose stack sintering, but commonly uses pressure on the powder aggregate to promote densification or a liquid phase for the same purpose. Most processes that involve sintering constitute one or more of the following:

1. Loose stack sintering. The loose powder stack is heated to a temperature near its melting point and densification occurs with time.
2. Pressed and sintered. Much or most of the densification of the powder aggregate is achieved by the application of high pressure preceding the sintering operation. Densification from the pressure occurs by plastic deformation and/or rearrangement of the particles.

3. Hot pressing. The application of pressure during the sintering process [4].

4. Liquid phase sintering. Sintering with the aid of a liquid phase [2,10].

The geometry of a loose stack of particles such as is found in normal, practical sintering appears complex. Some of the approaches that have been put forward to help in the understanding of sintering are the use of equi-sized particles, only two particles [11], a string of particles [12], a particle on a plane surface [13], three wires twisted together [4], spools of wire [4], constant temperature, and controlled atmosphere. The study of sintering in these relatively simple cases has given insight into the growth of weld necks and some understanding of the densification phenomenon, decrease in the relative volume of porosity, but have been generally unsuccessful in explaining the total sintering of even a simple shape which contained a large number of particles. Mathematical models can be formulated for simple cases and with the use of known physical parameters, mechanisms have been inferred. A basic fault with all the foregoing geometrically reduced experimental models is that the information is 1- or 2-dimensional and practical sintering is complex 3-dimensional. Some investigations of the three stages of sintering will now be presented.

The first stage of sintering includes weld neck growth and surface rounding. Surface rounding can be accomplished by evaporation of material from convex surface and condensation on concave, or less convex, surface [2,10]. Surface and volume diffusion [7,14] can cause

surface rounding by the net transfer of material from convex surface to concave surface. It should be noted that neither evaporation-condensation nor surface diffusion can cause significant densification in a powder aggregate [1,4,7]. It is thought that the growth of weld necks can be caused by several mechanisms. They are: evaporation-condensation [15], surface diffusion [4,11,12,16,17], volume diffusion [4,7,10,11,15,18,19,20], viscous flow [2,4], and plastic flow [7,20,21,22,23,24]. It is also believed that densification requires both creep and concurrent surface area minimization [25]. Calculations using the surface tension value obtained for copper (1400 dynes/cm) have shown that plastic flow is possible at least in the early stages of neck growth where contact area is very small [4]. Observations of weld necks formed in loose stack sintering experiments show that there is at least one of the mechanisms capable of surface rounding in operation during neck growth. The rounded neck surface could not have been created by plastic flow alone. In metal systems having low vapor pressure [11], the rate of weld neck growth, as indicated by experiments with particles on plane surfaces and pairs of particles, is believed to be either surface diffusion or volume diffusion controlled or both. Kuczynski [11] found for copper that surface diffusion was the dominant mechanism for small particles and low temperatures, while for large particles and high temperatures, volume diffusion was dominant.

Second stage sintering is characterized by densification of the body and the isolation of the pores that remain [1,7,8,9].

The connectivity of the porosity goes to zero [7]. There are three material transport mechanisms that various authors believe capable of causing densification. They are: creep [7,8,20,22,26], volume diffusion [4,14,26,27,28,29], and grain boundary diffusion [14,22,23; 29,30,31,32]. Sintering done under small loads [20,24] indicates that there is no change in mechanism as the sinter body densifies. This information supports the plastic flow theory. Support for the grain boundary diffusion theory may be found in the lowered sintering rate [27] after grain growth. Wire model experiments also show decreased pore size in the vicinity of grain boundaries. Volume diffusion of vacancies to the external surface from the internal pores has been generally discounted due to large distances involved [7].

Third stage sintering is usually defined as the elimination and/or coarsening [9] of the remaining isolated porosity. Plastic flow is believed responsible for elimination of pores by some and a theoretical model [22] for the shrinkage of these isolated pores by plastic flow has been derived. Coarsening of large pores at the expense of disappearance of smaller surrounding pores can be accomplished only by volume diffusion [9]. It has been shown by several authors [2,14,30] that the presence of grain boundaries can cause a significant increase in total densification; however, grain boundaries are not required for densification [4,9]. Volume diffusion is postulated by some [14,27,28] as the mechanism of pore shrinkage; whereas, others [7] believe volume diffusion of vacancies from an internal pore to the external surface cannot effect any significant densification of the total body. Densification rates based on volume diffusion data

indicate that the times required for densification are unreasonable and that geometry would require that the sinter body densify from the external surface inward, contrary to experimental observation [9,33].

It can be seen from the preceding paragraphs that considerable discussion of the exact nature of sintering still remains along with considerable, seemingly conflicting, experimental evidence. There is at present no formula in the literature into which one may insert the physical properties of a metal or a ceramic powder and predict the densification of a compact from a loose stack to a fully dense mass.

1.3 General Characteristics of the Creep Process

Creep is defined as the time dependent strain undergone by a material when subjected to a stress at constant temperature [34,35, 36,37,38,39]. At elevated temperatures where recovery processes are relatively active, small stresses which are a fraction of the tensile strength are capable of causing plastic deformation in metals. Some materials will show this phenomenon when subjected to room temperature tensile tests at different strain rates. This may be seen in the stress-strain curves of pure metals such as aluminum and zinc where the stress-strain curve of the tensile bar pulled at the slower strain rate shows a greater strain for a given stress.

Constant load tensile creep is generally thought of as possessing three stages [34,40]. The first stage is a period of decreasing creep rate where work hardening mechanisms are dominant [41]. In the creep of polycrystalline samples, the grains with orientations favorable to shear are the first to deform. This inhomogeneous

deformation produces elastic as well as plastic strains and these elastic strains are recoverable with time if the specimen is unloaded. This recoverable creep is called anelastic creep. The second stage is considered a stage of constant creep rate where the rate of work hardening being produced by the deformation is exactly counteracted by recovery processes [42,43] and/or reduction in cross-sectional area of the sample [39]. The third stage is generally characterized by an accelerating creep rate, intergranular cavity formation (at high temperature)[44,45,46], necking (at low temperature)[44], and ultimate failure. Constant stress and constant load compressive creep in ductile metals generally exhibits only the first stage of creep, and thus generally shows a monotonically decreasing creep rate throughout a test [47].

1.4 Background and Previous Investigations of the Creep Process

Creep is seen to be a sensitive function of temperature and for a given structural state has been shown to have an Arrhenius temperature dependence. Creep is therefore generally considered to be a thermally activated process [34,36,37,38]. Activation energies calculated from strain rate versus temperature data are usually close to the activation energies of self-diffusion when the creep temperature is between 0.5 and 1.0 T_m [34,36,38,48]. There is much discussion concerning the exact mechanism that allows creep to proceed. Some of the transport processes proposed as controlling the kinetics of the high temperature creep process are: diffusional creep (Nabarro-Herring creep

[36,40,49,50,51]) and others [52,53], dislocation intersection and jog formation [34,54,55,56], and climb of dislocations [36,56,57].

1.5 Dislocation Modelling

There are many formulas that have been used to model the first and second stages of creep [58,59]. Some of the equations have elements which match known physical parameters, whereas others are strictly empirical.

A few of the well-known creep laws or formulas will now be presented with explanations based on physical parameters where possible.

Logarithmic creep [34,40], $\epsilon = a \log(t) + c$. Log creep has been found in organics, glasses, metals, and ceramics and is generally found in experiments of moderate to low creep rates, small strains, and temperatures below $0.4 T_m$. This type of creep has a monotonically decreasing rate such as found in the transient, 1st stage of creep curves. Log creep can logically be reasoned to be a result of exhaustion of energy barriers to deformation capable of being overcome by the applied stress on a sample and local thermal fluctuations [34]. As the material deforms, the barriers to further deformation (dislocations, etc.), increase, thereby requiring more energy to overcome them and cause further deformation [60]. In constant stress creep there exists a constant external stress plus the thermal fluctuations. Thermal fluctuations are capable of helping overcome normal lattice coherency (Peierls force), but as deformation proceeds, these regions requiring minimum force to push a dislocation through are used up and only regions

requiring more energy (higher activation energy) remain. Thus the creep rate decreases. The log creep equation cannot account for steady state creep.

Andrade creep [59,61,62,63,64], $\epsilon = bt^{1/3}$. This type of creep has essentially no acceptable theory to explain it. The reason for the widespread use of the Andrade formula for transient creep is that many researchers [47,65,66] have found that it can be successfully used in plotting experimental results. The Andrade creep formula generally fits better in creep experiments where large creep strains and temperatures greater than about $0.4 T_m$ are involved. The basic Andrade creep equation will not fit curves where steady state creep has been involved, for steady state creep requires a linear term in time [40]. The fit of the Andrade creep formula can be improved in cases where steady state has occurred by the addition of a linear term, $\epsilon = kt$ ($k = \text{const.}$). A term for instantaneous strain on loading, ϵ_0 [67,68], is also frequently added, thereby making the Andrade equation, $\epsilon = \epsilon_0 + bt^{1/3} + kt$. For monotonically decreasing creep rates, the linear term, kt , is omitted. A constant creep rate (for a constant stress), implies that some recovery of the creep sample is taking place during the creep experiment. This dynamic recovery [69,70] is most likely cross-slip and climb. Under some conditions of stress and temperature, a combination of the log and Andrade creep equations fit the data best. Theory has of course been left far behind. Some authors do not find stage two creep for constant stress tensile tests [68,71] and observe a monotonically decreasing creep rate from the onset of loading to the initiation of failure.

Diffusional creep (Nabarro-Herring creep). Diffusional creep is believed by many authors to be stress directed self-diffusion. Atoms diffuse away from grain boundaries under compressive stress to grain boundaries under tensile stress, resulting in sample elongation in the tensile direction. The nature of diffusional creep is such that very high temperatures, very low loads, and a fine grain size are required for it to be the dominant creep mechanism. The strain rate for Nabarro-Herring creep may be given by the equation,

$$\dot{\epsilon} = (aD/L^2)(\sigma b/kT),$$

where $a = \text{const. about } 5$ for uniaxial stress, b is an atomic volume cm^3 where b is the Burgers vector and c is a constant about 0.7, D is the diffusion coefficient, and L is the grain diameter. That creep obeying this equation exists has been shown by several authors [36,40,49, 50,56].

None of the foregoing creep and creep rate equations is capable of modelling or predicting the occurrence of or the results of massive recovery such as recrystallization. Generally, when recrystallization occurs during a test, the creep rate increases [72,73].

There are many variables affecting the creep rates of materials, some of which are temperature, shear modulus, grain size and subgrain size, stacking fault energy, stress, composition, and diffusion rate. The manner in which some of these parameters are known or thought to affect creep will now be discussed.

Temperature. Creep is generally considered a thermally activated process because it has an Arrhenius temperature dependence; therefore,

the temperature at which a material undergoes creep deformation is of primary importance. Creep is usually thought of as a high temperature phenomenon, 0.3 to $1.0 T_m$, primarily because its effects are most commonly observed in this temperature range. However, creep has been reported at temperatures below 10°K . Thermally activated processes are exponential functions of temperature; i.e., $f(e^{-(\Delta H_c/RT)})$, and for most materials, ΔH_c , the apparent creep activation energy, is such that recovery processes become reasonably active above about $0.3 T_m$.

Diffusion. Self-diffusion is now generally accepted as being the ultimate controlling process in most high temperature creep [38]. Nabarro-Herring creep is generally thought to be stress directed volume diffusion (though not by all researchers)[51,52]. Climb of edge dislocations also has diffusion of vacancies to or from the dislocation core as the rate controlling step. Many experimentally determined high temperature creep activation energies for most metals and many ceramics are found to be identical to or very near the activation energy of self-diffusion. Creep rates are found to change abruptly with an abrupt change in diffusivity and in the same proportion. An example of this is found in the phase transformation of iron. In ceramic compounds, the high temperature creep activation energy is usually close to that of the diffusivity of one of the elements of which the compound is composed.

Shear modulus. [38]. The dependence of shear modulus on temperature is generally ignored. This is usually not critical, but significant deviations from creep rates predicted by self-diffusion data

have been corrected by introducing the temperature dependence of the shear modulus into the creep equation [74].

Stacking fault energy. In general, the lower the stacking fault energy, the lower the creep rate [35,38,75,76,77]. A low stacking fault energy allows widely split partial dislocations which must recombine for the dislocation to climb. Stacking fault energy is also a determining factor in the size of the substructure units (subgrains), formed during deformation.

Grain size. That grain size can in many cases have an effect on the creep rate of a material is accepted by most investigators [38,70,78,79,80]. Some authors show that a small grained material has a lower creep rate than the same material in large grain form at one temperature, while others see the opposite at another temperature [80]. Other authors have found a grain size effect only below a certain grain size [78]. The amount of grain boundary is that property which grain size determines which is of interest in creep. Grain boundaries, being discontinuities in a structure, act as barriers to the movement of dislocations. If the grain size is small enough for a significant portion of the work hardening to be a result of dislocations piling up at grain boundaries, then one could envision the effect of changing grain size (amount of grain boundary), in this grain size region. If one decreased grain size (increased grain boundary area), there should be a decrease in creep rate and vice versa. If, however, the grain size is large enough that the pileup of dislocations at grain boundaries is insignificant compared to pileups in the interior of the

grain, then varying the grain size would be expected to have little effect on creep rate. The grain size at which grain size becomes an important factor in determining creep rate depends upon properties of the material such as stacking fault energy and morphology (precipitates, etc.), although there is no uniformly accepted trend. The amount of grain boundary shear may also be tied to the amount of grain boundary. Grain boundary shear is the phenomenon in which the volume of a grain adjacent to a grain boundary shears to a greater extent than the bulk of the grain due to accelerated recovery [35,36,81] (generally polygonization)[82], of the crystal in this region. It has been shown in bicrystals [81] that a significant portion, 40%, of total shear can in some cases be attributed to grain boundary shear. Some authors state that grain boundary shear can be a significant portion of total creep in polycrystalline metals, while others discount its effect. Grain boundary shear appears to be important to the formation of cavities [83,84,85] leading to the commonly observed intercrystalline failure of high temperature creep samples [86].

Stress. The effect of stress on creep of materials and the resultant structure is complex. The stress dependence of creep is generally divided into three regions [7]. The low stress region where $\dot{\epsilon} \propto \sigma^1$, intermediate $\dot{\epsilon} \propto \sigma^5$, and high stress region where $\dot{\epsilon} \propto e^{b\sigma}$, $b = \text{constant}$. Most creep tests and engineering applications are concerned with the intermediate stress region where $\dot{\epsilon}$ is proportional to σ^5 . The effect of stress (strain rate) on structure is a complex function of temperature, stacking fault energy, modulus,

composition, etc., i.e., the mobility of dislocations and recovery processes. Generally in metals which form substructures, at a given temperature, the higher the stress and consequent strain rate the finer the substructure formed. The subgrain size formed in high temperature creep seems to be independent of deformation (creep or cold work), previous to a given test [35]. If, during a creep test the stress is changed, a new subgrain size will be formed which is characteristic of the new stress [35]. Recent work in pure aluminum indicates that increasing the temperature (and consequent strain rate) during a creep test will reduce subgrain size [82].

The primary problem in trying to determine the exact nature and influence of each of the aforementioned parameters is that it is difficult, if not impossible, to alter any one without affecting some or all the others. This is probably the basis of much of the conflict reported in the literature.

1.6 Purpose and Scope of This Research

The purpose of this research is to provide insight and quantitative data relating to the structural states through which a sintered nickel specimen goes during a compressive creep test. The nature of the interaction between the creep of sinter bodies and concurrent sintering is studied. Structural changes in a sinter body can most easily be studied through the use of quantitative metallography. Many of the well-known quantitative metallographic functions are used. They are: A_A , V_V , S_V , N_L , and N_A . A new quantitative metallographic function has been defined during the course of this research which has proved to be

a useful tool in predicting the strengths of sinter bodies. This function, A_{Af} , is a measure of the load bearing area in a sinter body. A_{Af} is the standard A_A count taken on the fracture areas of a fractured sinter body. When a sinter body is fractured, the fracture should take the path of least resistance, i.e., the weakest section. Thus, the measure of the area covered by fracture relative to the total cross section of the sinter body should be a measure of load bearing area in the sinter body.

This research encompasses a 400°C temperature range, a 4000 P.S.I. load range, particle sizes from -20 μ to 115 μ , and densities from loose stack to 100% dense. The response of sintered nickel bodies under various combinations of these parameters has been studied and presented. The creep and creep rate data have been modelled to the equation $\epsilon = \epsilon_0 + at^n$ and the effect of the various parameters on this equation are presented.

CHAPTER 2

MATERIAL SPECIFICATIONS

2.1 Material

The material used in the experimental creep work was nickel powder purchased from the Sherritt Gordon Company. The nickel powder was received in two lots, one of predominantly fine particle size (-270 mesh) and the other of predominantly coarse particle size (-48 + 200 mesh). The chemical analysis of each lot is given in Table 1. The powder was produced by an electrolytic process which resulted in an irregular particle at small size fractions which became more spherical as the powder size increased. All particles had a lumpy surface texture resembling that of a blackberry. The individual particles were not always solid and upon metallographic preparation intraparticle porosity could be seen as shown in Figure 1. Fractures of low density specimens of the coarse, -120 + 149, 115 μ , size fractions occasionally showed that the outer layer of one of the particles was torn from it at the point of fracture.

2.2 Particle Sizes Used

The powder, as received, was sieved through a set of U.S. Standard sieves made by the W. S. Tyler Company. Three of the size fractions used were sieve cuts from this series. The three size

Table 1. Chemical analysis of the Sheritt-Gordon
nickel powders used in the experimental
work.

Property	Lot #1	Lot #2
Composition wt %		
Nickel (includes Cobalt)	99.9	99.9
Cobalt	0.064	0.110
Copper	0.006	0.005
Iron	0.004	0.014
Sulfur	0.016	0.034
Carbon	0.005	0.016
Apparent Density (gm/cc)	4.61	3.76
Dominant Size Range (mesh)	(-48 + 200)	-270

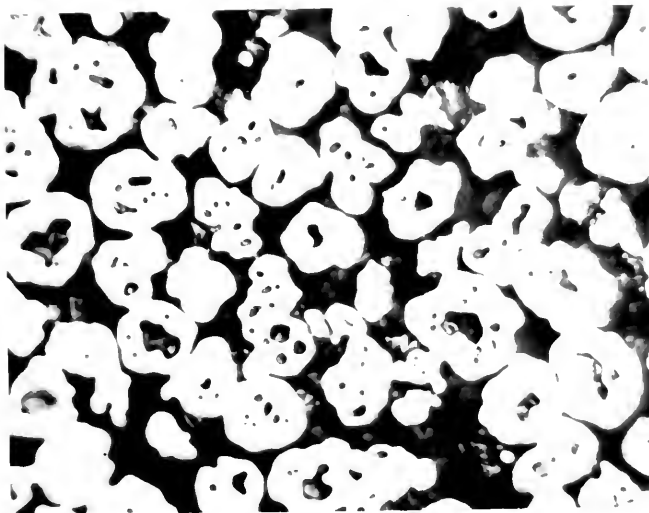


Figure 1. Intraparticle porosity in the nickel powder.

fractions from the Tyler sieves were: (1) coarse (-120 + 140, 115 μ), (2) intermediate (-230 + 270, 57 μ), and (3) fine (-400 + 500, 30 μ). A fourth size fraction was prepared by taking the fines which passed through the 500 sieve and further sieving it on screens in an Allen-Bradley Sonic Sifter. The size fraction used from this sieving was the powder which passed through the 20 μ screen, designated -20 μ . Scanning electron microscope photographs of these four size fractions may be seen in Figures 2 and 3. Specimen notation throughout the work is keyed by both a letter and a number. The letter denotes the size fraction from which the samples were prepared and the number denotes the chronological order of testing. The notation is as follows:

A # = -400 + 500, 30 microns (μ)

B # = -230 + 270, 57 microns (μ)

C # = -120 + 140, 115 microns (μ)

-20 microns = -20 microns + 0 (average 11 μ).

2.3 Sample Preparation

The procedure for manufacturing the loose stack sintered specimens was the following. Previously sized powder was poured into a graphite mold containing 10 to 12 flat-bottomed holes .375 inch in diameter and .75 inch in depth. The mold so charged was then inserted into a nichrome wound, silica tube, presintering furnace which was maintained at 1000°C. The atmosphere in the presintering furnace was wet hydrogen. Presintering time was 1 hour, after which the graphite boat was withdrawn from the furnace and the lightly sintered blanks were tapped out of the mold and the mold was reused.

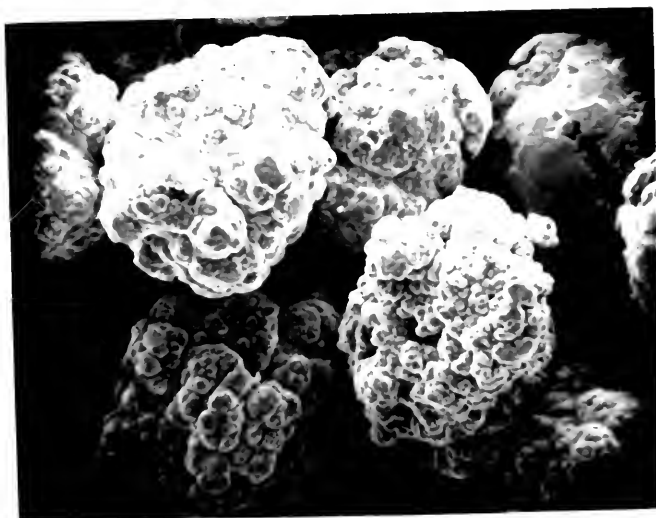


-20 μ
2000X

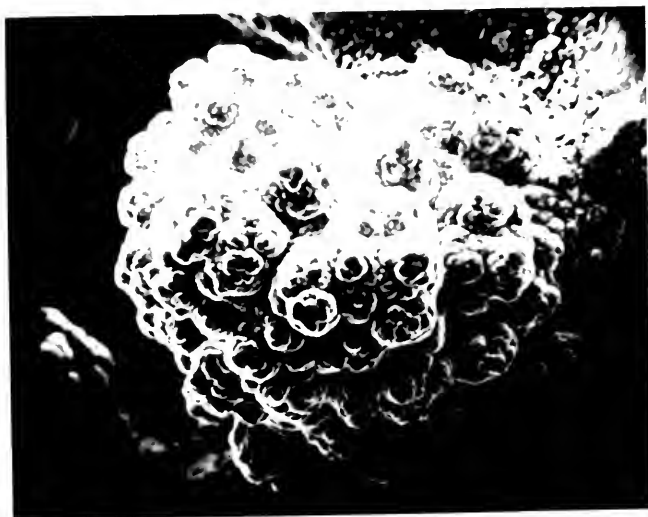


30 μ
1000X

Figure 2. Scanning electron photomicrographs of
-20 μ and 30 μ nickel powders.



57μ
500X



115μ
500X

Figure 3. Scanning electron photomicrographs of 57μ and 115μ nickel powders.

The temperatures used for sintering varied from 1100°C to 1400°C. The sintering furnaces were globar heated and had high purity impervious alumina tubes. The boats in which the presintered blanks were placed for sintering were also of high purity alumina. Any material with any appreciable trace of silica in the sintering environment resulted in destruction of the sintering blanks due to liquation at the surface of the blanks or, in some cases, complete melting. The dissociation of the water in the wet hydrogen atmosphere provided a back-pressure of oxygen which effectively retarded any SiO transport at sintering temperatures.

Samples above 93% relative density were made by hot-pressing the powder in a graphite mold at 1200°C. A 1-inch diameter blank was made in this way which was 91% dense. This large blank was then annealed in wet hydrogen at 1000°C and cold-pressed at 70,000 P.S.I. to 96.5% relative density. Several nominally identical high density specimens were then electro-discharge machined from this blank and annealed. Samples which were 100% dense were first hot-pressed to 97% relative density, annealed and swaged. All hot-pressing was done in graphite molds. This procedure resulted in the contamination of the specimen with enough carbon to cause melting at 1400°C. The samples were therefore given a decarburizing treatment at 1000°C which consisted of 1 hour in a slightly oxidizing atmosphere, commercial tank nitrogen, followed by 30 minutes under hydrogen.

Density measurements were made by using a wax impregnation Archimedes method. The sample was weighed (dry weight), impregnated

with wax, and weighed again (wax weight). The impregnated sample was then supported by a fine wire and weighed while immersed in water (H_2O weight). The wire weight was the weight of the wire suspended in the water. The density was determined from the following equation::

$$\text{Density (gm/cm}^3\text{)} = \frac{\text{Dry weight}}{\text{Wax weight} - (\text{H}_2\text{O weight} - \text{Wire weight})}$$

Relative density could then be obtained by dividing by 8.906 gm/cm^3 , the theoretical x-ray density of nickel. If the desired density of nickel had not been reached, the wax was burned out in air and the blank returned to the sintering furnace for further sintering. This process was repeated until the blank had a measured density equal to the density desired, $\pm 0.5\%$.

A blank of the desired density was then machined on a Schaublin 70 high precision lathe. The specimen was a right circular cylinder with a tolerance of ± 0.0002 inch on the diameter and with the ends within 0.0002 inch of being parallel.

2.4 Experimental Investigation into the Creep of Sintered Nickel

The experimental investigation of sintered nickel was done in compression, encompassing a wide range of loads, temperatures, particle sizes, and densities.

2.4.1 Equipment (Creep Apparatus)

The creep apparatus consisted of a globar furnace with an impervious alumina tube in which the sample and loading rig were inserted for the test. A complete view of the creep apparatus in

operation is shown in Figure 4. The loading rig in which the sample was placed for testing consisted of three $\frac{1}{2}$ -inch diameter molybdenum rods bolted to a $1\frac{1}{2}$ -inch diameter molybdenum base plate which supported the samples. Loading was effected by means of a fourth $\frac{1}{2}$ -inch diameter molybdenum rod which used the three support rods as guides (see Figure 5). The support rods were bolted to a stainless steel plate which was bolted to a large aluminum plate which served as the working surface for the remainder of the creep apparatus. The stainless steel plate also had a gas outlet in it as well as holes for the loading rod and measuring thermocouple which was positioned next to the test sample. A photograph of this part may be seen in Figure 6. Loading was accomplished by a 3 to 1 lever which had a ball bearing pivot. The load was transferred to the loading rod from the lever arm through a ball bearing set into a piece of steel. This ball bearing had a flat ground on it on which the dial gage rested. With the dial gage directly over the sample, one could read deflection of the sample directly during the test. The dial gage had a range of 0.4 inch and direct readings to 10^{-4} inches with estimates to 10^{-5} inches. The height of the lever arm pivot and the dial gage was adjustable to accommodate different length specimens. The working surface of the apparatus is shown in Figure 7.

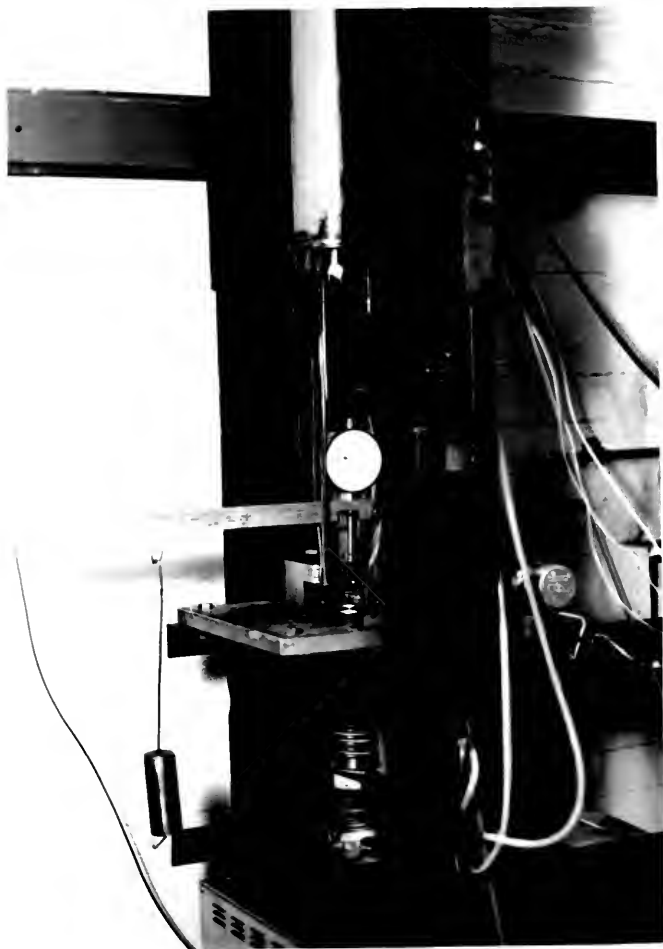


Figure 4. Creep furnace in operation.



Figure 5. Molybdenum creep rig with sample in test position.

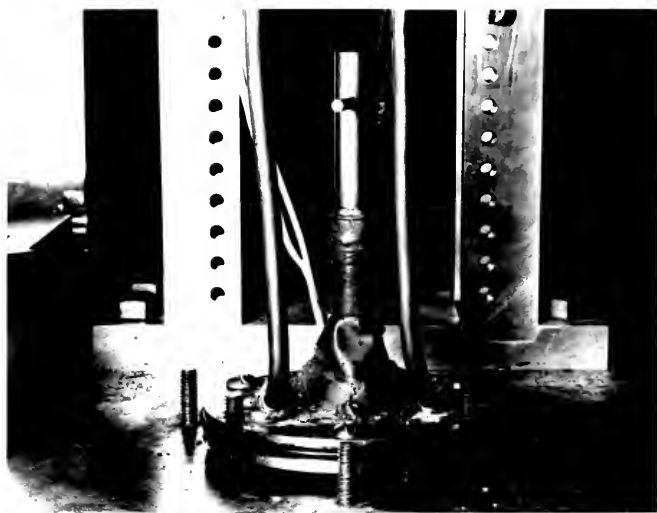


Figure 6. Stainless steel plate supporting the molybdenum creep rig.

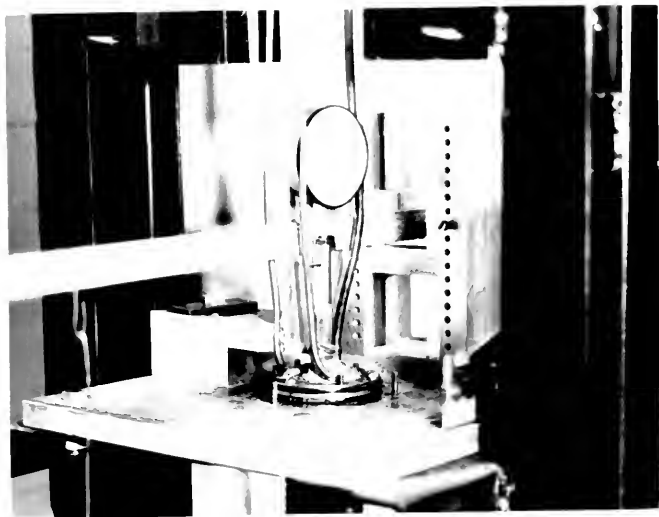


Figure 7. Working surface of creep apparatus as in operation.

2.4.2 Test Conditions

The range of conditions of the test parameters is as follows:

1. Temperature - 700°C - 1100°C
2. Load - 25 P.S.I. - 4000 P.S.I.
3. Density - 60% - 100% Rel. Density
4. Atmosphere - Wet Hydrogen.

2.5 Experimental Procedure

A specimen machined to the desired size was measured with a micrometer before inserting into the creep apparatus while outside the furnace. The specimen sat on an alumina disk and had one resting on it. The loading rod was then lowered onto the sample to avoid sample movement and consequent misalignment during insertion of the rig into the furnace. The rig was lowered into the hot zone of the furnace, at which time the loading rod was lifted from the sample and remained off until the sample temperature had risen to test temperature and the creep test was to begin. While the sample was coming to temperature, as measured by a thermocouple placed next to the sample, the lever arm was placed over the loading rod and the dial gage was locked into place directly over the rod. When the test was to begin, the loading rod was lowered to contact the sample, an initial dial reading was taken, and the load applied at time zero, t_0 , for the start of the test. Dial readings were taken at intervals to record the creep curve and a temperature reading at the same time. At completion of the run, the load was removed from the sample and the entire rig was removed from the hot zone of the furnace. The loading rod was lifted from the sample

immediately at the end of the test. Elapsed time from the end of the creep test, removal of load and loading rod from the sample, to removal of the sample from the furnace hot zone was generally 3 to 5 minutes.

All creep work was done in a hydrogen atmosphere to prevent oxidation of the sample and the molybdenum creep apparatus.

When the sample had cooled, the final length was measured and the per cent error of creep measurement was calculated according to the following formula:

$$\% \text{ Error} = \frac{(D_0 - D_f) - (L_1 - L_2) \times 100}{(L_1 - L_2)}$$

where

D_0 = Initial dial reading

D_f = Final dial reading

L_1 = Initial sample length as measured by micrometer

L_2 = Final sample length as measured by micrometer .

This error was usually less than 6%. If the error was greater than 15%, the test was automatically discarded.

CHAPTER 3

EXPERIMENTAL RESULTS

The experimental work was designed to provide information on the creep of sintered nickel under conditions of varying particle size, density, temperature, and load. Studies of sintering kinetics were performed on the various particle size powders independent of creep testing. Densification rates of loose-stack sintered specimens can be translated into lineal shrinkage which may be significant in compressive creep testing. The density was monitored both before and after creep testing. Quantitative microscopy was used as a means of following the evolution of microstructure in loose stack sintering as well as in creep testing.

3.1 Densification and Shrinkage in Sintering

The densification (shrinkage) of nickel powder aggregates was measured as a function of particle size, density, temperature, and time. The first step needed to understand the creep of sintered nickel was to determine the sintering kinetics of the various powders. This information was needed to determine what fraction of the length change in a creep test was ascribable to loose stack sintering phenomena in a compressive creep test.

As a powder aggregate sinters and densifies, the lineal dimensions decrease. If the sintering is isotropic (under no force except that of surface tension), the lineal shrinkage may be calculated according to the following equation:

$$\frac{\Delta L}{L_0} = 1 - \left(\frac{\rho_0}{\rho} \right)^{1/3} = 1 - \left(\frac{1 - V_{V_0}}{1 - V_V} \right)^{1/3} \quad (1)$$

where L_0 is the initial length, ρ_0 is the initial density, V_{V_0} is the initial volume fraction porosity, and ρ and V_V are final states, respectively. From equation (1), the amount of strain in a creep test that is attributable to loose stack sintering may be subtracted from the total strain. The densification curves for the four particle sizes used in the creep experiments at three temperatures are given in Figures 8 to 10. The incremental average shrinkage rates versus percent density, corresponding to the densification curves are given in Figures 11 to 13. The incremental average lineal shrinkage rate is calculated according to the following formula:

$$\Delta L/L_0/\text{hr} = 1 - \left[\rho(t_1)/\rho(t_2) \right]^{1/3} / t_2 - t_1 \quad (2)$$

where $\rho(t_1)$ and $\rho(t_2)$ are the densities after sintering for times t_1 and t_2 , with $t_2 > t_1$. The $\Delta L/L_0/\text{hr}$ is calculated between each time interval and is plotted versus the density at the end of the time interval $\rho(t_2)$. All densification and corresponding $\Delta L/L_0/\text{hr}$ data for Figures 8 to 13 are given in Table 2. Loose stack sintering and creep are parallel mechanisms in the shortening of a porous sintered sample in compressive creep. Any change in the creep conditions which would

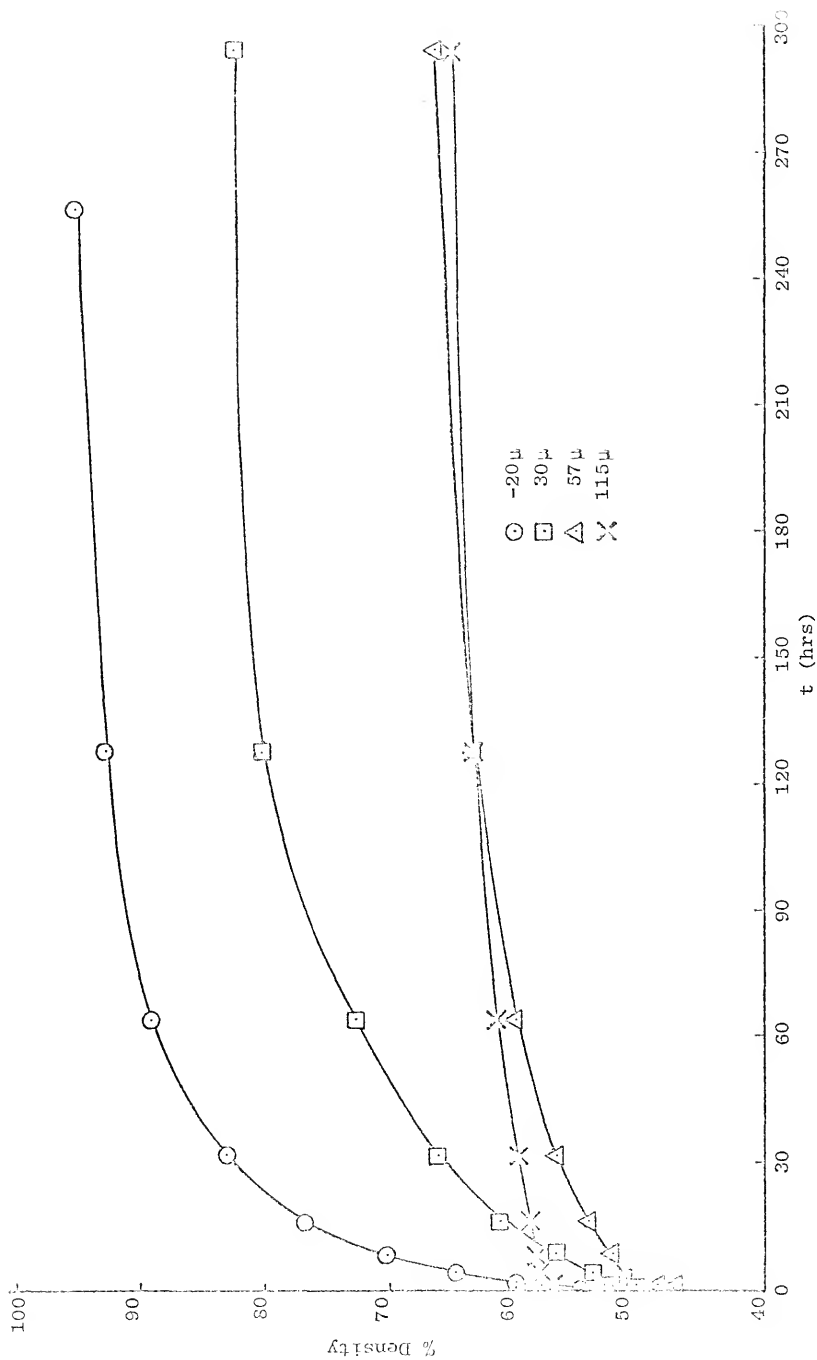


Figure 8. Densification curves for the four particle sizes when loose stack sintered at 1100°C.

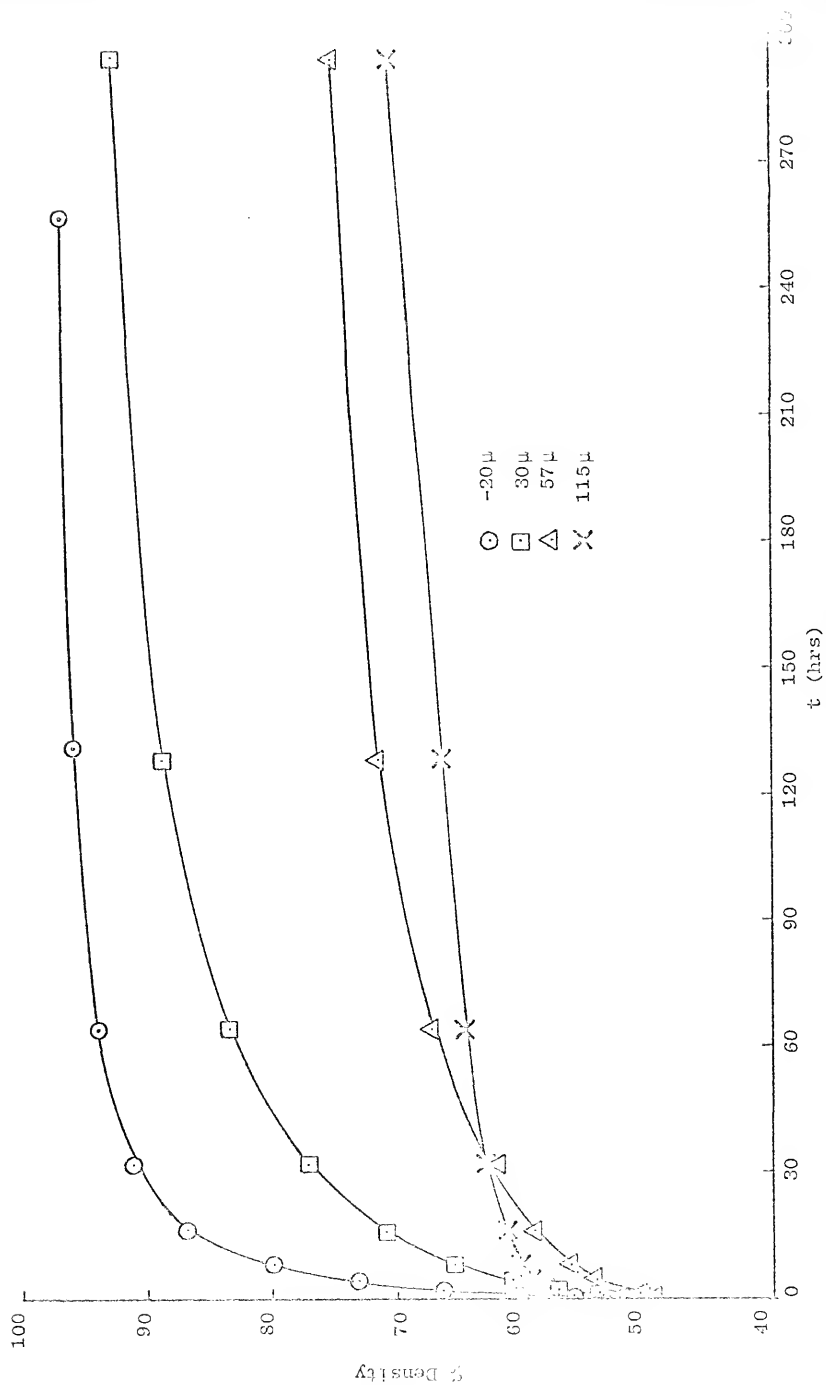


Figure 9. Densification curves for the four particle sizes when loose stack sintered at 1250°C.

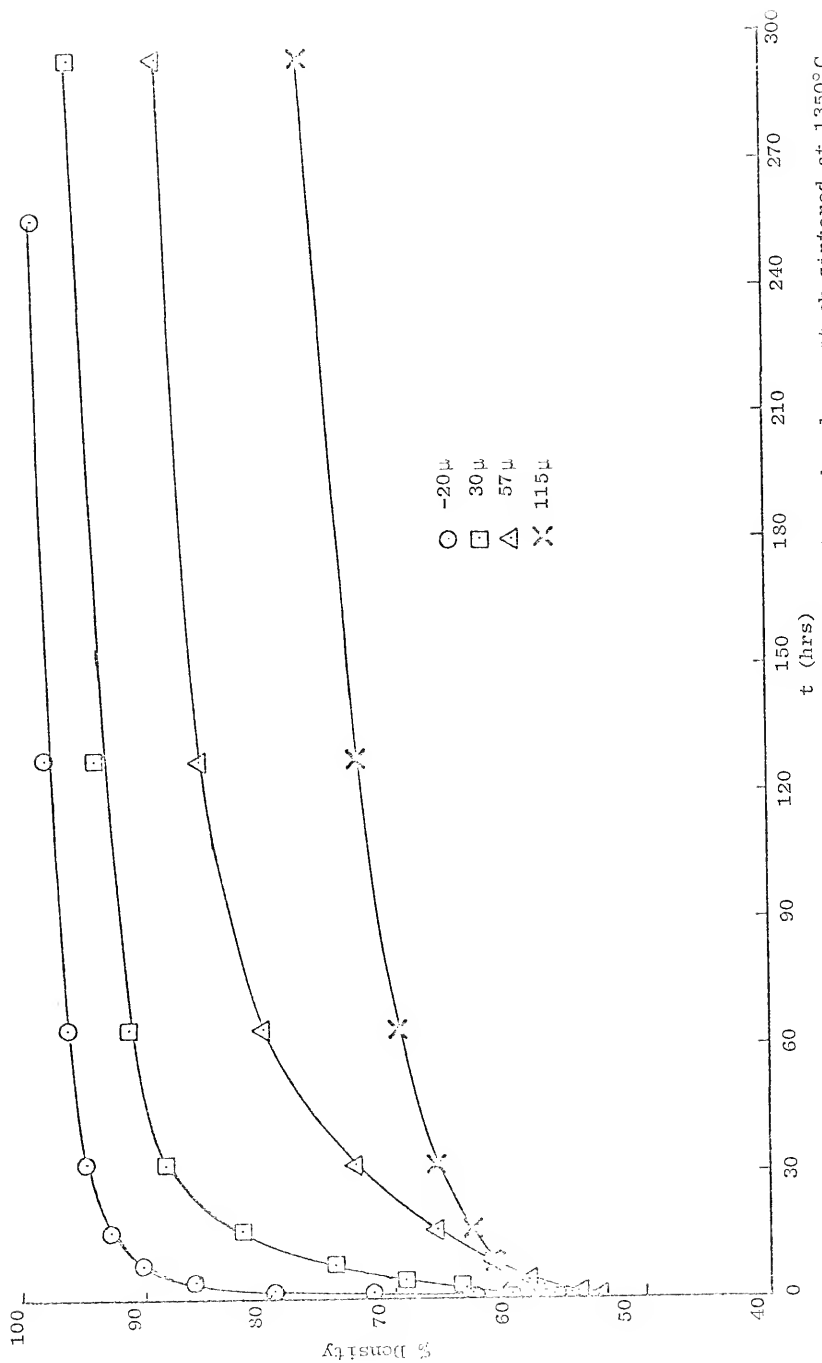


Figure 10. Densification curves for the four particle sizes when loose stack sintered at 1350°C.

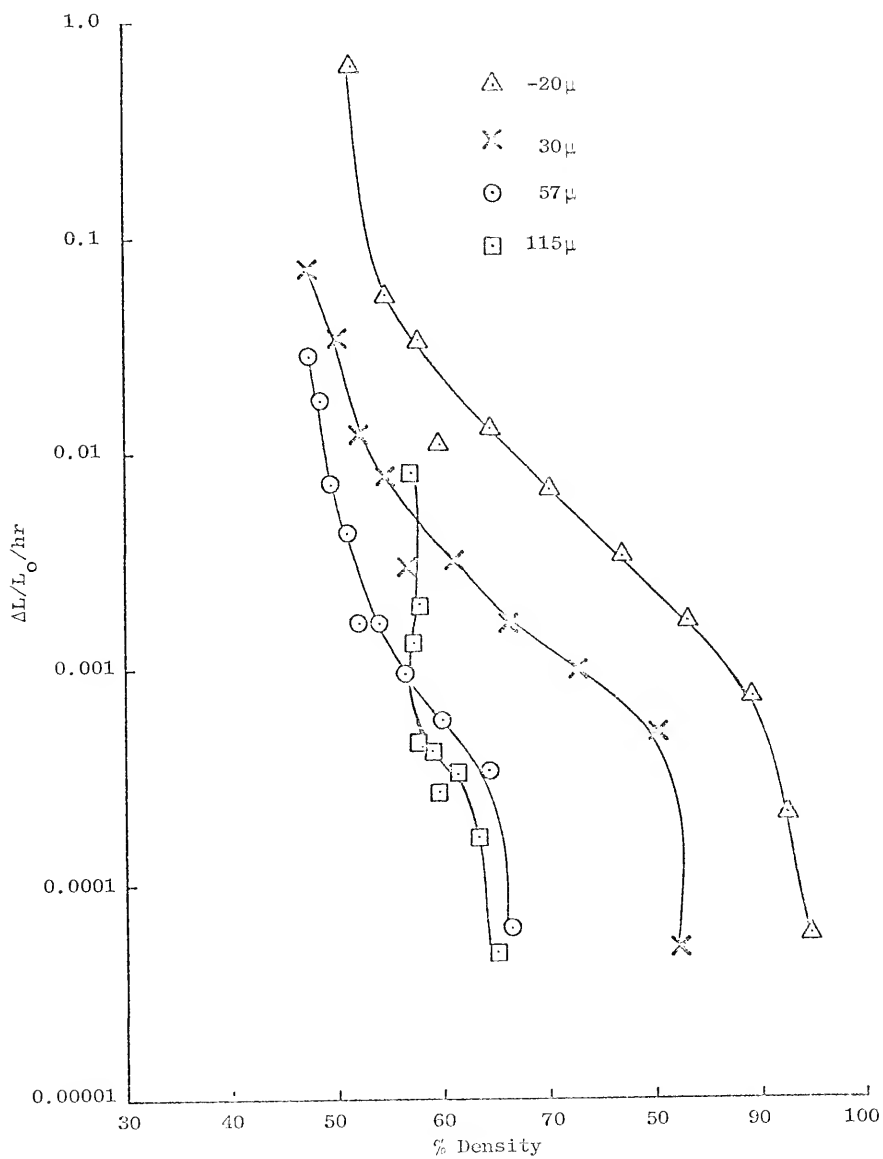


Figure 11. Shrinkage rates of -20μ , 30μ , 57μ , and 115μ nickel powder specimens at 1100°C .

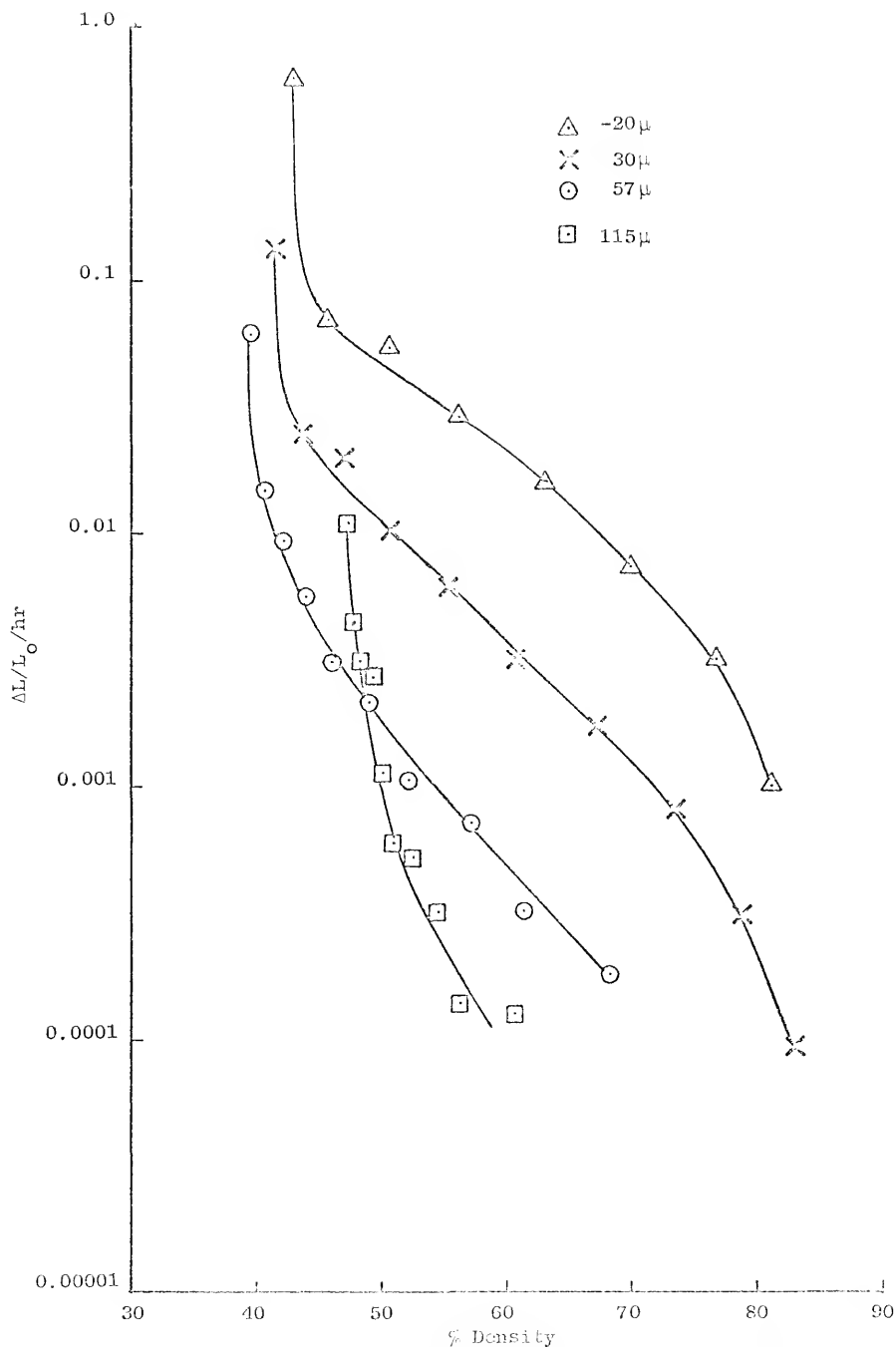


Figure 12. Shrinkage rates of -20μ , 30μ , 57μ , and 115μ nickel powder specimens at 1250°C.

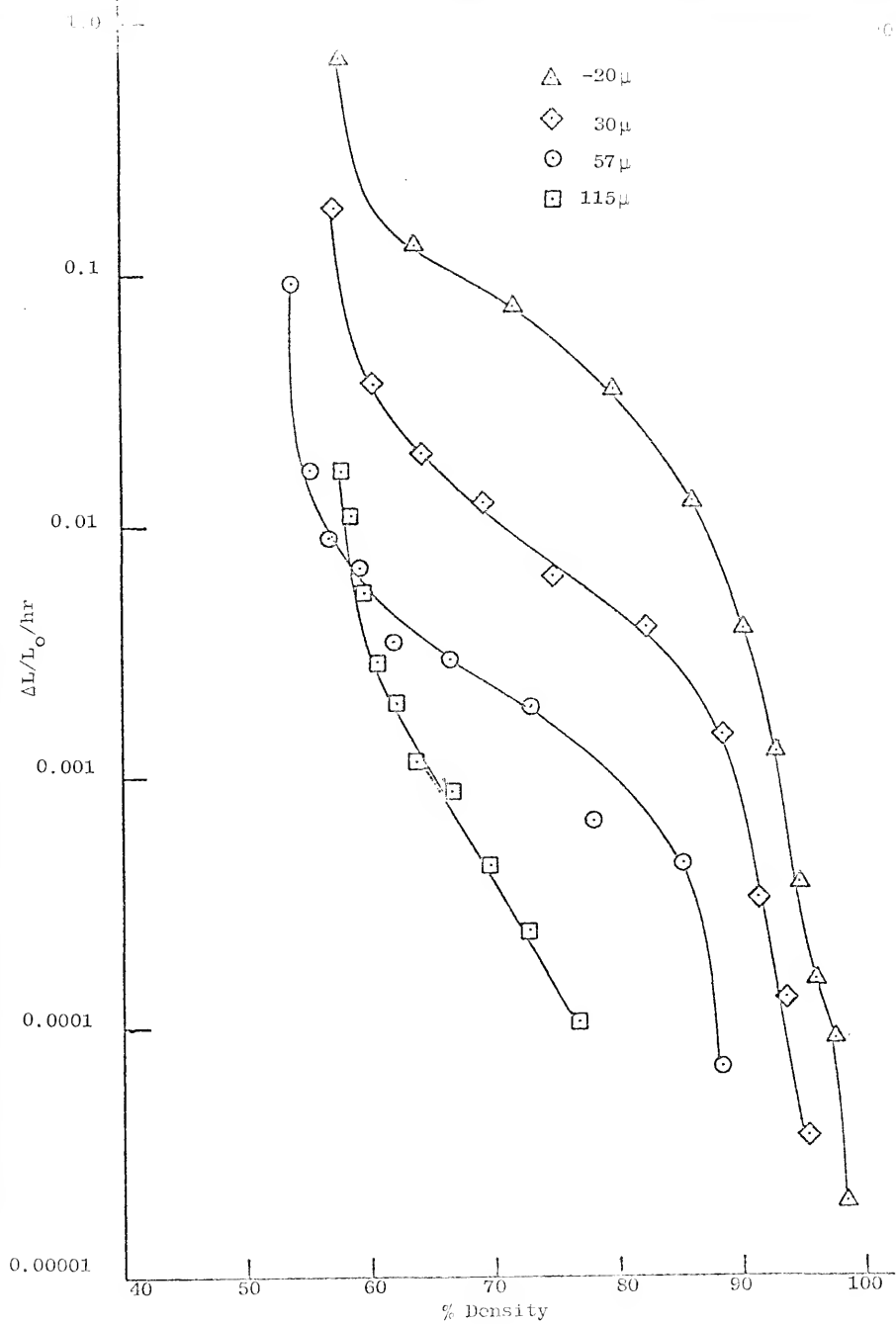


Figure 13. Shrinkage rates $\Delta L/L_0/hr$ for -20μ , 30μ , 57μ and 115μ nickel powders at $1350^\circ C$.

Table 2. Loose stack densification data for -20μ , 30μ , 57μ , and 115μ nickel powders at 1100°C , 1250°C , 1350°C and the corresponding calculated incremental average shrinkage rates.

Particle Size, Temp. Total			time (hrs) = t				
Loose Stack, ρ_o (%)			.25	.5	1	2	4
-20μ	1100°C	% ρ after t	52.5	54.67	57.75	59.7	64.58
$\rho_o = 31.5\%$		$\Delta L/L_o/\text{hr}$.626	.0536	.0362	.011	.0129
-20μ	1250°C	% ρ after t	53.04	55.91	60.73	66.31	73.04
$\rho_o = 31.5\%$		$\Delta L/L_o/\text{hr}$.637	.0696	.0544	.0289	.0159
-20μ	1350°C	% ρ after t	57.88	63.8	71.6	79.7	86.00
$\rho_o = 31.5\%$		$\Delta L/L_o/\text{hr}$.734	.128	.0754	.0351	.0125
30μ	1100°C	% ρ after t		47.5	50.24	52.12	54.63
$\rho_o = 42.5\%$		$\Delta L/L_o/\text{hr}$.0728	.0370	.0122	.00778
30μ	1250°C	% ρ after t		51.75	53.72	57.08	60.73
$\rho_o = 42.2\%$		$\Delta L/L_o/\text{hr}$.1315	.0248	.0200	.0102
30μ	1350°C	% ρ after t		57.31	60.53	64.20	69.24
$\rho_o = 42.7\%$		$\Delta L/L_o/\text{hr}$.187	.0361	.0194	.0124
57μ	1100°C	% ρ after t		47.3	48.56	49.62	51.01
$\rho_o = 45.33\%$		$\Delta L/L_o/\text{hr}$.0282	.0174	.00717	.00458
57μ	1250°C	% ρ after t		49.68	50.81	52.27	54.10
$\rho_o = 45.2\%$		$\Delta L/L_o/\text{hr}$.0620	.0149	.00940	.00570
57μ	1350°C	% ρ after t		53.88	55.25	56.76	59.12
$\rho_o = 46.6\%$		$\Delta L/L_o/\text{hr}$.0945	.0167	.00895	.00675
115μ	1100°C	% ρ after t		57.0	57.0	57.22	57.90
$\rho_o = 56.32\%$		$\Delta L/L_o/\text{hr}$.00798	0	.00128	.00197
115μ	1250°C	% ρ after t		57.45	57.84	58.39	59.36
$\rho_o = 56.5\%$		$\Delta L/L_o/\text{hr}$.0111	.00451	.0315	.00274
115μ	1350°C	% ρ after t		57.71	58.67	59.64	60.68
$\rho_o = 56.3\%$		$\Delta L/L_o/\text{hr}$.0164	.011	.00545	.00287

Table 2 (Extended)

8	16	32	64	128	256	294
70.13	76.78	83.07	89.08	92.77	95.18	
.00678	.00361	.00164	.000719	.00021	.0000665	
	+ .5 hr	- .5 hr		+ 3 hr		
79.96	86.79	91.07	94.11	96.11	97.25	
.00743	.00317	.00103	.000335	.000104	.0000314	
90.13	92.88	94.58	95.98	97.67	98.43	
.00388	.00125	.000377	.000153	.0000906	.00002	
56.63	61.12	66.15	72.71	80.18		82.23
.00298	.00314	.00163	.00097	.000501		.0000501
65.43	70.93	77.17	83.51	88.73		92.96
.00614	.00332	.00173	.000812	.000313		.0000928
74.72	82.28	88.33	91.24	93.59		95.32
.00627	.00395	.00147	.00033	.000132		.0000367
52.01	54.06	56.61	59.91	63.33		66.36
.00161	.00160	.000953	.000585	.000366		.0000621
56.15	59.17	62.33	67.2	71.53		78.39
.00308	.00216	.00107	.000774	.000322		.000181
62.00	66.55	73.05	77.96	85.22		88.22
.00393	.00292	.00191	.00067	.000457		.000104
58.21	58.81	59.57	61.45	63.42		64.97
.00445	.000427	.000267	.000322	.000163		.0000483
60.17	61.04	62.61	64.56	66.34		70.74
.00113	.000597	.000527	.000318	.000141		.000128
62.11	63.87	66.64	69.58	72.91		76.83
.00193	.00116	.000878	.000446	.000242		.000104

increase the relative importance of sintering with respect to that of creep will increase that portion of the measured strain which is attributable to sintering and vice versa. For example, at a given temperature and compressive strain rate, a sample of lower density and lower load would have a greater portion of its strain attributable to sintering than one of higher density and higher load.

The densification rates are entirely consistent, with the finest nickel powder sintering faster than the coarser powder at each density and temperature level. It can easily be seen that the shrinkage rates due to loose stack sintering would be lower for temperatures lower than those in Table 2 and for densities higher than those in the table. Densification rates for all powders fit the following equation:

$$P = \exp - \left[a(D_0)^{-n} e^{-Q/RT} (t)^n \right] \quad (3)$$

where P is a porosity parameter equal to V_V/V_{V_0} , where V_V is the porosity at time (t), and V_{V_0} is the loose stack porosity, D_0 is the starting particle size microns, $T = ^\circ K$, $t = \text{time (hrs)}$, R is the gas constant, 1.987 cal/mole $^\circ K$, $a = 1550$, $n = 1$, $Q = 16,200$ cal/mole, and $m = 0.4$. The -20 μ powder had an effective D_0 of 11 μ .

3.2 Calibrate ΔL in Creep as a Function of Particle Size, Density, Load, Temperature, and Time

The main thrust of the experimental creep work has been the characterization of the effects of the different conditions of creep testing. There were systematic series of creep tests run to separate

the effects of particle size, density, temperature, and load on creep rates and total creep. The data obtained were curve fitted to an Andrade type equation.

$$\epsilon = \epsilon_0 + at^n \quad (4)$$

The exponent of time, n , varied with stress as did ϵ_0 and a . These "constants" were plotted as a function of stress on the minimum sample cross section (σA_{Af}), for samples of the 115 μ particle size crept at 1100°C. From the functional dependence of these constants, ϵ_0 , a , and n , one can then write an equation that models creep of the 115 μ particle size samples as a function of stress at 1100°C. This equation is:

$$\epsilon = \left(\frac{\sigma A_{Af}}{4000} \right)^{1.42} + \left(\frac{\sigma A_{Af}}{2350} \right)^{2.146} (t) \left(\frac{\sigma A_{Af}}{100} \right)^{-0.246} \quad (5)$$

Creep data on all samples used in this research are given in Table 3.

A basic assumption has been made in the tests that were undertaken to model the effects of temperature, load, and density. This assumption was that the densification effect of sintering is negligible. This means that the dimensional change in a creep sample caused by loose stack sintering densification during a test was small enough to be ignored. To this end, the largest size fraction of powder was used in most experiments, with the choice of the other conditions to be held constant selected accordingly.

Table 3. Creep data containing before and after densitics, loads, temperatures, total creep, total test time, and Andrade constants ϵ_0 , a , and n .

#	Part. Size μ	ρ Before %	Temp. °C	Load P.S.I.	ρ After %	Time (min)	Creep %	ϵ_0	a	n	Fig. #
C21	115	84.6	1100	1000	88.2	300	12.5	1.36	.333	.614	26
C22	115	85.1	1100	500	89.4	1096	5.25	.464	.0074	.957	19
C23	115	84.9	1100	250	82.2	3020	5.12	.16	.0069	.817	20
C24	115	85.7	1100	100	86.0	4050	2.10	.0053	.136	.32	26
C25	115	75.8	1100	1000	79.8	21	15.5	1	3.13	.404	24
C31	115	80.0	1100	500	86.2	534	10.96	.251	.512	.513	-
C32	115	79.8	1100	250	79.4	1770	6.05	.19	.006	.92	20
C33	115	80.2	1100	100	82.9	3450	1.24	.00467	.00313	.77	21
C34	115	64.8	1100	500	70.0	21	16.02	2.54	3.75	.42	19
C36	115	65.2	1100	250	69.2	60	10.36	.225	2.12	.38	20
C37	115	64.7	1100	100	68.8	300	7.82	.864	.247	.59	21
C38	115	64.63	1100	50	68.5	1746	9.28	.162	.124	.58	22
C41	115	69.2	1100	1000	76.4	10	15.32	2.61	4.81	.425	23
C42	115	70.2	1100	100	75.4	1910	6.10	.0093	.0012	.83	21
C43	115	65.57	1100	1000	-	5	19.02	3.98	7.5	.43	22
C44	115	80.2	900	1000	81.17	122	3.74	.8	1.13	.293	15
C17	115	80.3	900	1000	80.95	120	4.72	.105	.99	.32	18
C18	115	69.9	900	1000	74.10	60	6.18	.0027	1.7	.313	18

Table 3 (Continued)

#	Part. Size in	ρ Before %	Temp. °C	Load P.S.I.	ρ After %	Time (min)	Creep %	ϵ_o	a	n	Fig. #
C83	115	84.7	1100	628	85.84	120	1.82	.214	.226	.405	-
C89	115	65.27	1100	167	66.86	120	8.59	0	.65	.54	22
C90	115	64.54	1100	333.8	67.4	120	16.37	.613	1.42	.493	22
C91	115	85.00	1100	1257	85.47	120	8.53	.594	.491	.575	-
C92	115	75.1	1100	375	75.72	120	4.19	.470	.112	.737	24
C93	115	76.1	1100	755	78.43	120	9.05	.361	1.09	.434	24
C94	115	63.63	1100	67.88	65.19	120	5.00	.050	.258	.620	22
C104	115	100	1100	1500	100	120	5.66	-	-	-	40
A45	30	80.4	900	1000	-	120	4.07	0	.335	.529	15
A66	30	80.0	1100	506	80.7	120	6.21	.363	.099	.85	-
A79	30	79.7	1100	500	81.28	120	5.89	.388	.081	.88	14
A82	30	79.6	700	2000	80.01	150	3.73	.625	.247	.501	16
A99	30	100	900	1000	100	1440	1.29	.244	.195	.230	16
D54	57	79.5	900	1000	81.4	120	3.82	.219	.267	.544	15
L81	57	79.5	1100	500	80.69	120	5.50	.272	.125	.78	14
L83	57	79.7	700	2000	80.43	150	3.18	.630	.217	.492	16

Table 3 (Continued)

#	Part. Size μ	ρ Before %	Temp. °C	Load P.S.I.	ρ After %	Time (min)	Creep %	ε ₀	a	n	Fig. #
C49	115	79.7	900	500	81.23	2730	4.19	.186	.009	.47	27
C50	115	80.0	900	2000	87.48	54	8.17	.0075	2.07	.334	27
C53	115	96.4	900	1000	97.35	2880	2.73	.318	.284	.265	18
C55	115	79.9	900	4000	85.02	6	17.23	1.91	10.16	.25	27
C56	115	79.7	1000	1000	85.5	120	7.53	.149	1.55	.326	17
C57	115	80.1	1100	1000	85.3	120	10.53	.416	1.3	.426	17
C58	115	79.9	850	1000	80.4	120	2.92	.368	.482	.35	17
C59	115	79.7	700	1000	80.2	630	2.80	.472	.267	.342	17
C60	115	75.1	900	2000	78.3	120	12.50	.801	2.83	.293	-
C62	115	75.1	900	2000	79.2	60	10.1	.761	2.97	.277	-
C64	115	100	900	1000	100	1410	2.07	.006	.550	.180	15b
C70	115	80.0	700	2000	80.1	150	2.94	.929	.303	.375	16
C74	115	74.94	1100	250	76.13	450	5.48	.586	.0095	.645	20
C75	115	70.6	1100	250	74.09	420	8.68	.251	.388	.322	-
C76	115	70.05	1100	500	74.96	180	12.23	.67	1.71	.432	19
C77	115	74.6	1100	500	77.92	180	9.23	.108	1.3	.376	19
C80	115	79.9	1100	500	82.77	120	4.71	.251	.387	.512	14
C81	115	80.3	700	2000	83.61	150	2.68	.445	.236	.459	16c
C86	115	66.4	1100	25	65.798	540	.977	0	.0078	.768	22
C87	115	70.02	1100	250	70.99	360	8.64	0	.469	.498	20

Table 3 (Continued)

\pm	Part. Size μ	σ Before %	Temp. °C	Load P.S.I.	σ After %	Time (min)	Creep %	ϵ_o	α	n	Fig. #
-20 ₀	93	-20	80.29	1100	87.09	120	18.4	.171	.528	.745	-
-20 ₀	96	-20	80.43	900	83.1	120	7.1	.115	.104	.88	15
-20 ₀	97	-20	79.59	700	80.37	120	4.71	.73	.079	.82	16a
-20 ₀	98	-20	80.0	1100	85.34	120	13.05	.252	.315	.777	14
-20 ₀	102	-20	100	1000	100	1440	.59	.1	.128	.185	16b
-20 ₀	105	-20	60.17	1100	79.98	10	18.05	-	-	-	40
-20 ₀	106	-20	70.47	1100	77.72	60	17.58	-	-	-	40
-20 ₀	108	-20	79.5	1100	84.66	120	15.22	-	-	-	40
-20 ₀	109	-20	100	1300	100	120	5.0	-	-	-	40

3.2.1 Particle Size Effect

There were four particle sizes tested under creep conditions. They were: -20μ , $-400 \pm 500(30\mu)$, $-230 \pm 270(57\mu)$, and $-120 \pm 140(115\mu)$. Comparisons of the creep of the three particle sizes were run at three different load-temperature combinations, 1100°C and 500 P.S.I., 900°C and 1000 P.S.I., and 700°C and 2000 P.S.I. The results of these twelve tests may be seen in Figures 14 to 16a. For these tests, all samples started at 80% dense. In all cases, the finer the powder from which the sample was made, the greater the percent creep at the end of the two-hour creep tests. The wide difference in the amount of creep cannot be explained from shrinkage due to loose stack sintering densification. Samples of the various powders at 100% relative density showed that the finer the starting powder, the lower the creep rate. This effect at 100% density is due to the purity of the nickel powder decreasing with decreasing particle size, Figure 16b and Table 1.

3.2.2 Temperature Effect

The temperature effect on creep was studied in a series of 80% dense, 115μ samples under a load of 1000 P.S.I. The creep curves for these five samples may be seen in Figure 17. The results are as expected, with total creep and creep rate increasing with increasing temperature.

3.2.3 Effect of Starting Density

The effect of starting density on creep rate was predictable with total creep and creep rate increasing with a decrease in density

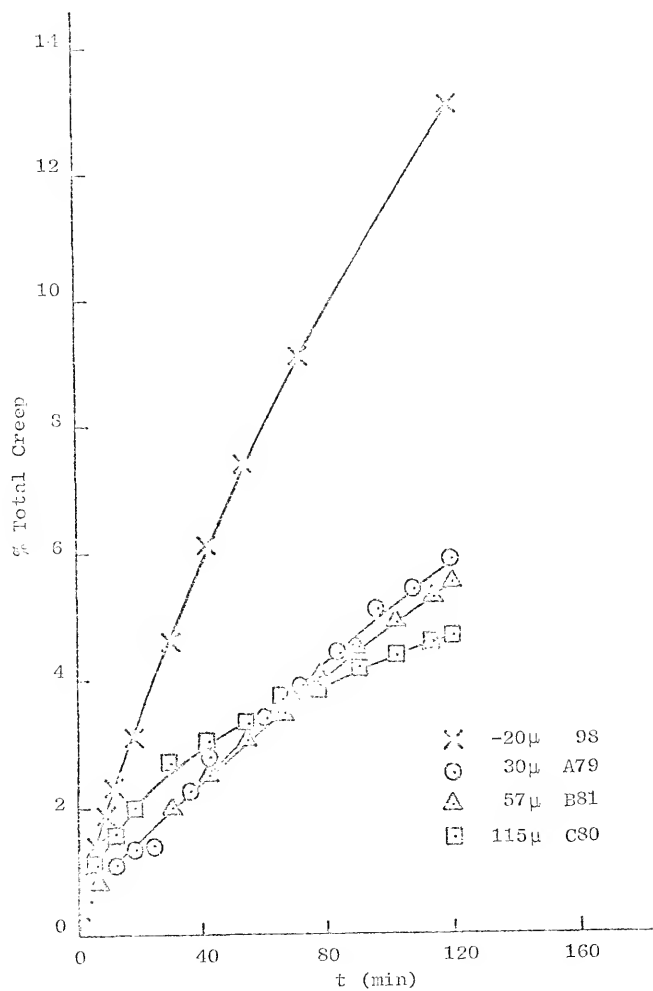


Figure 14. The creep of 80% dense nickel samples of four different size fractions versus time at 1100°C and 500 P.S.I.

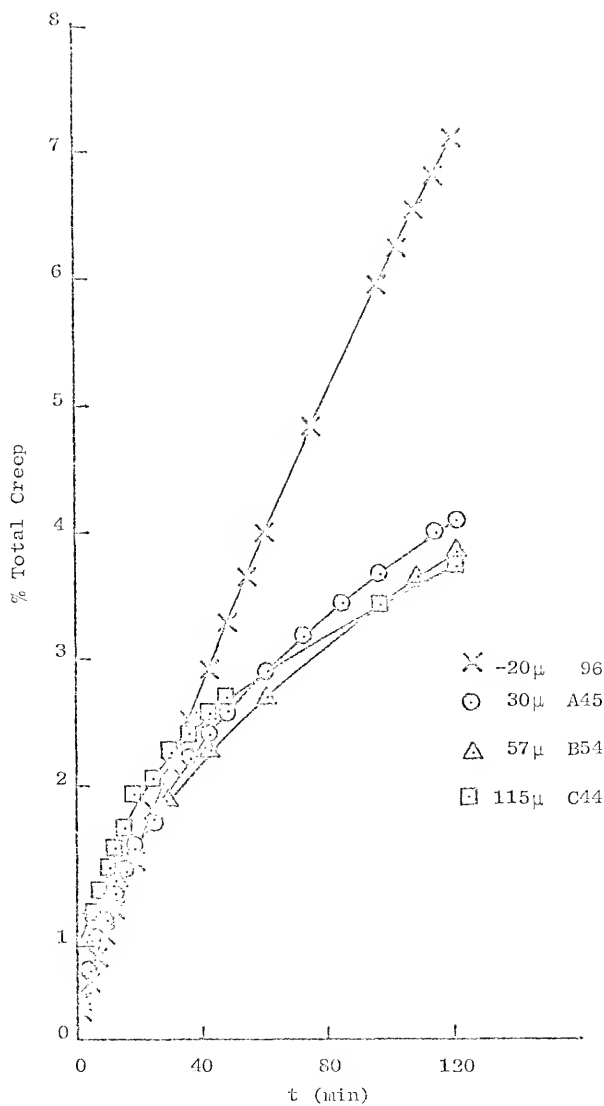


Figure 15. The creep of 80% dense nickel samples of four different size fractions versus time at 900°C and 1000 P.S.I.

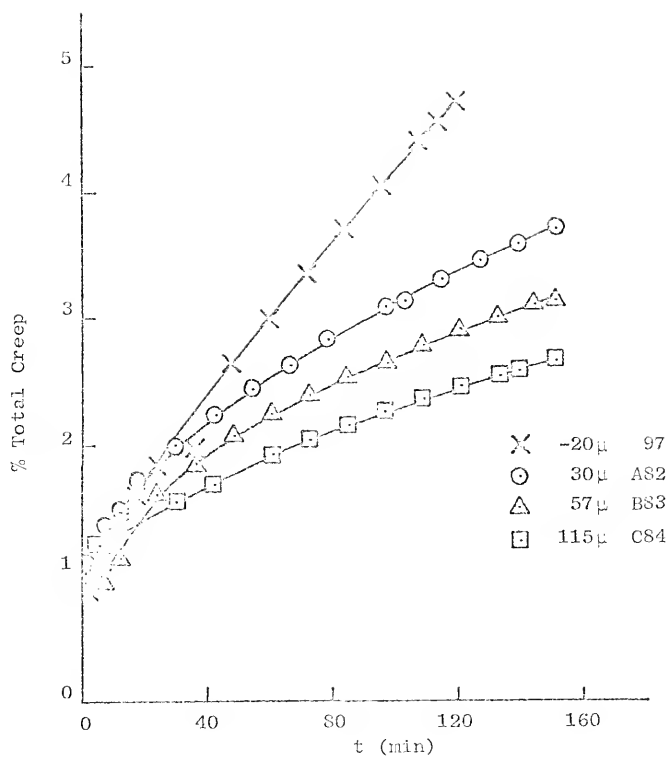


Figure 16a. The creep of 80% dense nickel samples of four different size fractions versus time at 700°C and 2000 P.S.I.

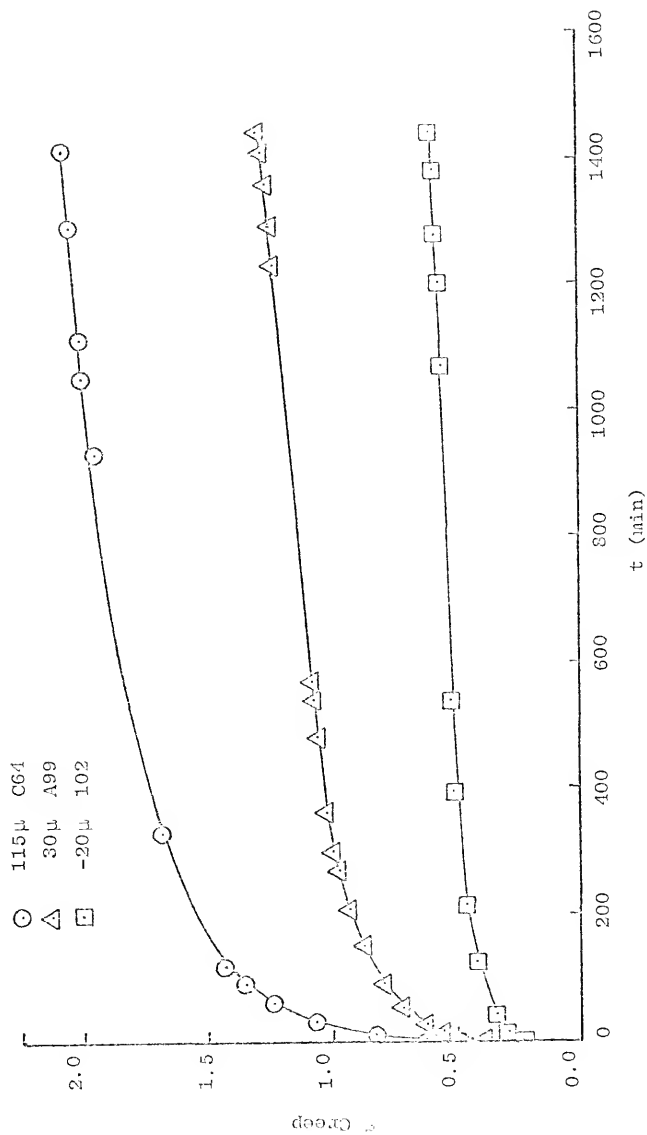


Figure 16b. Creep curves of 100% dense samples made from -20μ, 30μ, and 115μ particle size fractions at 1000 P.S.I. and 900°C.

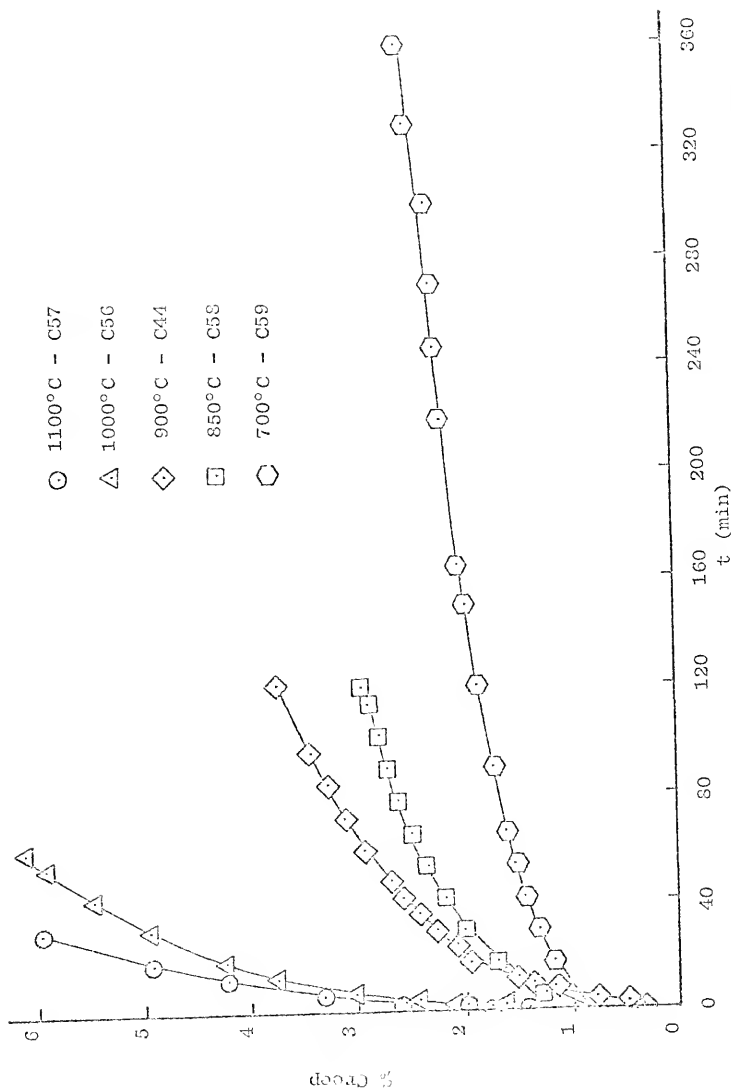


Figure 17. The dependence of the creep of 80% dense 115 μ particle size samples on temperature at a constant load of 1000 p.s.i.

for a set temperature and load. Figures 18 to 21 show the results of varying the density of samples while holding particle size, temperature, and load constant.

3.2.4 Stress Effect

The creep rate of sintered nickel increases with an increasing stress. Figures 22 to 27 show the results of creep experiments over a wide range of loads and densities at two temperatures. In each series, the temperature, density, and particle size were held constant.

3.3 The Quantitative Microscopy of Sintered Nickel Creep Samples

Quantitative microscopy has been established as a useful tool for the description of microstructures. In the course of this work, quantitative microscopic measurements were taken as a means for understanding microstructural changes that occurred when a porous body underwent creep.

3.3.1 Quantitative Microscopy on Polished Surfaces

The quantitative microscopic measurements were first taken on samples in the as sintered state for use as controls, then on samples which had undergone creep testing. The quantitative metallographic data taken on polished sections of loose stack sintered samples and crept samples may be found in Table 4. A plot of S_v versus porosity is given in Figure 28 for 30μ , 57μ , and 115μ loose stack sintered samples. On crept samples, quantitative metallography data were taken in two directions, one parallel to the creep direction and one

Table 4. Quantitative microscopy data on polished sections.
Creep Samples

#	Part. Size μ	Temp. °C	Load P.S.I.	ρ before 3 gm/cm ³	ρ after 3 gm/cm ³	Creep %	S_V
C21	115	1100	1000	7.54	7.85	12.5	128.16 144.4
C22	115	1100	500	7.58	7.96	5.25	121.53 123.20
C25	115	1100	1000	6.76	7.10	15.5	213.57 232.30
C26	115	1100	500	6.71	7.12	13.37	191.28 204.32
C30	115	1100	1000	7.13	7.78	13.09	128.55 160.24
C31	115	1100	500	7.13	7.68	10.96	157.46 177.34
C39	115	1100	500	6.24	6.95	13.4	210.72 224.52
C40	115	1100	250	6.23	6.84	12.05	227.70 231.62
C41	115	1100	1000	6.21	6.81	15.32	249.44 262.44
C47	115	900	1000	7.15	7.21	4.72	165.10 173.08
C48	115	900	1000	6.23	6.60	6.18	241.88 248.60
C49	115	900	500	7.11	7.24	4.19	173.24 178.96
C50	115	900	2000	7.13	7.79	8.17	152.78 180.78

Table 4 (Extended)
Creep Samples

$\Omega S_V = \Omega N_L$	$T_{A_{net}} \times 10^{-3}$	$\Omega T_{A_{net}}$	$M_V \times 10^{-3}$	(\bar{H}/cm)	$\bar{\lambda} \times 10^4$ (cm)
	- 9.48		- 29.8	- 23.24	37.14
.8875	- 9.36	1.013	- 29.21	- 20.37	32.96
	- 9.56		- 30.0	- 24.70	35.10
.9863	- 8.77	1.09	- 27.5	- 22.35	34.63
	- 14.50		- 36.1	- 16.91	38.06
.9193	- 10.86	1.33	- 34.1	- 14.69	34.99
	- 9.32		- 29.3	- 15.31	42.01
.9361	- 9.88	.944	- 31.0	- 15.19	39.33
	- 10.71		- 33.6	- 26.16	39.49
.8022	- 10.43	1.03	- 32.8	- 20.45	31.68
	- 8.18		- 25.7	- 16.32	35.00
.8878	- 10.43	.784	- 32.8	- 18.48	31.15
	- 10.27		- 32.3	- 15.31	41.76
.9385	- 9.05	1.135	- 28.4	- 12.66	39.10
	- 8.10		- 25.4	- 11.17	40.81
.9833	- 7.90	1.025	- 24.8	- 10.72	40.13
	- 7.51		- 23.6	- 9.45	37.80
.9506	- 7.98	.9406	- 25.1	- 9.48	35.93
	- 8.41		- 26.4	- 16.01	46.23
.9538	- 7.38	1.145	- 23.1	- 13.34	44.09
	- 9.13		- 28.7	- 11.85	42.88
.9729	- 10.27	.9729	- 32.3	- 12.98	41.72
	- 7.82		- 24.6	- 14.18	43.29
.968	- 6.99	1.11	- 22.0	- 12.27	41.91
	- 8.69		- 27.3	- 17.93	33.04
.8424	- 9.56	.9091	- 30.0	- 16.61	27.83

Table 4 (Continued)
Creep Samples

#	Part. Size μ	Temp. $^{\circ}\text{C}$	Load P. S. I.	ρ before gm/cm^3	ρ after gm/cm^3	Creep $\%$	S_V
C51	115	900	4000	7.12	7.84	22.14	137.68 174.38
C55	115	900	4000	7.12	7.58	17.23	143.72 172.48
B54	57	900	1000	7.09	7.25	3.82	295.80 306.37
-20 μ 105	-20 μ	1100	292.5	60.17	69.98	18.05	852.88 904.10
-20 μ 108	-20 μ	1100	517.5	7.08	7.54	15.22	504.3 518.3

Table 4 (Extended)
Creep Samples

$\Omega S_V = \Omega N_L$	$T_{A_{net}} \times 10^{-3}$	$\Omega T_{A_{net}}$	$M_V \times 10^{-3}$	\bar{H} (1/cm)	$\bar{\lambda} \times 10^4$ (cm)
	- 12.05		- 37.8	- 27.49	34.89
.7895	- 10.15	1.187	- 31.9	- 18.29	27.55
	- 10.07		- 31.6	- 22.02	34.62
.8332	- 8.57	1.175	- 26.9	- 15.61	34.89
	- 30.42		- 95.6	- 32.31	25.21
.9654	- 28.33	1.074	- 89.0	- 29.05	24.34
	- 689.4		-2165.8	-2524.55	14.02
.9489	- 776.3	.8881	-2438.8	-2697.5	13.31
	- 981.7		-3084.2	-6115.8	12.12
.9230	- 999.5	.9822	-3140.0	-6055.8	11.86

Table 4 (Continued)
Loose Stack Sintered Samples

Part. Size μ	δ $\left(\frac{\text{gm}}{\text{cm}^3}\right)$	V_V Porosity	S_V (cm^{-1})	M_V $(\text{cm}^{-2}) \times 10^{-5}$	\bar{H} (cm^{-1})	$\bar{\lambda}$ (cm)
30	7.81	.104	293	- 2.62	-894	.0014
	7.23	.158	556	- 2.05	-369	.0011
	6.65	.221	790	- 5.15	-652	.0011
	6.11	.283	923	- 5.44	-589	.0012
	5.35	.354	1230	- 5.84	-475	.0011
	4.96	.397	1370	-12.8	-934	.0011
57	4.85	.462	845	- 4.84	-573	.0021
	5.08	.393	708	- 1.95	-275	.0022
	5.52	.368	701	- 2.84	-405	.0020
	5.98	.322	624	- 2.36	-378	.0020
	7.05	.176	407	- 1.87	-459	.0017
115	5.49	.402	417	- .914	-219	.0038
	5.95	.333	281	- .082	- 29.1	.0047
	6.31	.287	254	- .202	- 79.5	.0045
	7.09	.224	179	- .237	-132	.0050
	7.45	.131	126	- .286	-227	.0042

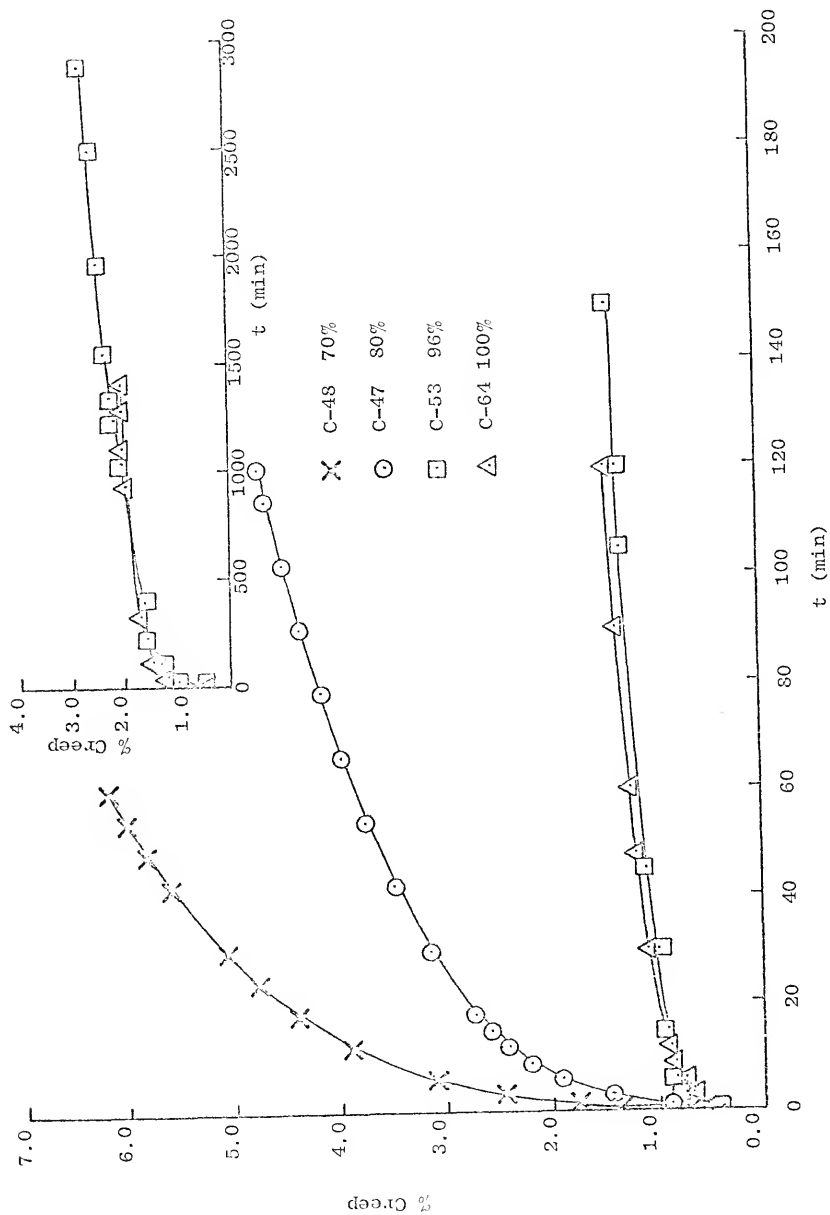


Figure 18. The effect of starting density on creep of samples made of 115μ powder and tested at 900°C and 1000 P.S.I.

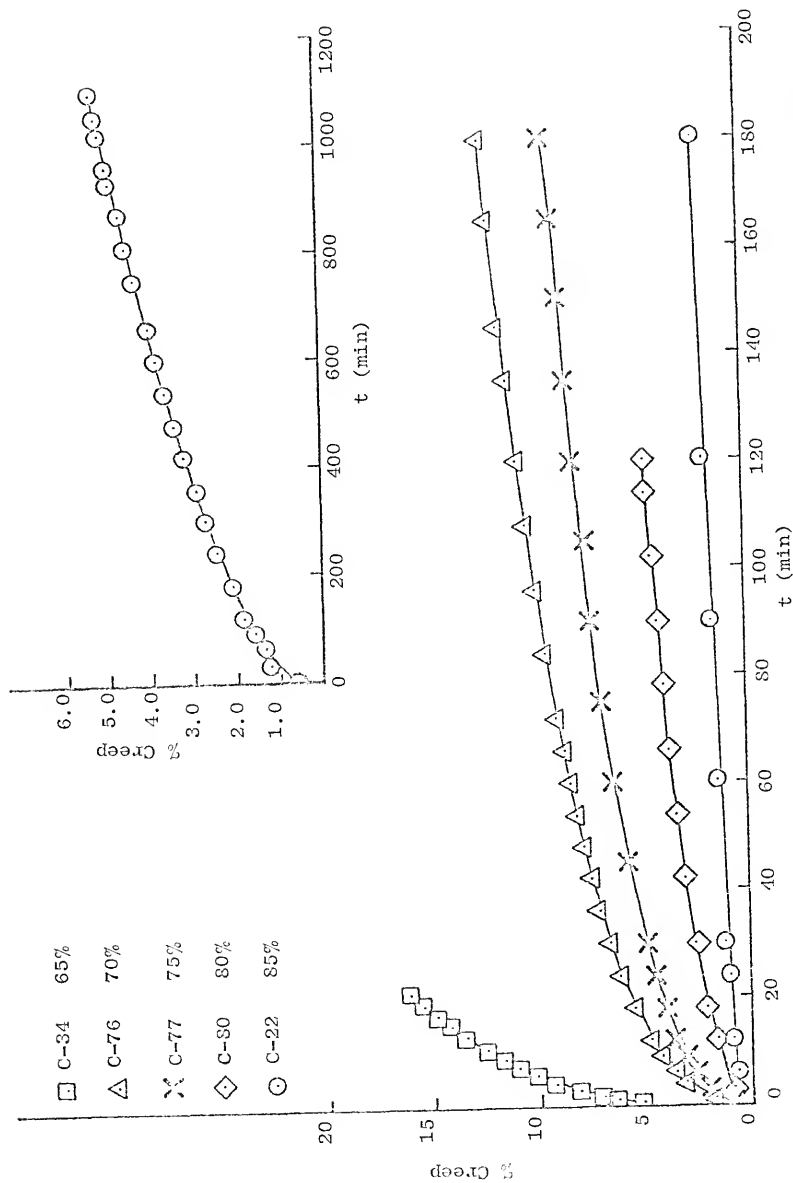


Figure 19. The effect of starting density on creep of samples made from 115 μ powder and tested at 1100°C and 500 P.S.I.

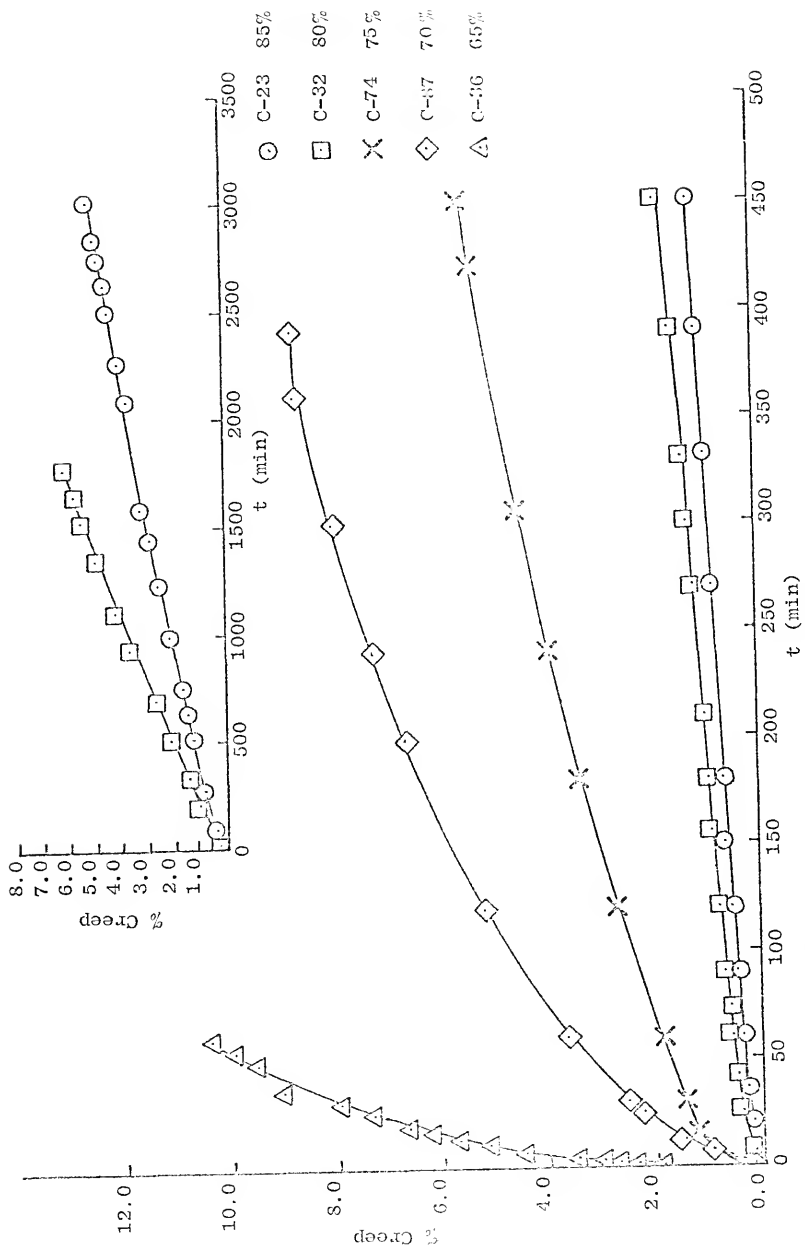


Figure 20. The effect of starting density on creep of samples made from 115μ powder at 1100°C and 250 P.S.I.

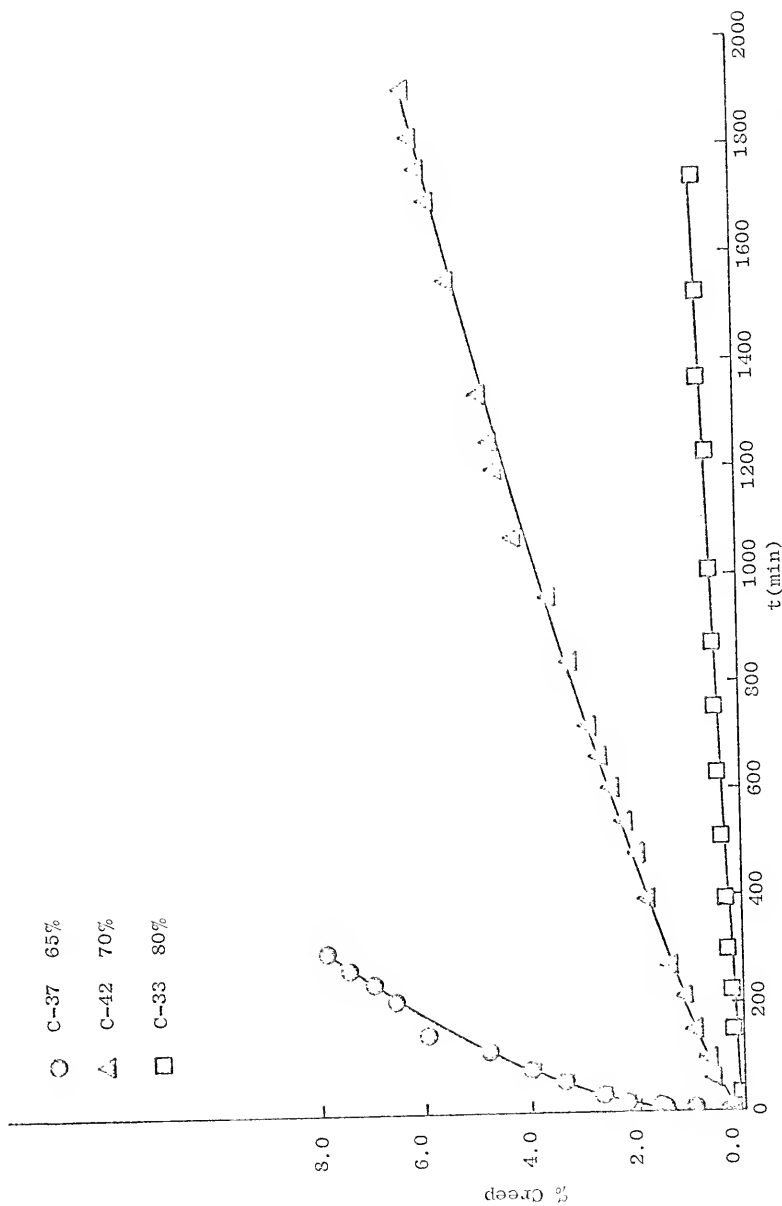


Figure 21. The effect of starting density on creep of samples made from 115μ powder and tested at 1100°C and 100 P.S.I.

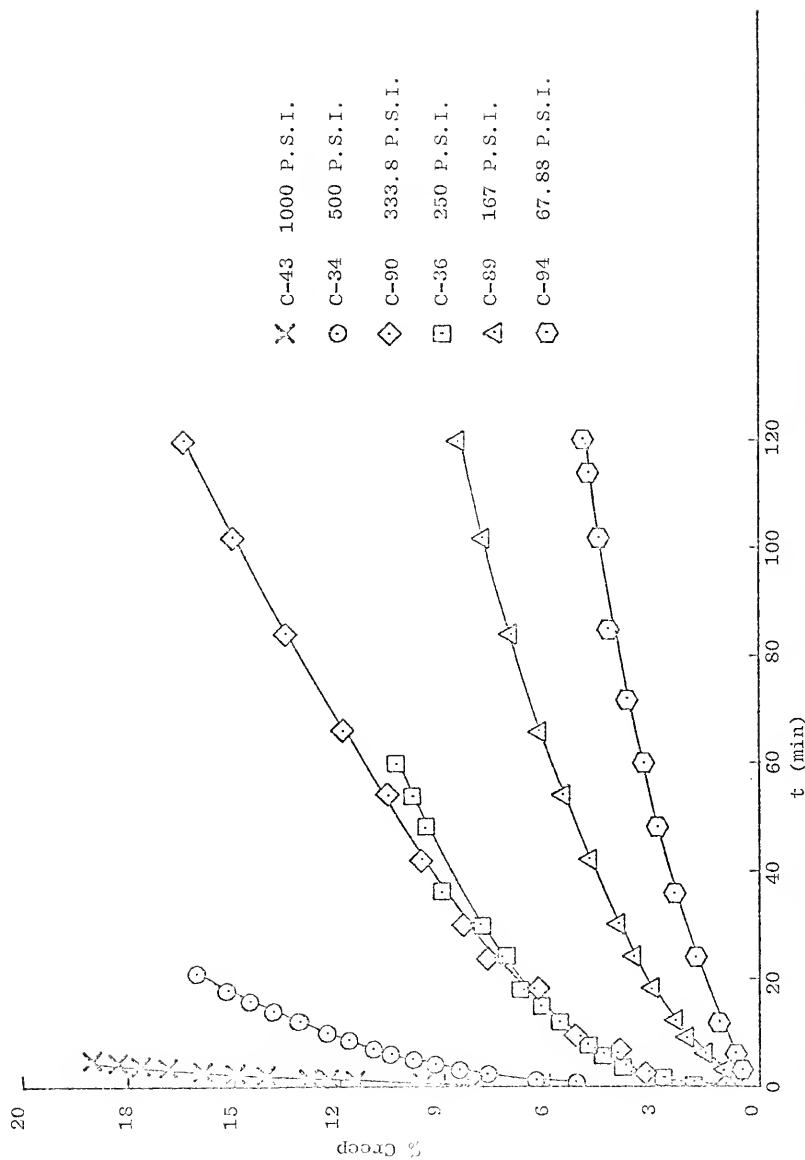


Figure 22a. The effect of stress on 65% dense samples made from 115 μ powder and tested at 1100°C.

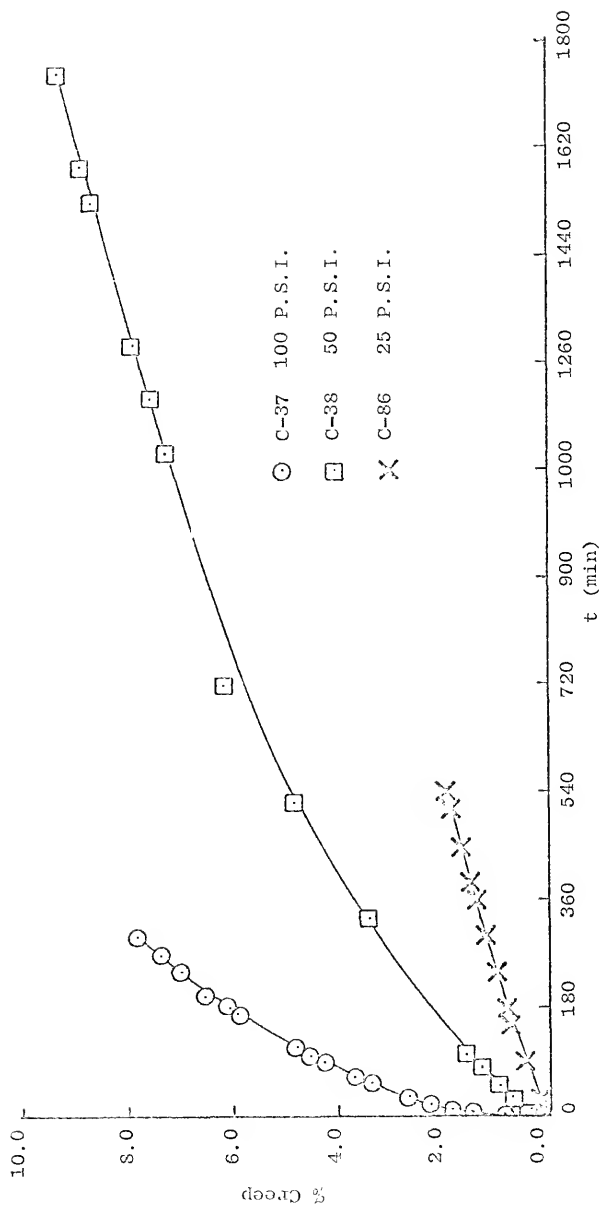


Figure 22b. The effect of stress on 65% dense samples made from 115 μ powder and tested at 1100°C.

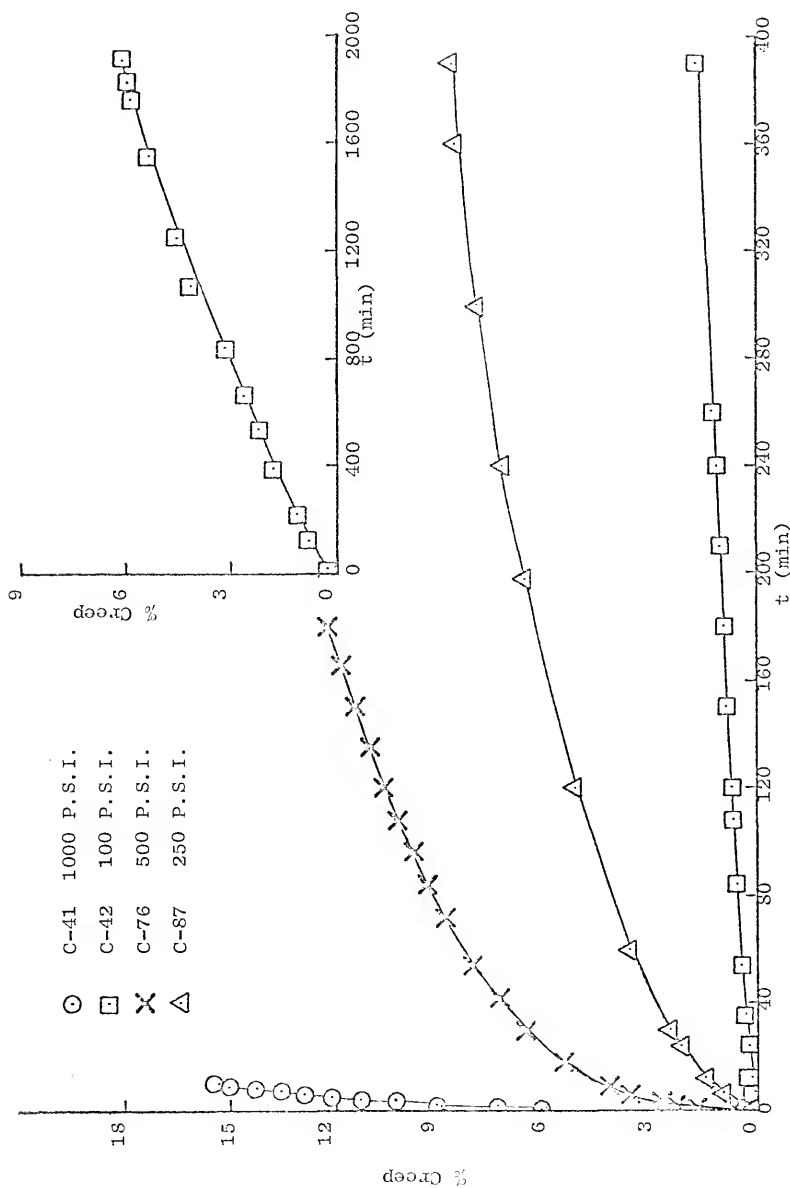


Figure 23. The effect of stress on 70% dense samples made from 115 μ powder and tested at 1100°C.

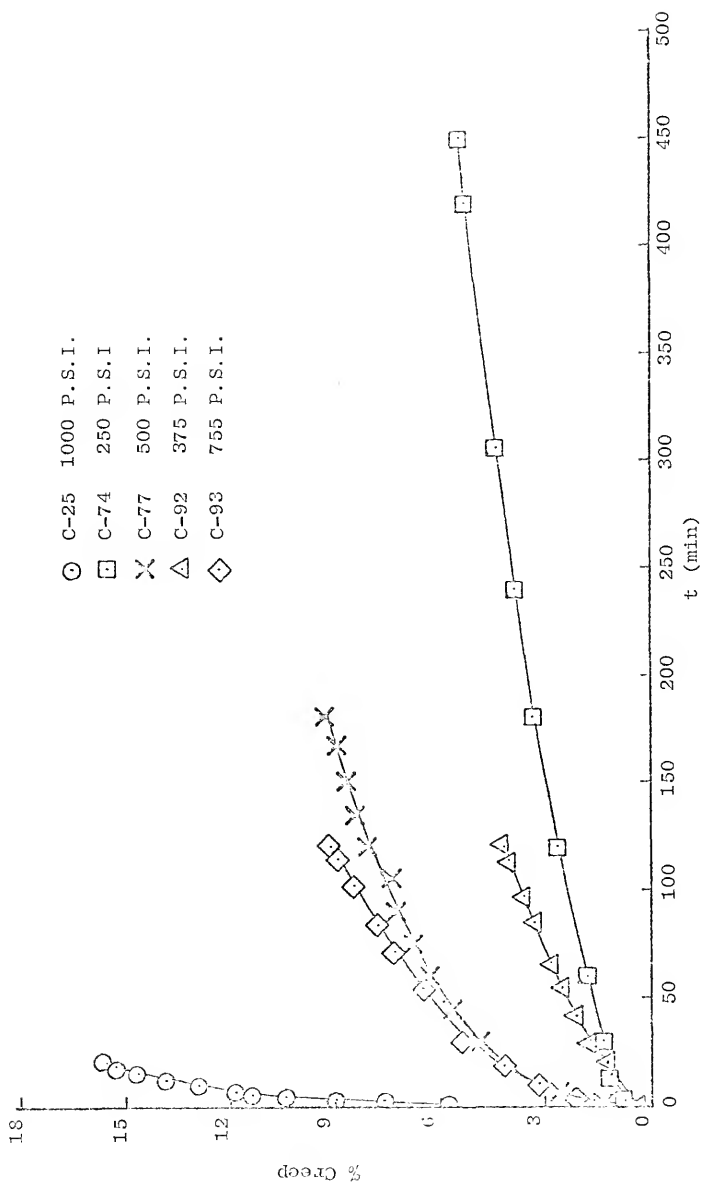


Figure 24. The effect of stress on 75% dense samples made from 115 μ powder tested at 1100°C.

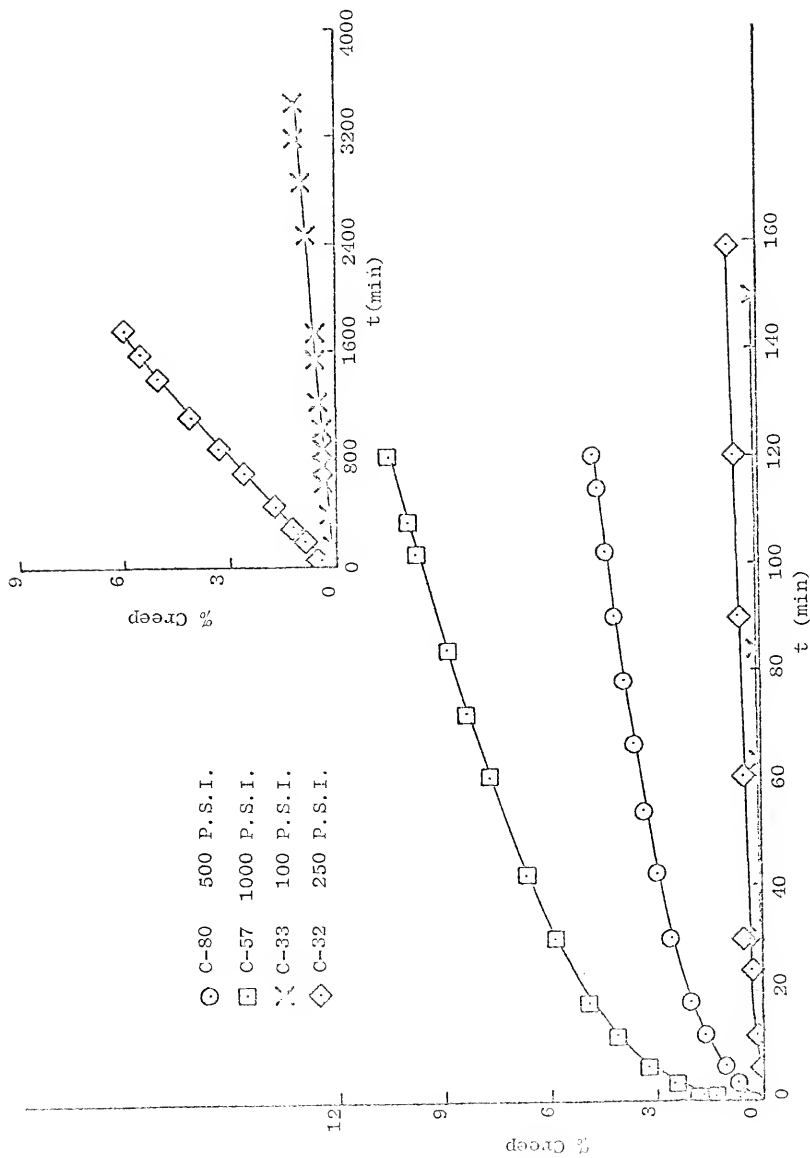


Figure 25. The effect of stress on 80% dense samples made from 115 μ powder tested at 1100°C.

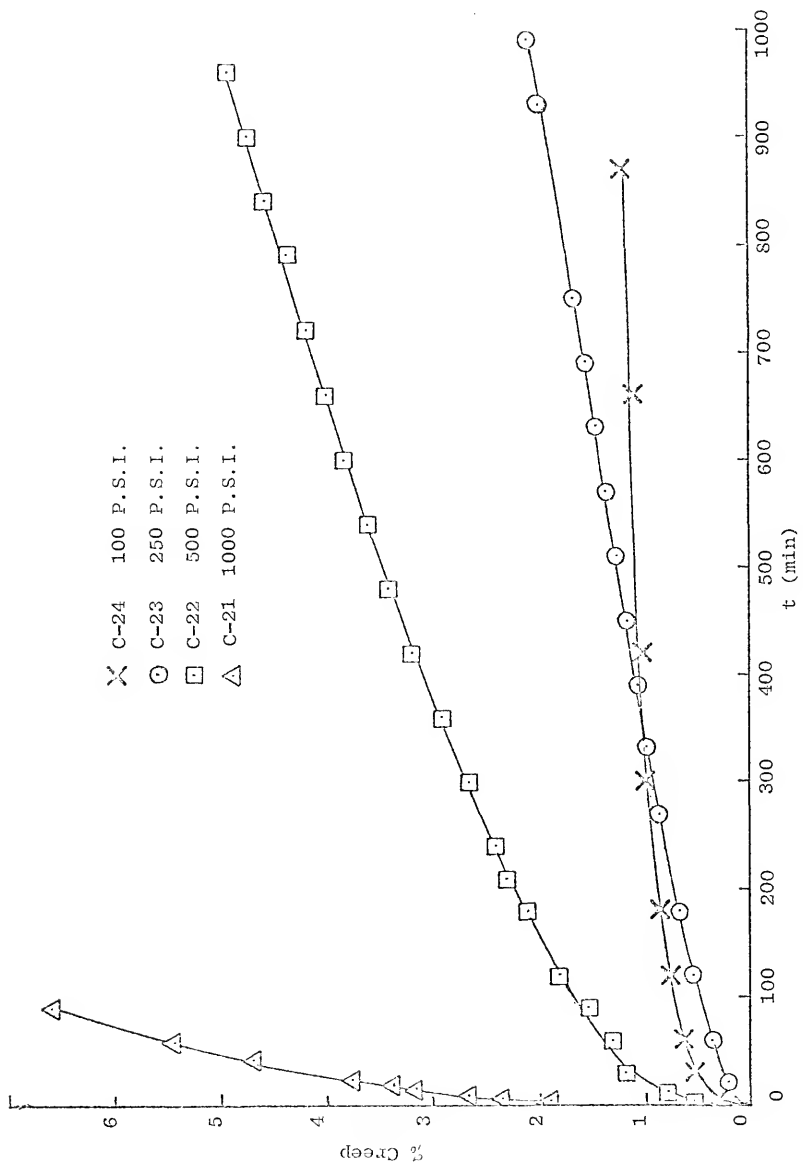


Figure 26. The effect of stress on 85% dense samples made from 115 μ powder and tested at 1100°C.

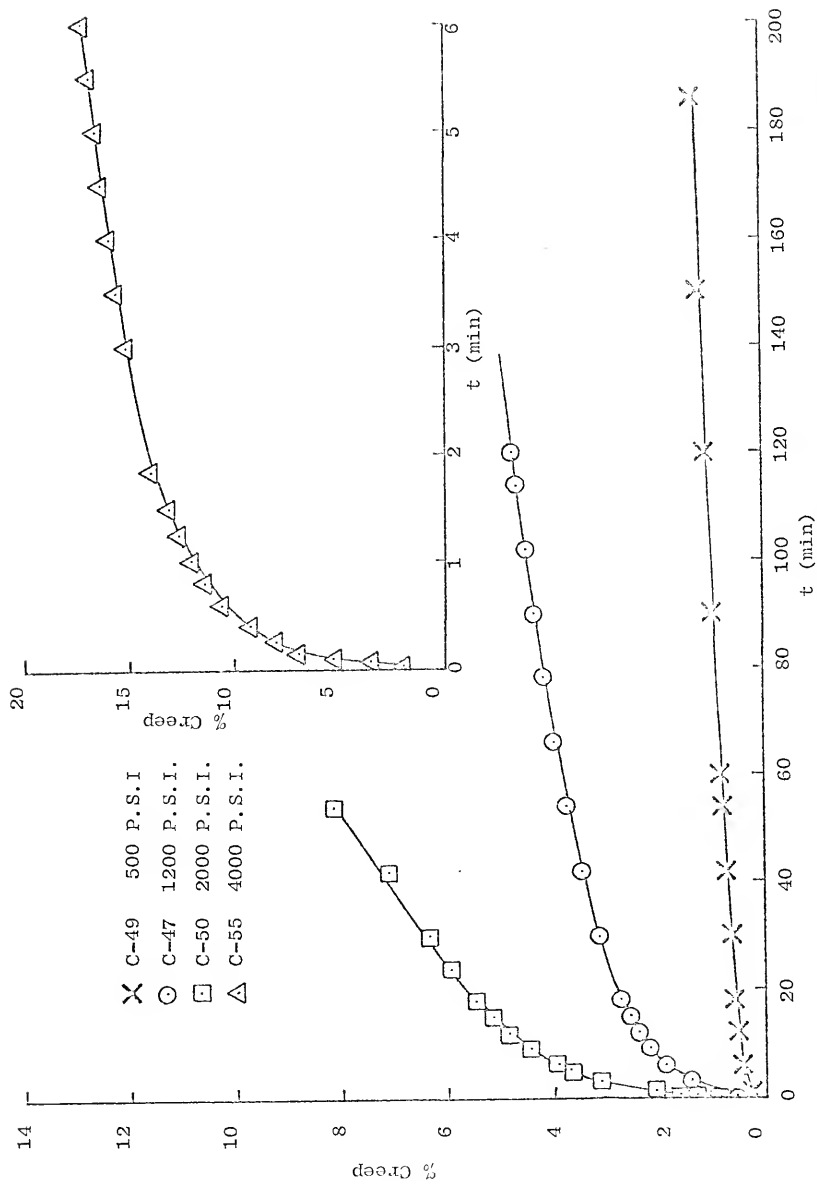


Figure 27. The effect of stress on 80% dense samples made from 115u powder and tested at 900°C.

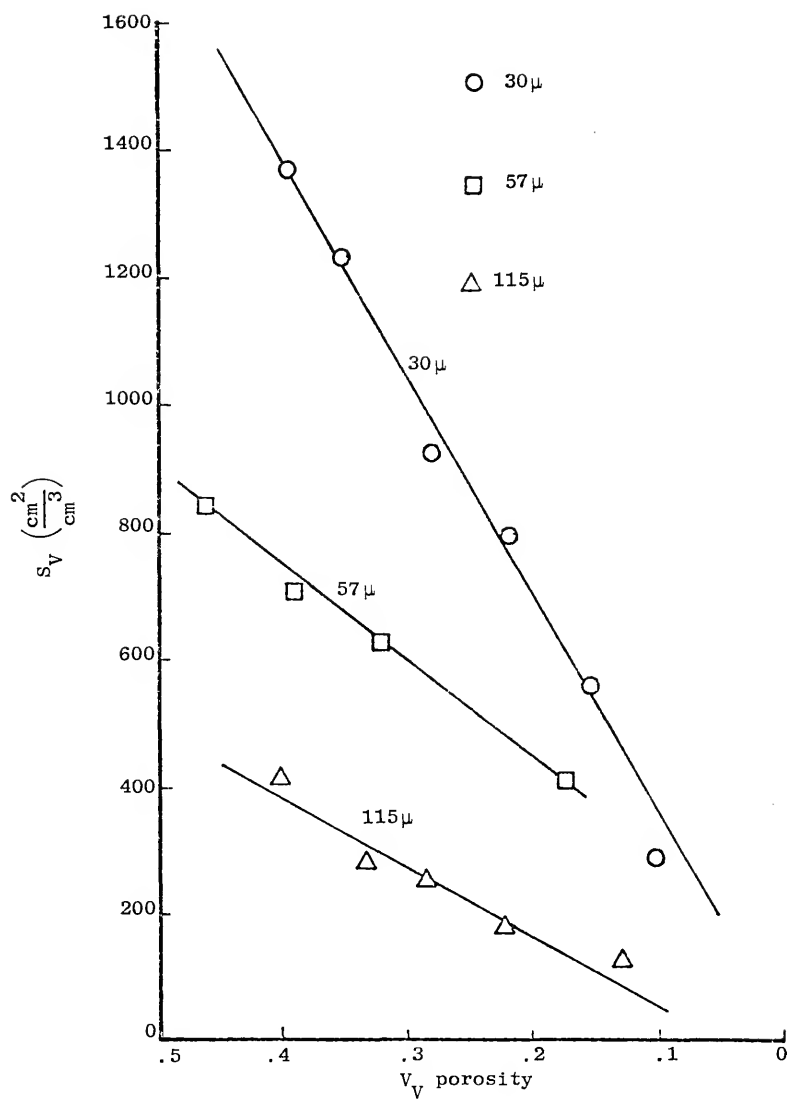


Figure 28. Surface area (S_V) versus volume fraction porosity (V_V) for the 30 μ , 57 μ , and 115 μ nickel powders loose stack sintered to different densities.

perpendicular to the creep direction, rather than randomly as is generally done. This counting in specific directions shows the anisotropy created in the pore structure by creep deformation.

In loose stack sintering, S_V varies linearly with V_V once the conditional minimal surface area has been reached in second stage sintering. The effect of creep in all cases has been to increase S_V relative to the S_V of a loose stack sintered sample which is of the same density as the creep sample after a creep test. This may be seen in Figure 29 where S_V is plotted versus V_V for many crept samples of 115μ powder and all points lie to the high side (surface excess side) of the loose stack sintered line.

An anisotropy factor was defined as

$$a = \frac{\text{Property in perpendicular direction}}{\text{Property in parallel direction}}.$$

The anisotropy of S_V , ΩS_V , is plotted versus percent creep in Figure 30. Anisotropy varied roughly linearly with percent creep in the 30μ nickel samples, but showed much scatter in the 57μ and 115μ samples.

3.3.2 Quantitative Microscopy on Fracture Surfaces

Fractured surfaces of sintered and sintered and crept samples were also amenable to quantification by quantitative metallography. The quantitative metallographic parameters used in the quantification of fracture areas were: A_{Af} , N_{Lf} , and N_{Af} . These quantitative metallographic measurements were taken from irregular internal surfaces which were exposed when the porous samples were fractured. Note must be made that these measurements are not taken from plane polished

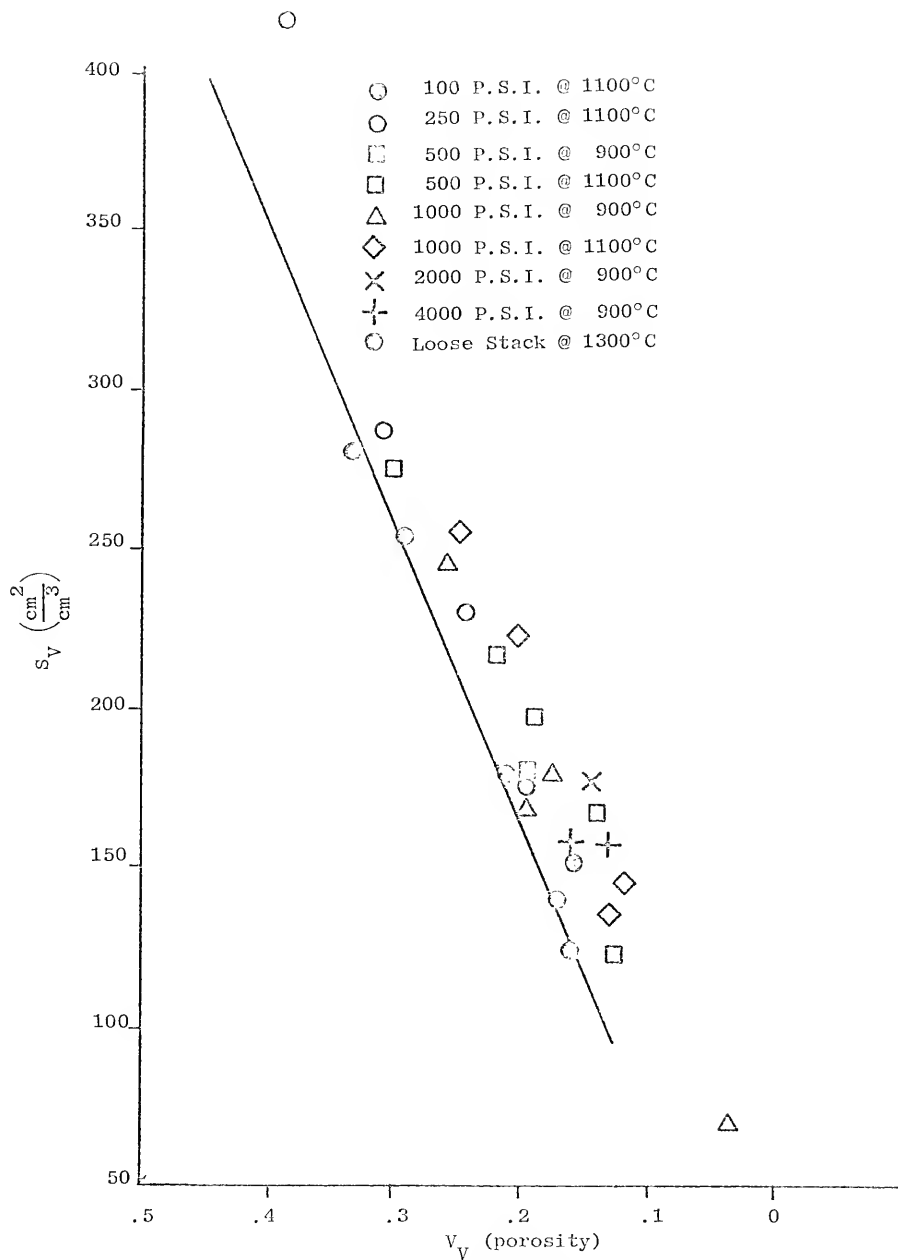


Figure 29. S_V versus V_V for crept 115 μ samples compared to S_V versus V_V for loose stack sintered samples.

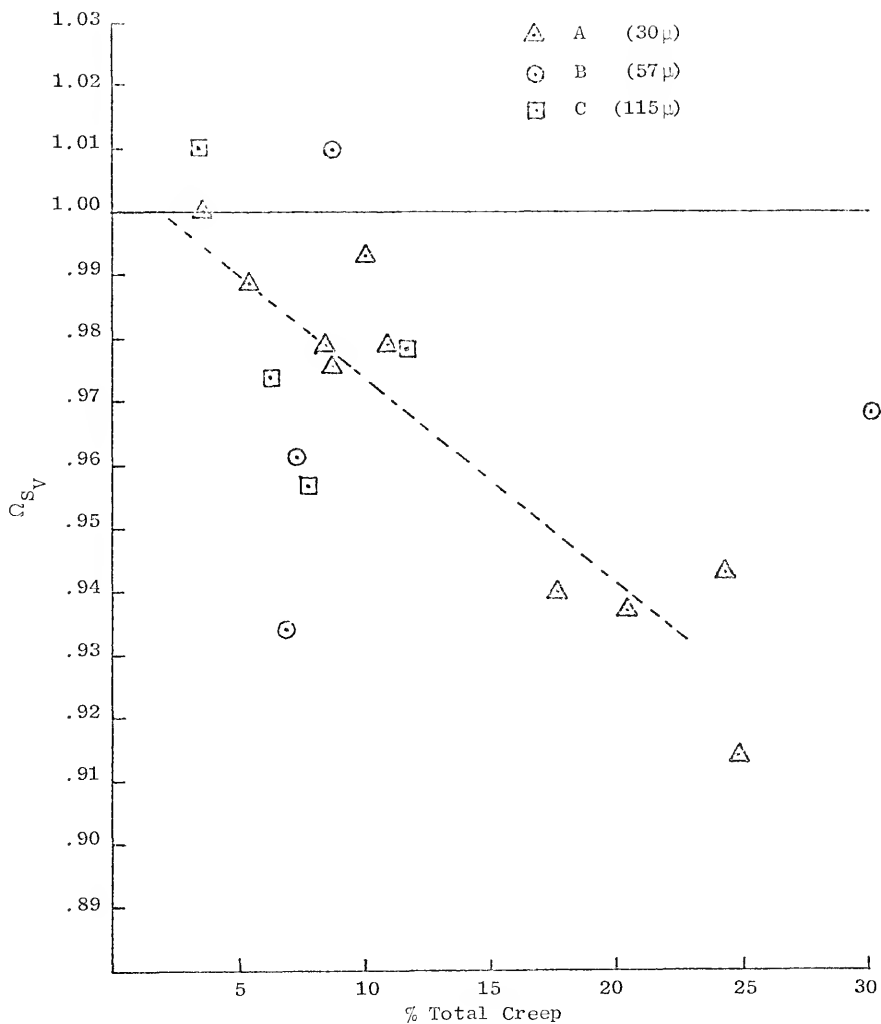


Figure 30. Anisotropy in surface area of crept samples, plotted as a function of the amount of creep. Data include a broad range of sample configurations and test conditions.

surfaces as in most quantitative metallography. The A_{AF} measurement is defined as the area fraction of fractured surface and is simply the fraction of the total projected area occupied by fracture. N_{Lf} is the line intercept count taken on the perimeters of the fractured areas. The N_{Af} count is simply the number of distinct fracture areas recorded per unit area.

A series of four samples, three of which were crept and one control sample, made from 115μ nickel powder were measured for A_{Af} , N_{Lf} , and N_{Af} . All samples were notched and then fractured in the apparatus shown in Figure 31. The notched sample was inserted into the apparatus with the notch toward the bottom. The knife edge was rested against the sample opposite the notch. The apparatus, thus assembled, was then immersed in a container of liquid nitrogen. When the nitrogen boil subsided, the knife edge was struck a sharp blow with a hammer, fracturing the specimen. The fracture mode was completely ductile. A section of the fracture surface was cut out with a jeweler's saw, with care taken not to include any area deformed by the knife edge. These sections were then mounted and inserted into a scanning electron microscope. All counting was done by using a 5×5 grid of points and lines held against the display tube by the tube cover plate.

The A_{Af} , N_{Lf} , and N_{Af} counts on the 115μ samples were taken at 500X magnification. The results of the change in A_{Af} with percent creep are shown in Figure 32. All quantitative metallography data taken on fracture surfaces are in Table 5. The N_{Lf} and N_{Af} counts

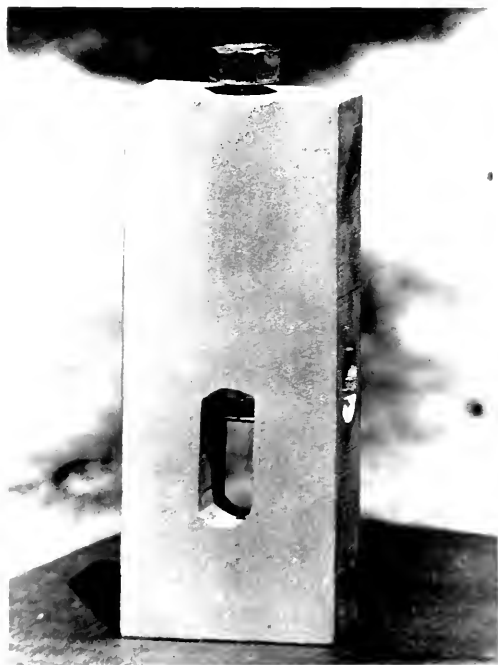


Figure 31. Apparatus used to fracture notched, sintered samples for quantitative metallography of fracture surfaces.

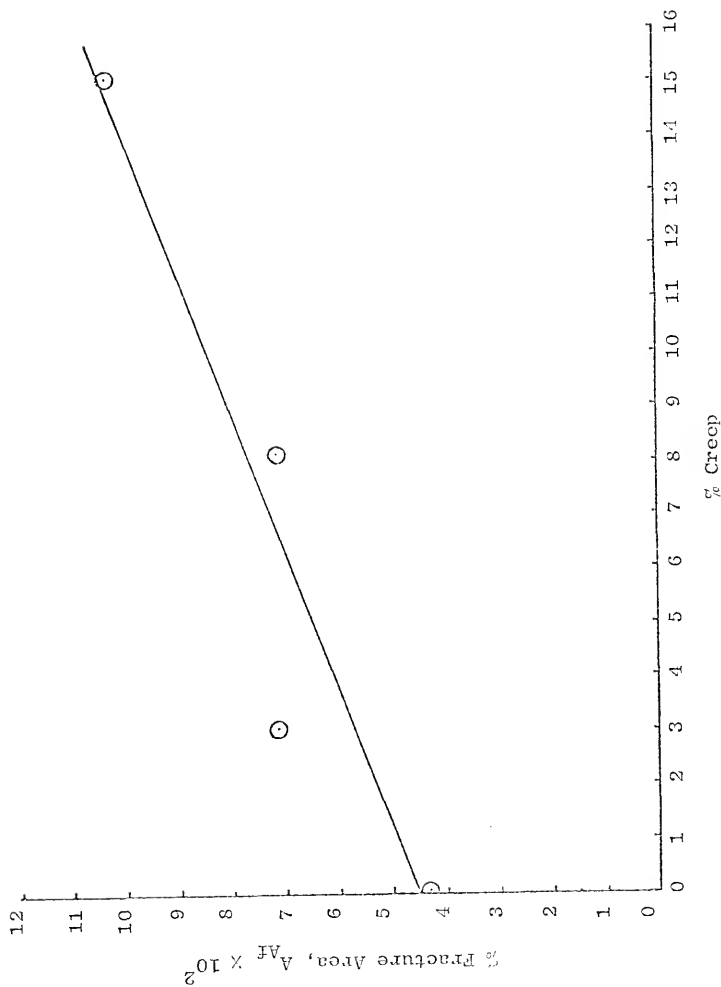


Figure 32. The percent fracture area versus percent creep undergone by 63% dense, 115 μ samples at 700°C.

Table 5. Quantitative metallography of fracture surfaces.

Quantitative microscopy of fractured as sintered samples

Particle Size	ρ %	A_{Af}	Particle Size	ρ %	A_{Af}
115 μ	56.5	0*	30 μ	41.8	0*
"	63.0	.045	"	51.2	.0873
"	70	.1655	"	70.79	.2057
"	75	.25			
"	80	.331			
48 μ	45.5	0*	-20 μ	31.5	0*
"	62.0	.13	"	62.66	.213
"	70.75	.18	"	79.64	.345
"	76.5	.285			

* Loose stack density.

Quantitative metallography of fractured creep samples

Particle Size	% Creep	A_{Af}	N_{Lf}	N_{Af}
115 μ	0	.045	59.75	14.2×10^3
"	3.05	.0713	55.93	12.9×10^3
"	8.17	.0715	65.95	12.5×10^3
"	15.12	.1028	96.07	16.8×10^3

versus percent creep on the fractured areas (Figures 33 and 34) have an initial decrease in value with percent creep, then increase as expected. The initial decrease in N_{Lf} and N_{Af} leading to these minima is attributed to the close proximity of the initial contacts between particles. These multiple contacts derive from the lumpy, blackberry-shape of these nominally spherical surfaces. With small compressive strains, these multiple contacts coalesce, initially decreasing both N_{Lf} and N_{Af} . For smooth spherical powders, the N_{Lf} and N_{Af} measurements on the fractured surfaces would be expected to increase with increasing creep from the outset.

A series of A_{Af} measurements was made on samples made from different size fractions of powder at various densities. Figure 35 shows the results of these A_{Af} measurements plotted versus V_V porosity. The specific A_{Af} values may be found in Table 5. It is clear from these curves that A_{Af} is sensitive to particle shape, i.e., loose stack density, at low densities. The plots of A_{Af} for the different particle sizes converge in the range of 0.3 to 0.2 V_V porosity and are identical from 0.2 to 0.0 V_V porosity. These data were used to calculate the creep loads which would give the same normalized stress on the load bearing areas of two series of 115 μ creep samples. From the results in Figures 36 and 37, the postulate that A_{Af} is a measure of load bearing area is substantiated. Severe distortion of the areas around the fractures made it difficult to distinguish fracture from distorted metal surrounding the fracture at density levels above 80% dense.

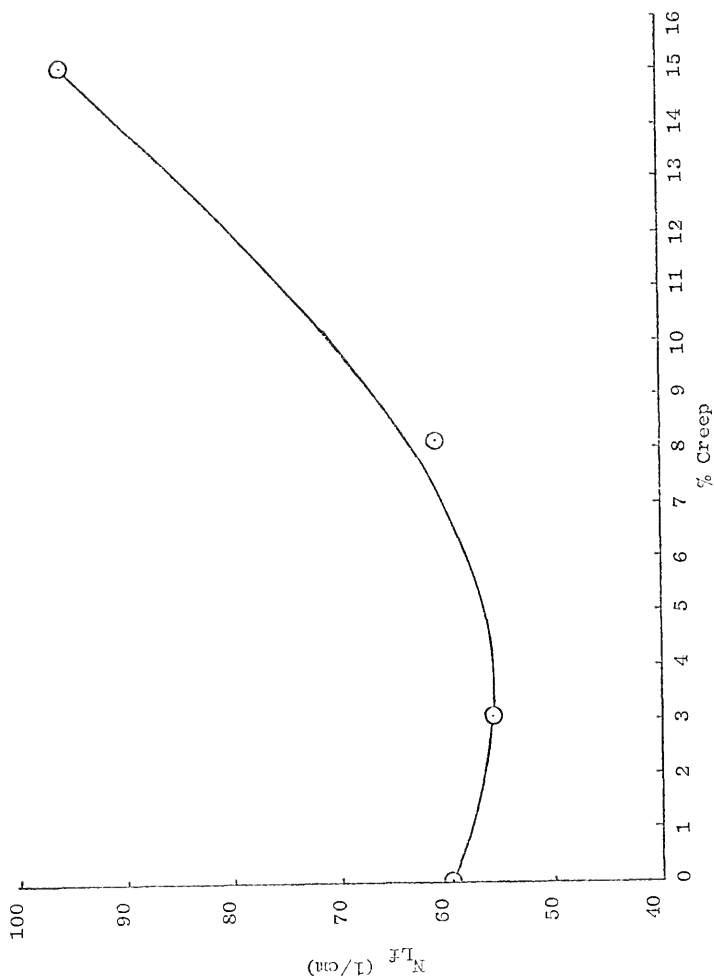


Figure 33. Number of intersections of fracture outline with test probe per unit length of probe, N_{Lf} , plotted against percent creep undergone by 63% dense, 115μ samples at 700°C .

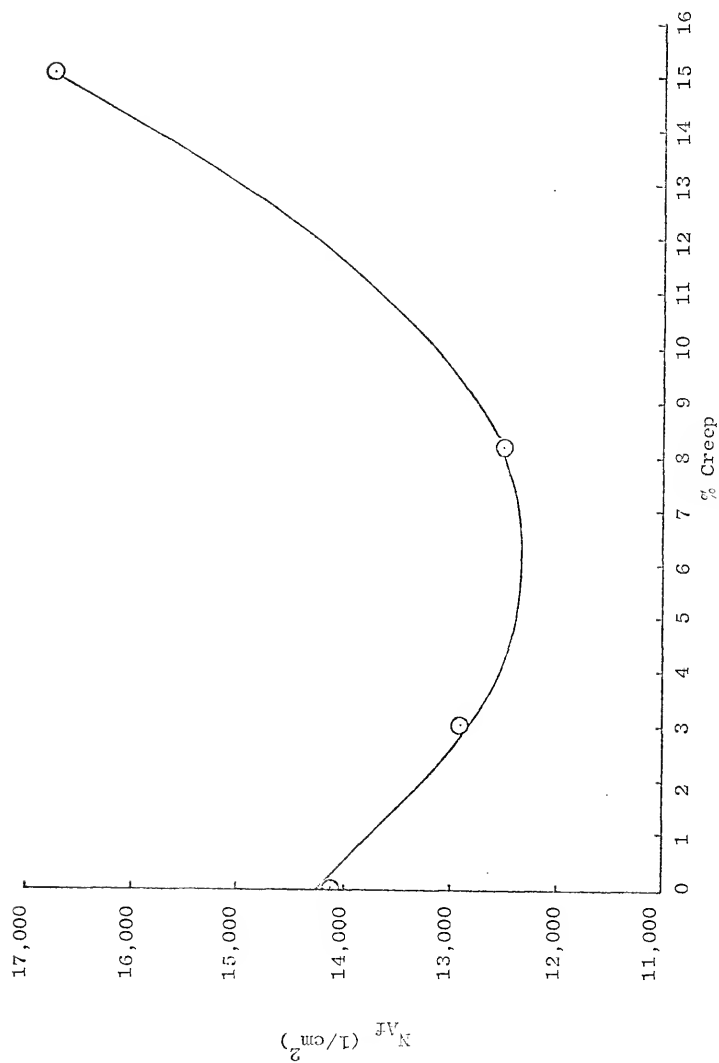


Figure 34. Number of fracture areas per unit area of exposed fracture, N_{Af} , plotted against percent creep undergone by 63% dense, 115 μ samples at 700°C.

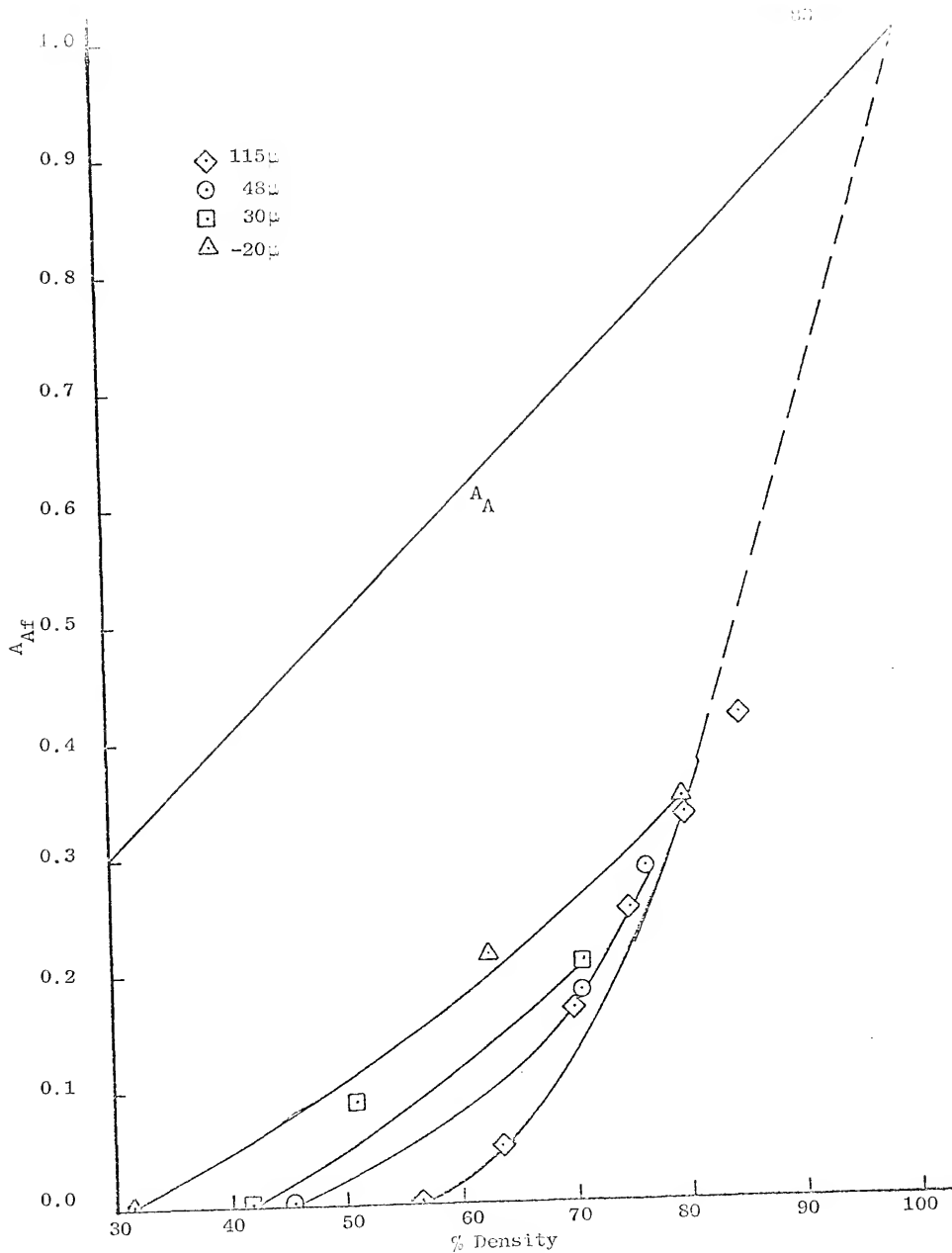


Figure 35. A_{Af} versus percent density for samples of -20μ , 30μ , 48μ , and 115μ samples.

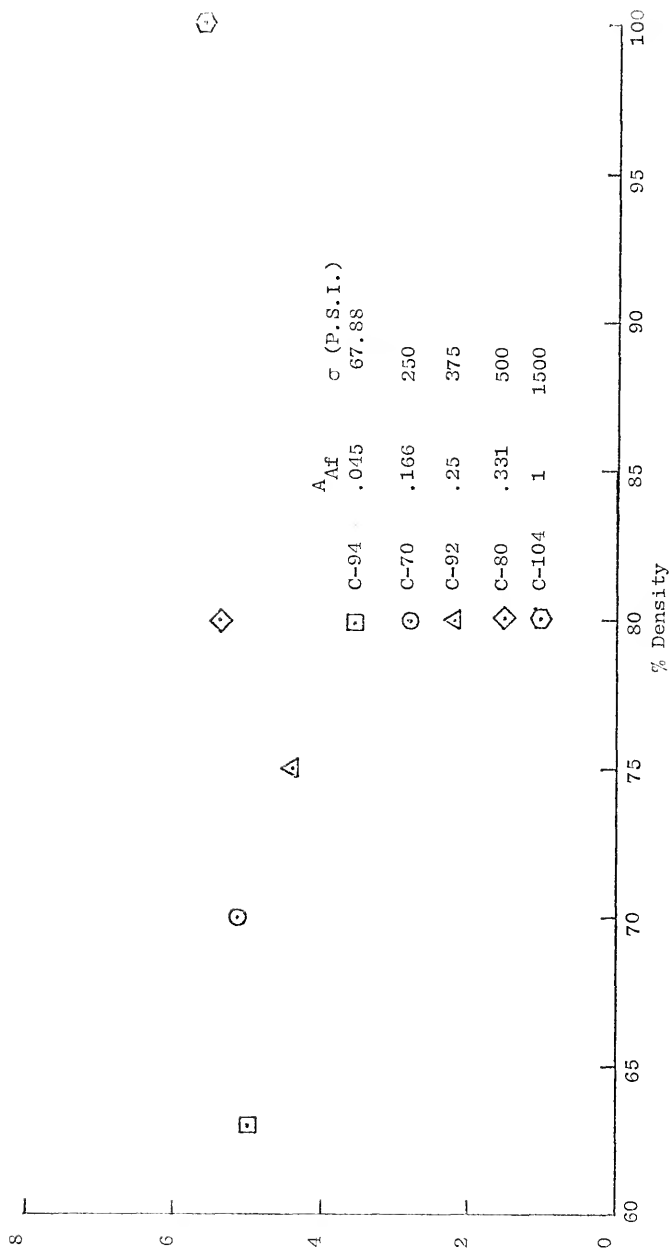


Figure 36. Total creep after two hours for five densities at 1100°C with $\sigma_{Af} = 1510$ P.S.I.

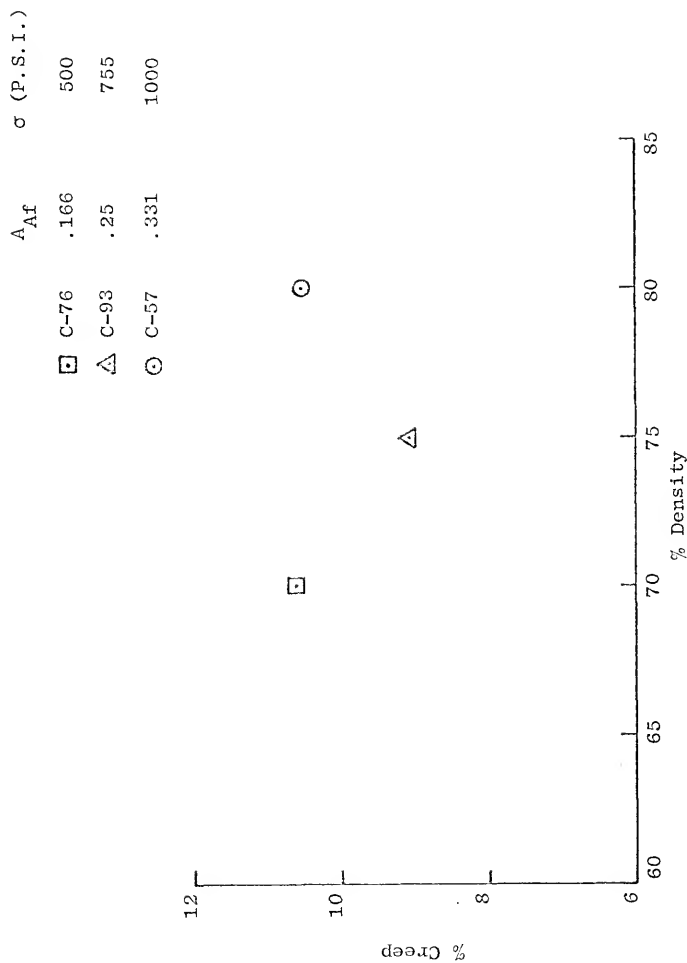


Figure 37. Total creep after two hours for three densities at 1100°C
with $\sigma_{A_{Af}} = 3020$ P.S.I.

Room temperature tensile tests were made on specimens of varying densities and varying starting particle sizes. A plot of normalized fracture stress plotted versus V_v porosity may be seen in Figure 38 [87]. As can be seen, the tensile strength of the sintered samples follows A_{Af} , the minimal sample cross section measured on the fracture surface.

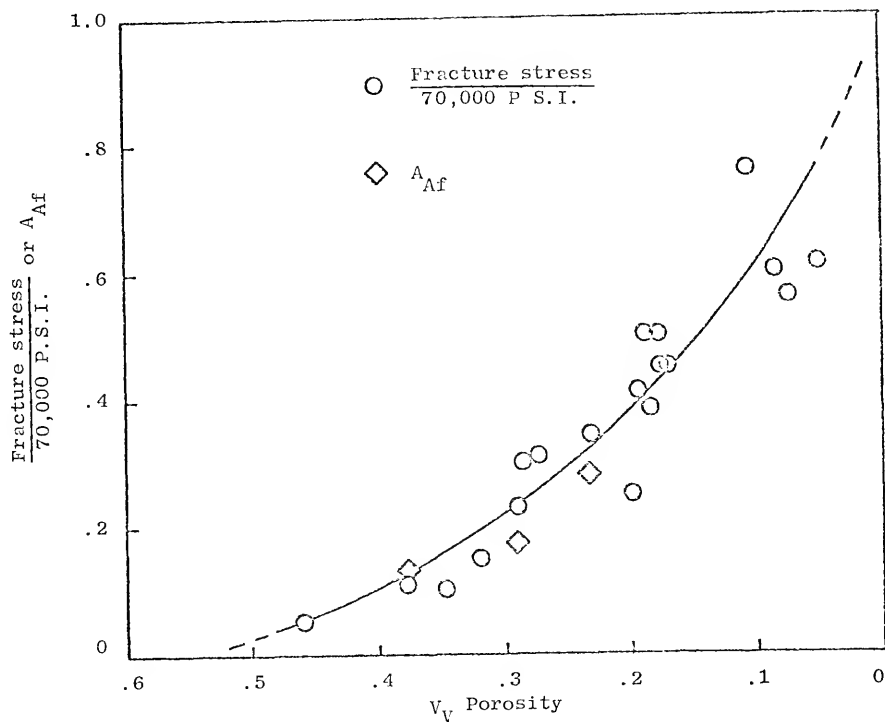


Figure 38. Normalized fracture stress and area fraction of fractured surface plotted against volume fraction porosity for sintered nickel tensile bars.

CHAPTER 4

DISCUSSION OF RESULTS

4.1 Description of Physical Aspects of a Sample Undergoing Creep

This research was performed with the objective of gaining an understanding of the nature of high temperature creep deformation of porous sintered nickel. To this end, a general survey was made with particle size, temperature, load, and density as the variable parameters. Quantitative microscopy of polished sections and of fracture surfaces was used extensively to determine the structure and geometry of samples in the as sintered state and to follow the structural changes which took place during creep as a means to provide insight into the process of creep in porous sintered nickel.

The question now arises as to what happens to a porous sinter body when loaded compressively at high temperature. With the application of the load, the body begins to deform. The first part of this deformation is simply the elastic response of the sample to the stress and is not time dependent. Further deformation which is time dependent (i.e., creep) also begins at the time of loading. As the deformation proceeds, the energy state which exists in the pore-solid interface by virtue of surface tension is disrupted. This disruption is the change of shape of this internal interface. The sample is under a triaxial

compressive stress from surface tension and although the value of the force exerted by surface tension on the sinter body may vary locally according to the Gibbs equation for pressure across an interface; eq. 6, the net effect is a hydrostatic compression on the sample as a whole.

$$\Delta P = \gamma \left(\frac{1}{r_1} + \frac{1}{r_2} \right) \quad (6)$$

where ΔP is the pressure differential across an interface, γ is the surface tension and r_1 and r_2 are the normal radii of curvature at a point on the surface. The application of the external compressive creep load alters this uniform compressive stress by increasing the load on the sample in the vertical direction and sample deformation (with attendant flattening of pores) changes the surface tension stress pattern further. A model of a spherical pore (radius r) is used to illustrate the changes in stress distribution (Figure 39).

Figure 39, part a, describes the stress from surface tension as uniformly hydrostatic throughout; i.e., the curvature is equal at all points. Part b shows the change in the state of stress on the material after loading, but before pore deformation. There is an increase in total force in the vertical direction from the external load, but the forces from surface tension remain the same. Part c shows the pore deformed into an ellipsoid. If the deformation has been uniform, the three axes of the ellipsoid are now (r_1 , x direction), (r_2 , y direction), and (r_3 , z direction), with $r_1 = r_2 > r_3$. The radius of curvature at point (0,0, r_3) is r_c in both the x-z and y-z planes. At point (0, r_2 ,0) the radii of curvature are r_a in the

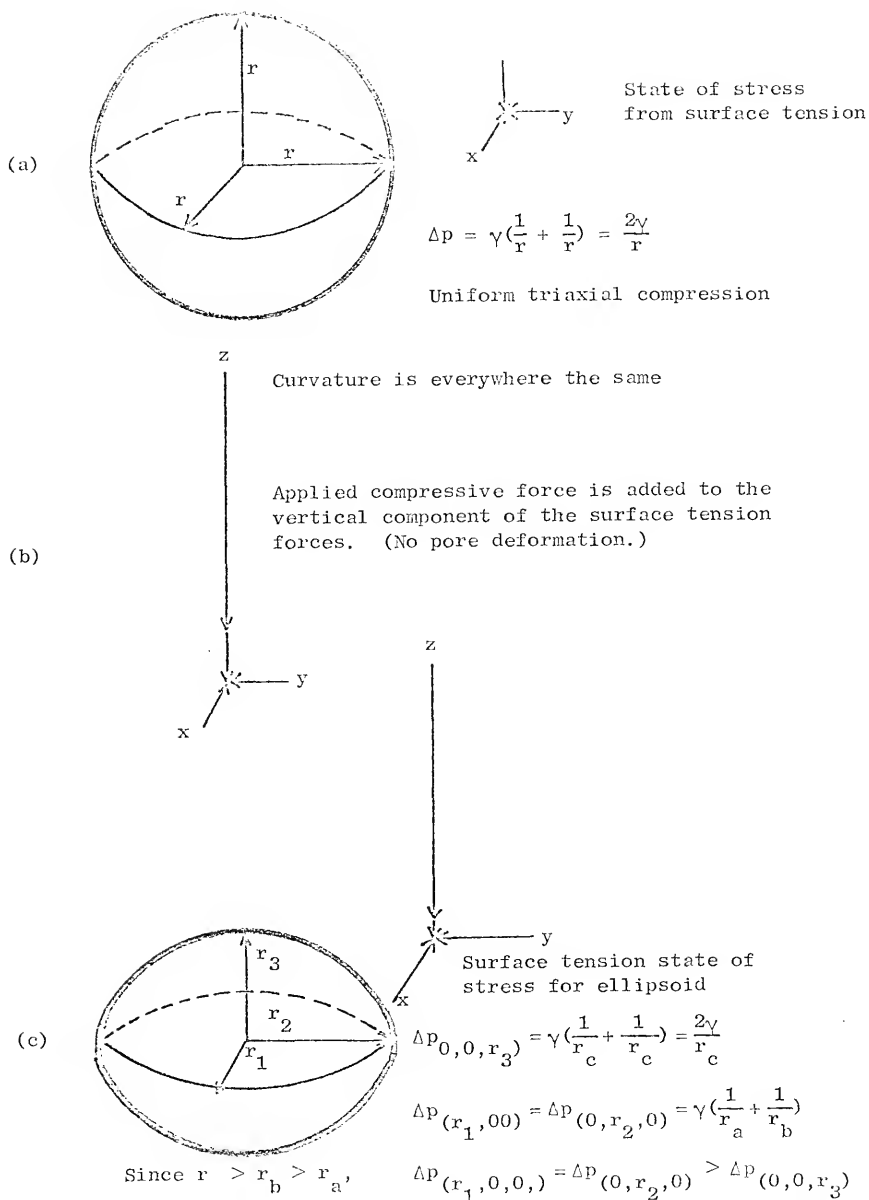


Figure 39. Model showing change in state of stress of a spherical pore from the addition of an external compressive load.

y-z plane and r_b in the x-y plane. Point $(r,0,0)$ has the same radii of curvature as point $(0,r_2,0)$. The relative magnitudes of the radii of curvature are $r_c > r_b > r_a$. The resulting surface tension forces are then

$$\Delta P_{(0,0,r_3)} = \gamma \left(\frac{1}{r_c} + \frac{1}{r_c} \right)$$

and

$$\Delta P_{(0,r_2,0)} = \Delta P_{(r_1,0,0)} = \gamma \left(\frac{1}{r_c} + \frac{1}{r_b} \right).$$

Since r_a and r_b are both smaller than r_c , it follows that the surface tension force is greater at points $(r_1,0,0)$ and $(0,r_2,0)$ than at $(0,0,r_3)$. This change in curvature causes a potential gradient down which a net migration of material can occur. Surface tension forces act toward the center of curvature of a surface and will try to reduce surface area (and total surface energy) by moving a surface toward its center of curvature. The potential gradient thus results in the net migration of material by diffusion to the areas of high curvature from the areas of low curvature.

This sintering action results in the reduction of total surface and a reduction in the anisotropy of the surface as measured by the N_L count. There are then two forces working against each other in terms of pore shape; the external load causing the anisotropy through specimen deformation with partial pore collapse in the creep direction and the local diffusion action trying to make the porosity isotropic again. The relative rates of these two actions are measured by the anisotropy of the N_L count across the pore-solid interface.

Compressive deformation of a porous body results in densification through partial collapse of the porosity. There is therefore not as much barreling in a porous body which undergoes plastic deformation as is found in a solid body which cannot alter its volume upon deformation. The densification effected upon a porous sinter body by compressive deformation is seen to be generally slightly higher in high temperature creep than in room temperature compression for the same amount of deformation, Figure 40.

4.2 Sintering Process in Creep

When a porous body is held at high temperature, sintering is expected to take place. Sintering phenomena may be divided into surface changes and volume changes with surface tension as the driving force for both changes.

Early in the sintering process, there is a considerable portion of the surface energy expended just in local surface minimization. There is considerable densification in early stage sintering although it is not simply related to the total expenditure of surface. As sintering proceeds, the surface area reaches the minimum it can have for the given density of the sample. From this point, until isolated porosity appears, there must be densification for a reduction in surface area to be effected. At this point in the process all interparticle porosity is interconnected and the surface is referred to as a conditional minimal surface. This condition may be thought of as having the surface stretched taut over the solid network. Densification occurs as pore channels are pinched off. As soon as a channel is eliminated, the

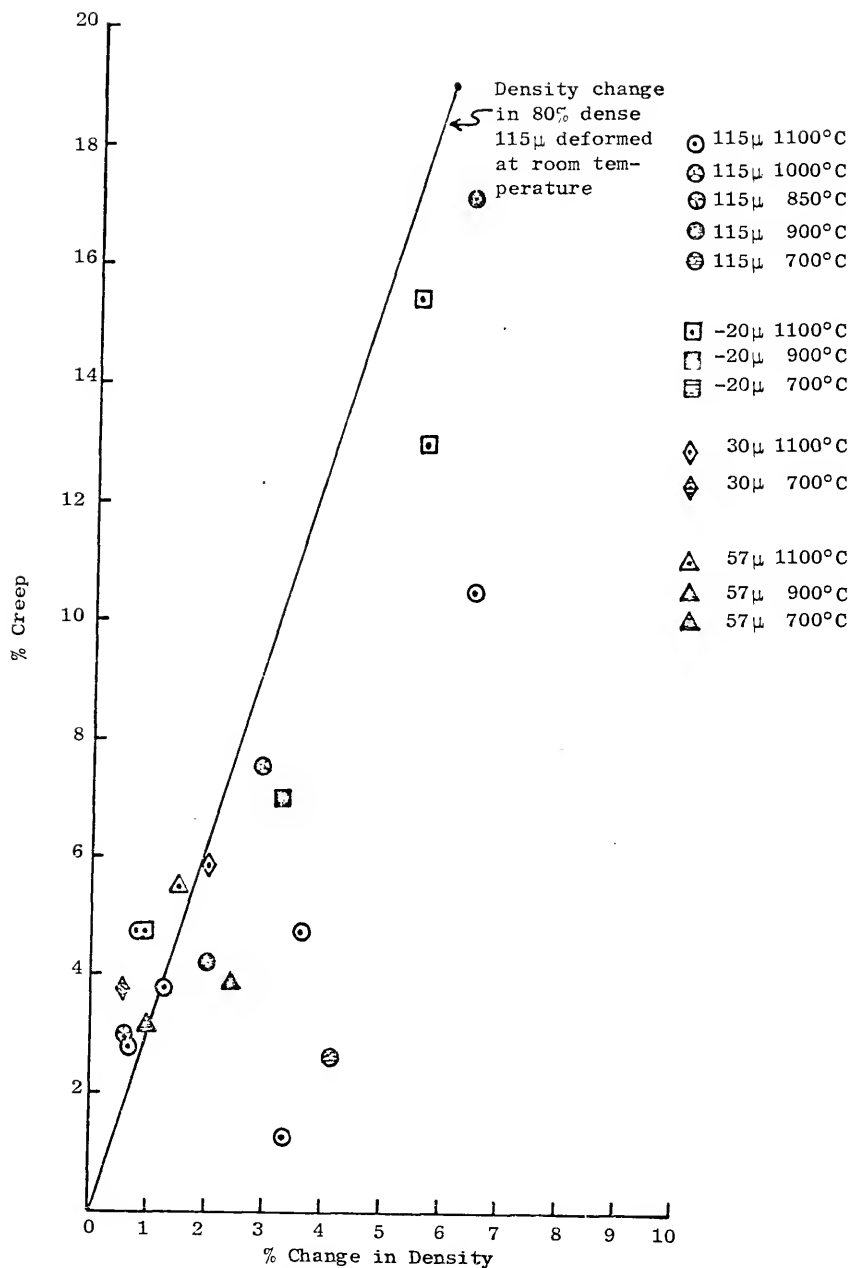


Figure 40. Density change undergone by 80% dense creep samples at various temperatures and varying amounts of creep.

surface springs back to a new local minimal surface. This state of conditional minimal surface is maintained until isolated porosity appears. The expenditure of surface energy is linearly related to densification, while the system maintains this conditional minimal area state.

What is the contribution of loose stack sintering to the total deformation found in a compressive creep test? Using the rate and volume equations (equations 1, 2, and 3 of Section 3.1), one finds that the shortening of a sample due to loose stack sintering in these creep tests is negligible in all cases except in the -20μ (smallest powder) samples where it was a small, but significant portion. As mentioned in Section 4.1, sintering action in these creep tests is primarily localized and it attempts to take the anisotropy out of the surface which is undergoing mechanical deformation in creep. The pore volume is decreased by the creep deformation by collapse in the creep direction. This collapse in the vertical direction is the primary source of the anisotropy in the pore structure.

The contribution of sintering in the creep of sinter bodies is local action involving particle size distances attempting to maintain a minimal surface, and pore isotropy.

4.3 Creep

Creep rate of a dense specimen depends on many factors. Composition, crystal structure, and morphology of a specimen are material factors and temperature, load, and time are test conditions which alter creep rate. Most samples in this research have two more

variables which are particle size and sample density. The following discussion is concerned with the effects of particle size, temperature, density and stress on the creep of porous nickel samples.

4.3.1 Particle Size Effect

It was found that the particle size from which a porous sample was made has a large effect on creep rate. It was always found that the finer the powder from which a porous sample was made, the more the sample would creep under a given set of conditions. It might at first be supposed that the difference in creep rates might be explained by the faster sintering rates of the samples made from the finer powders. Reference to the $\Delta L/L_0/\text{hr}$ values in Table 2 show that the sintering rates of the different powders are far too slow to make the magnitude of difference seen in these tests. From the chemical analyses of the powder lots received, it is known that the purity of the powder decreased with decreasing particle size. When 100% dense samples made from the different particle sizes were tested, it was found that the finer the particle size from which a sample was made, the less it crept! This result is believed to come from the purity effect as these samples are geometrically identical. That is, with the elimination of internal porosity, there cannot be any sintering phenomena operating. On the other hand, the higher creep rate of fine particle specimens at significant porosity levels (80% dense and less) must be the result of a phenomenon characteristic of the size of the particles from which the samples were made and which has much stronger and opposite effect on creep than the purity difference. Further discussion of the particle size effect follows in Section 4.4.

4.3.2 Temperature Dependence

The temperature dependence of creep is generally found to be of the Arrhenius type. From the Arrhenius temperature dependence it is commonly found that high temperature creep activation energies are equal to the activation energy for self-diffusion in fully dense materials. This is usually taken to signify that the ultimate controlling mechanism is diffusion. Activation energy may also vary with temperature [48]. In nickel, the activation energy for creep has been found to decrease the self-diffusion activation energy of 66.5 kcal/mole as the temperature decreases below 700°C and approaches 23 kcal/mole at 500°C [48]. Seeger [88] reports that an activation energy of about 1 ev (23 kcal/mole) is characteristic of dislocation intersection in nickel.

In these experiments, the exact nature of the temperature dependence was difficult to determine as the creep apparatus was not capable of fast temperature cycling. The activation energy analysis was therefore performed on separate samples that had the same particle size, starting density, and load, but were crept at different temperatures. To have the samples as structurally similar as possible, the analysis was performed, using the creep rates at equal amounts of creep. The creep activation energies found for the 115 μ particle size samples were generally in the range of 23 to 40 kcal/mole which is suggestive of dislocation intersection.

As an Arrhenius temperature dependence implies, the creep rate is very sensitive to temperature and increases with increasing temperature.

4.3.3 Density Effect

As a sinter body densifies, the amount of metal per unit cross section increases. For this reason, for a given external load, the unit stress on the load supporting cross section is reduced the denser the specimen and less creep occurs. The average cross section of a porous body, A_A , increases linearly with increase in density. This average cross section is in fact a direct measure of the density. If a sample is 60% dense, then the A_A is .6, at 80% dense, $A_A = .8$, and at 100% density, $A_A = 1$. Another cross section found useful in this research has been A_{Af} . This is considered to be the average minimal cross section in a porous body and is measured by taking an A_A count of the fracture areas exposed when a sample is fractured in tension. A_{Af} does not increase linearly with increase in density and depends upon the original stacking of the loose powder. The density at which a given particle size stacks when poured into a mold depends upon the particle shape. The more regular the particle (spherical), the higher the loose stack density. Thus the difference in loose stack density found in this research is a result of the smaller particles being more irregular than the larger particles. The finer particles, i.e., -20μ , also do not appear to be as "filled in" as the 115μ powders. The density from which A_{Af} begins to increase with sintering from approximately zero is the loose stack density, regardless of what that loose stack density is. The rate of increase of A_{Af} with increasing sintering densification is slow as the sample starts densifying and the rate increases as densification continues until the density for which this

particle shape (and stacking) reaches its minimal surface area configuration. This minimal area configuration is reached when the A_{Af} of a sample intersects the A_{Af} versus density line that is representative of a sample which had its particles most densely stacked in the loose stack condition, i.e., a sample of smooth, spherical particles. In this research, the 115 μ particles closely approximate spheres and normal spherical stacking. Thus it is seen that the A_{Af} s of the smaller, more irregular powder samples approach the 115 μ A_{Af} versus density line and are identical to this 115 μ A_{Af} line as the samples of the smaller size fractions continue to densify past the point of juncture. A result of this factor is that the A_{Af} of a sample of a smaller size fraction (in this research) is always equal to or larger than the A_{Af} of a sample from a larger size fraction.

A_{Af} has been found to be a measure of the load supporting area in tensile tests. If the stress is reversed to a compressive test the area supporting the load should be the same. It follows then that for small deformations, in which the load bearing area A_{Af} does not significantly change, A_{Af} should be predictive in compression. That this has been found for 115 μ samples is discussed in the next section.

4.3.4 Stress Effect

The stress effect is such that an increase in stress produces an increase in creep rate. The stress, σ , listed for a given test is the stress on the gross sample cross section. To find the true maximum stress on the minimal cross section, one must divide the listed sample

stress by the A_{Af} of the sample. The creep stress is the highest on the minimal cross section; therefore, most of the creep deformation is concentrated there, as strain rate is proportional to σ^n where n is usually 3 to 6. All creep tests were constant load tests. This condition leads to a monotonically decreasing effective stress from the outset of creep.

In coarse size fraction (115μ), the load and density effects could be combined into a single term of the use of the A_{Af} measurement at a particular density. Using the effective stress, $\sigma_{A_{Af}}$, on the minimal cross section of the 115μ samples, the creep rate remained the same regardless of starting density. For example, an 80% dense sample made from 115μ powder has an A_{Af} of 0.331. In this case $\sigma_{A_{Af}} = \frac{\sigma}{0.331}$ = approximately 3σ . At 100% density, $\sigma_{A_{Af}} = \frac{\sigma}{1} = \sigma$. The postulate was made that the area represented by A_{Af} is the true load bearing area in a porous sintered sample. If this postulate is valid, then a creep load of $\frac{\sigma}{3}$ on an 80% dense sample will produce the same creep as a load of σ on a 100% dense sample. There are further requirements which must also be met for the creep of the 80% and 100% dense samples to be equal. They are:

1. The samples must be metallurgically stable (no grain growth, etc.) throughout the test.
2. Densification of the porous sample due to loose stack sintering must be negligible during the test.
3. Creep must not be affected by the scale of the system (grain size, subgrain size, or proximity of surface) over the range of densities involved.

The results of creep tests on two series of 115μ samples at varying densities with $\sigma_{A_{Af}}$ constant may be seen in Figures 36 and 37. Although there is scatter in the results, the agreement is close and justifies the postulate that the A_{Af} of a sintered sample is the load bearing area.

As these tests are constant load tests, the stress on A_{Af} is continually decreasing. As creep proceeds the $\sigma_{A_{Af}}$ must decrease proportionally on samples of all densities as the A_{Af} increases. In the 100% dense sample, the increase in cross-section is all barreling, whereas in a porous sample, the A_{Af} increases as well as the gross sample cross-section. The total load supporting cross-section, A_{Af}^a , where a is the gross sample cross-section, must increase proportionally in the samples of all densities to keep the $\sigma_{A_{Af}}$ equal on all samples as creep proceeds. If this increase were not proportional, the $\sigma_{A_{Af}}$ on the different samples would be different as would the resulting creep rates and the total creep in a given time.

4.4 Specimen Examination

Metallographic examination of 115μ samples that have undergone creep shows virtually no variation in the makeup of the particles in the density range of 60% to 80%. The particles have internal porosity and 5 to 7 grains on a polished cross section. Numerous annealing twins are present as well as occasional serrated grain boundaries. The 100% 115μ samples had grain diameters up to 1 mm to 3 mm or roughly the same diameter as a 1/8-inch diameter creep sample. The observation of no effect on creep of 115μ particle size samples of a variation in grain size from roughly 40μ diameter as seen in samples where particle identity is retained, to 1000μ to 3000μ grain diameter means that the creep

mechanism is not structure sensitive, i.e., grain size sensitive, in this size range.

The effect of particle size on creep shows that the scale of the system is of importance when there is a significant porosity level. The degree of the effect is small until a critical size range is reached. For instance, Figure 14 shows the creep curves of 80% dense samples tested under 500 P.S.I. at 1100°C for four different particle sizes. It can be seen that there is only a small size effect on creep between the 115 μ and the 30 μ samples. There is almost a factor of 4 difference in the average particle diameter which produces only a factor of 1.25 difference in total creep in 2 hours. If one now compares the 30 μ sample with the -20 μ (11 μ average) where there is only a factor of three difference in diameter, one sees that the -20 μ sample has crept 2.2 times as much as the 30 μ sample. Obviously, the scale of the system is much more important in this particle size range than in the size range of 30 μ to 115 μ . It has previously been shown that at 100% density, the creep rate varies directly with the particle size from which the samples were made, Figure 16b. From these two observations (creep at 100% density and creep at 80% density), one would expect to find creep at constant $\sigma_{A_{Af}}$ to be density dependent in samples made from the 57 μ , 30 μ , and -20 μ powders. The strongest dependency should be found with samples made from the -20 μ powder. To check the density effect on creep in this size fraction, samples of 60%, 70%, 80%, and 100% density were crept with different starting loads which produced a $\sigma_{A_{Af}}$ of 1500 P.S.I. in each sample. The results in Figure 41 show an extreme sensitivity to density.

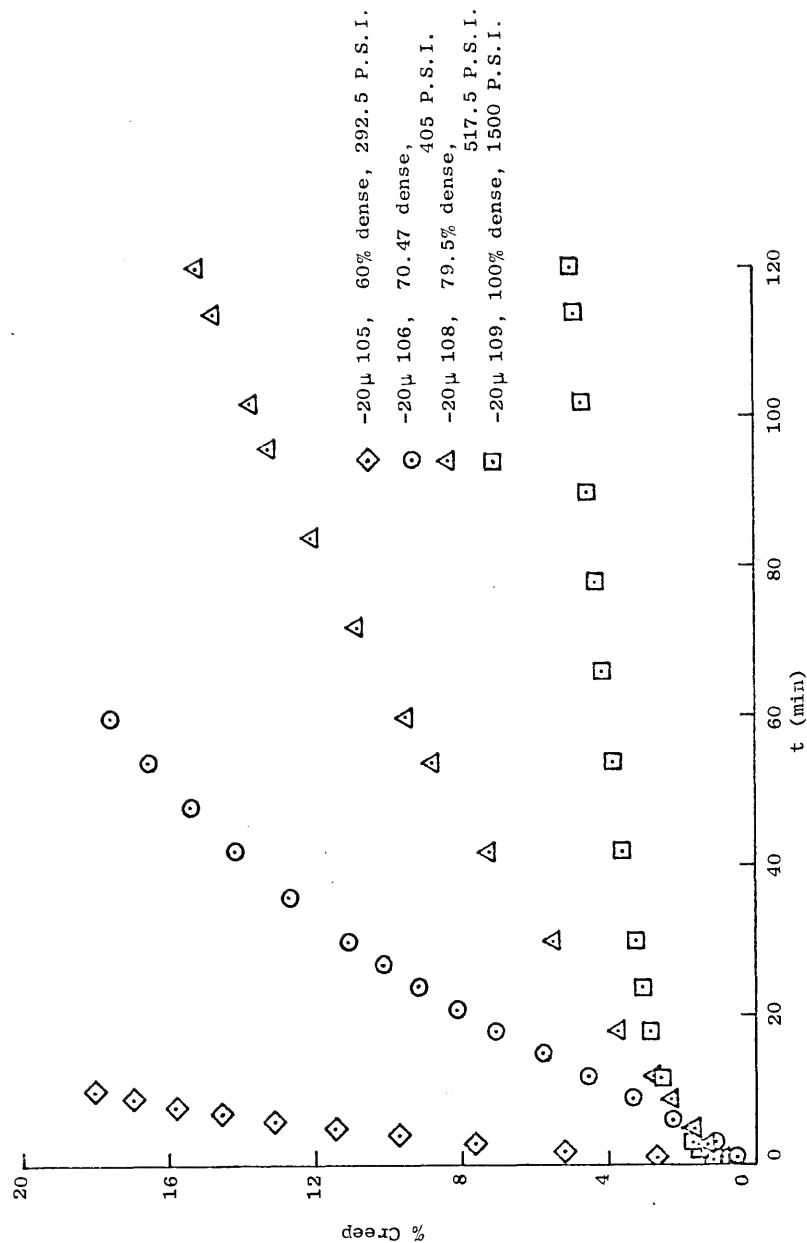


Figure 41. Creep of -20μ samples at four densities at 1100°C with $\sigma_{Af} = 1500$ P.S.I.

An explanation of the particle size effect is based on dislocation motion and stoppage. First, consider the deformation of a dense, polycrystalline piece of metal where dislocation glide is the method of deformation and dislocation accumulation is the strengthening mechanism. Next, consider the effect of grain boundaries and subgrain boundaries on the movement of dislocations. Grain and subgrain boundaries are lattice discontinuities through which dislocations often penetrate with much difficulty; therefore, dislocations accumulate behind them. As grain size decreases, grain boundary area increases and a dislocation travels a shorter distance before encountering a boundary, thus the common observance of increased strength and creep resistance with a decrease in grain size. Now imagine this polycrystalline piece of metal pulled apart at the grain boundaries and the effect these boundaries would now have on stopping dislocation movement. When dislocations reach a grain boundary and the boundary is not restrained by another grain or oxide, the dislocation may put a step in the surface, thereby leaving the interior of the grain. This results in negligible strengthening of the crystal. Relate this analysis to the structure of a porous sinter body. If the particle size from which the sinter body is made is large compared to the grain or subgrain size, then the probability of a dislocation being caught by an interior boundary of the particle and causing hardening or strengthening is much higher than the probability of the dislocation traveling to the pore-solid interface and escaping as a step on the surface. As a sinter body densifies, the average distance a dislocation would have to travel before

reaching a free surface (pore-solid interface) increases. In the case of the particle size being large compared to the grain or subgrain size so that the dislocations are already caught inside the particle, this increase in average distance is of no consequence. Such is the case with the 115μ samples where there is a large amount of intraparticle boundary. If however, the particle size is small enough for an active dislocation to have a high probability of reaching the pore-solid interface, then densification with the attendant average increase in distance a dislocation must travel to reach a free surface would increase the probability of the dislocation being trapped in the solid. Such is the case with the -20μ (11μ average) samples. As the -20μ particle size samples densify, they approach the same situation as found in the large particle size samples and at 100% density, the two are geometrically identical. A comparison of the creep of the 100% dense samples made from 115μ and -20μ powders in Figure 41 show this. The two intermediate particle sizes, 30μ and 57μ , are intermediate cases between the two extremes. Metallographic examination of -20μ samples revealed that the particle were either single crystals or bicrystals and 3μ to 15μ in size, which is the size generally reported for subgrain in hot worked and crept nickel [35,89].

4.5 Quantitative Microscopy in the Creep of Sinter Bodies

Many quantitative microscopy data were taken in the course of this work. These measurements included A_A (area fraction), S_V (surface area/unit volume), M_V (total curvature), \bar{H} (average mean curvature) and $\bar{\lambda}$ (mean pore intercept) on polished sections, and A_{Af} (area

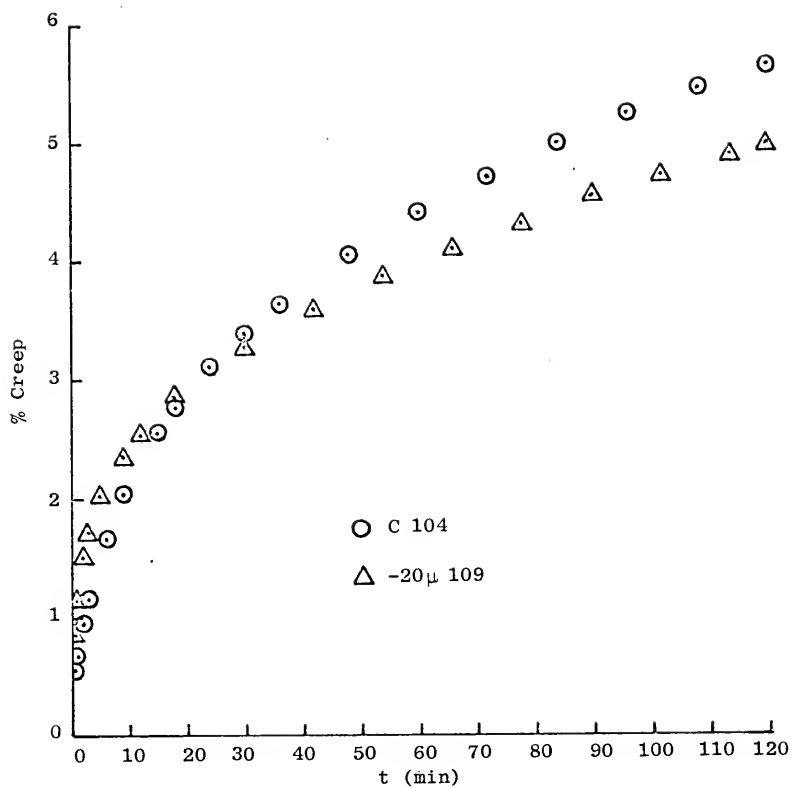


Figure 42. Creep curves of 100% dense, -20μ and 115μ samples at 1100°C and 1500 P.S.I.

fraction of fracture surface), N_{Lf} (number of intersections on fracture surface/unit length of test line) and N_{Af} (number of fractures/unit area) on fracture surfaces. The line intercept count, N_L , was the most widely studied of the measurements on the polished sections. The N_L count is related to S_V by the equation $N_L = \frac{1}{2} S_V$. S_V , surface area/unit volume, was used as one indicator of how the creep process affected the amount of internal surface in a sinter body. The S_V values were determined for the 115 μ , 57 μ , and 30 μ powder samples at various densities in the as-sintered condition (uncrept). These "standard" values were then compared with the S_V values obtained from samples which had undergone creep. In loose stack sintering, there is a linear correlation between S_V and V_V once second stage sintering and the conditional minimal surface condition have been reached. The effect of creep was to increase the value of S_V over that which would be associated with loose stack sintering, Figure 30. Sintering phenomena, especially surface rounding, continually strive to bring the surface area back to the balance line, the $S_V - V_V$ equilibrium line. The N_L count from which the S_V calculation is made has been used to measure the distortion in the pore-solid interface left by the creep process. Rather than taking the N_L counts randomly on the polished sections of creep samples, the counts were made parallel to and at 90 degrees to the creep direction. The ratio of these two measurements has been designated by the term ΩN_L , N_L (transverse direction)/ N_L (longitudinal direction). For a loose stack sintered sample which has not undergone creep, $\Omega N_L = 1$. For crept samples, $\Omega N_L < 1$.

For the porous nickel used in this research, the compressive deformation is thought of as consisting of three parts. Part of the overall study has been to separate and quantify these parts. The first part, called normal creep, is the creep which takes place with no influence from sintering phenomena. This creep is similar to that found in fully dense material, but is nevertheless tied to the geometry of the porous structure. The anisotropy of the N_L count, ΩN_L , is taken as the measure of this creep. This measurement reveals the degree of flattening of the internal porosity of a creep sample in the creep direction. This flattening is purely mechanical and would be expected to be maximized when deformation takes place under conditions where thermal readjustment of internal surface is minimal. The second portion of the total deformation is the shrinkage of the sample attributable to loose stack sintering. This is the dimensional change in the creep direction which the sample would undergo due to normal sintering (no load) at the test temperature for the time of the test. This length change may be calculated using equations 1, 2, and 3 of Section 3.1. The third portion of the total sample deformation is attributed to the fact that the creep stress is acting on a porous body rather than on a fully dense bulk sample. This portion is referred to as stress assisted sintering. Stress assisted sintering results from the fact that the creep process results in more than the equilibrium amount of surface that a sinter body of a given particle size, genus, and density were obtained through loose stack sintering and the fact that the porosity has been made anisotropic. Local sintering action

attempts to return the sample to the minimal surface and remove the anisotropy put in by the purely mechanical creep.

A simple model was devised for the analysis of the different parts that make up the total creep deformation of a porous sinter body. In this model, the porosity has been segregated to one end, Figure 42a. Figure 42b shows the model divided into the various components of deformation under study. The notation is as follows:

L_o = sample length before creep test

L = sample length after creep test

h_{pb} = height of pore before creep test = $L_o (1 - \% \rho_{\text{before}})$

h_{pa} = height of pore after creep test = $L (1 - \% \rho_{\text{after}})$

h_m = height of metal = $L_o (\% \rho)$

h_{an} = height lost in test due to normal creep processes
as measured by anisotropy of $N_L = h_{pa} \frac{(1-\Omega)}{\Omega}$

h_{us} = height lost due to loose stack sintering densification

h_{as} = height lost in test due to stress assisted sintering
 $h_{as} = h_{pb} - h_{pa} - h_{an} - h_{us}$

This model is used as a method of following the anisotropy of the pore shape and h_{an} and h_{as} should not be taken as the actual percentages of the total deformation undergone by a porous creep sample.

The results of this analysis are found in Table 6. This analysis has shown that for the 115μ particle size sample, h_{us} is negligible and the total creep may be thought of as consisting of h_{an} and h_{as} . Figure 43 is a plot of the percent total creep versus the percent of the total calculated to be activated sintering. There is

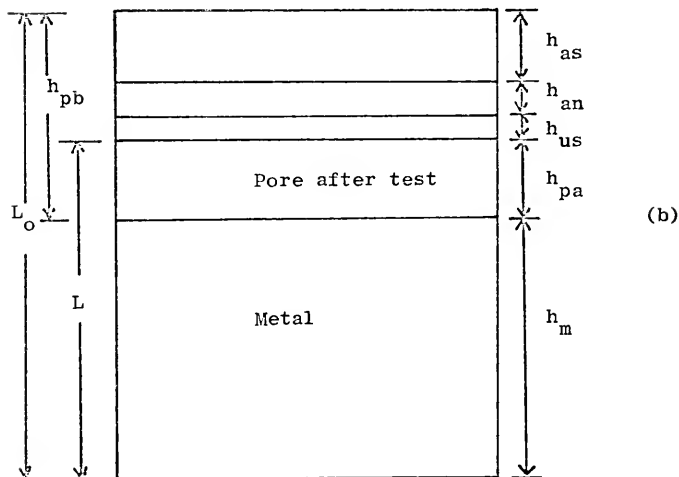
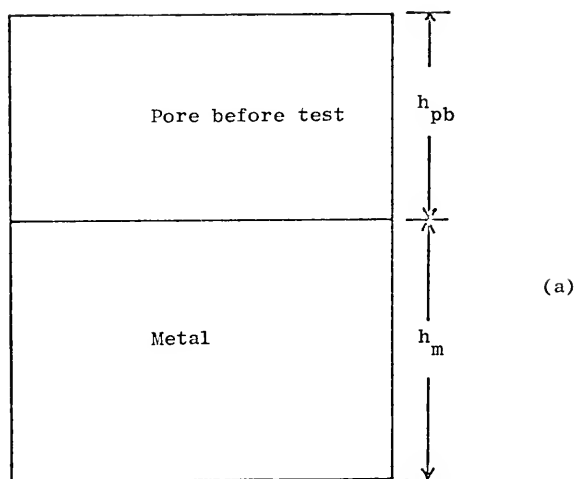


Figure 43. Model used in the analysis of creep and stress assisted sintering.

Table 6. Calculations of the components of the stress activated sintering model.

#	Temp.	ρ before	ρ after	L_o	L	h_{pb}
C21	1100°C	84.6	88.2	.2950	.2601	.04543
C22	"	85.1	89.4	.3507	.3413	.05345
C25	"	75.8	79.8	.3992	.3404	.09661
C26	"	75.4	79.9	.3972	.3473	.09771
C30	"	80.0	87.3	.3334	.2932	.06668
C31	"	80.0	86.2	.3715	.3340	.0743
C39	"	70.0	77.9	.4740	.4150	.1422
C40	"	69.9	76.7	.4163	.3702	.1253
C41	"	69.7	76.4	.3685	.3150	.111F
C48	900°C	69.9	74.1	.3967	.3737	.11941
C49	"	79.7	81.25	.3860	.3709	.07836
C50	"	80.0	87.48	.3145	.2904	.0629
C51	"	80.0	88.03	.3496	.2674	.06992
B54	"	79.5	81.4	.3452	.3345	.070766
C55	"	79.9	85.02	.3338	.2800	.06709
-20 μ 105	1100°C	60.17	69.98	.5474	.4400	.2180
-20 μ 108	"	79.5	84.66	.3231	.2784	.06624

Table 6 (Extended)

h_{pa}	h_m	h_{an}	h_{us}	h_{as}	σ	$\frac{\sigma}{\epsilon_c}$ Creep	time (min)
.03069	.24957	.00389	5.6×10^{-6}	.01085	1000	12.5	300
.03618	.30525	.000503	"	.01677	500	5.25	1096
.06876	.30259	.00604	"	.02181	1000	15.5	21
.06981	.29949	.00477	"	.02313	500	13.39	120
.03724	.26672	.00918	"	.02026	1000	13.09	60
.04609	.2972	.00582	"	.02239	500	10.96	534
.09172	.3318	.00601	"	.04447	500	13.4	120
.08626	.29099	.001465	"	.03757	250	12.05	420
.07434	.2568	.00386	"	.0335	1000	15.32	10
.09679	.2773	.002696	"	.01992	1000	6.18	60
.06954	.3076	.002299	"	.00652	500	4.19	2730
.03636	.2516	.006802	"	.01934	2000	8.17	54
.03201	.27968	.008535	"	.02938	4000	22.14	6
.0622217	.274434	.002299	"	.006319	1000	3.82	120
.04194	.26671	.008396	"	.01675	4000	17.23	6
.13389	.3293	.007214	.0016	.0753	292.5	18.05	10
.04271	.2569	.001204	.001315	.02101	517	15.22	120

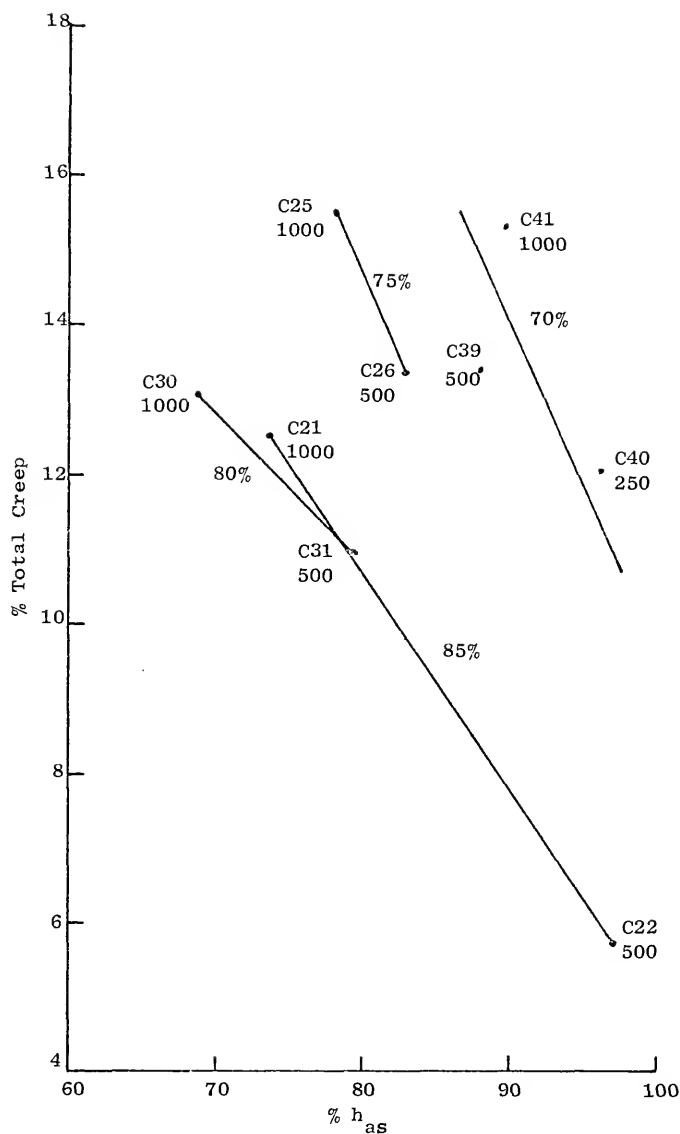


Figure 44. Total creep in test versus percent calculated from the model to be stress activated sintering. Sample numbers and corresponding loads (P.S.I.) are given.

a striation of the data according to the starting density of the samples. This striation of the 1100°C, 115 μ data with density shows that at a given total creep, the portion of the total creep which is attributed to activated sintering is larger the lower the density. The data are further ordered within each density according to the time of testing and load. For a given starting density, the lower the load and longer the test time, the larger the percentage of creep attributed to stress activated sintering. Figure 44 is a plot of the same samples with time of creep testing plotted versus percent of total creep attributed to activated sintering. With $h_{us} = 0$, one has only the two remaining parts to add up to the total creep; namely, the normal creep as measured by the anisotropy of the porosity, h_{an} , and the stress activated sintering, h_{as} . Any test condition which would reduce the anisotropy of the porosity would necessarily increase the share of the total creep attributed to activated sintering because the calculation of activated sintering is done by difference. Although the time, temperature, and particle sizes involved in these tests are such that sample length changes due to loose stack sintering are negligible, local rounding takes place with surface diffusion. The longer times involved with creep testing at the smaller stresses result in a loss of anisotropy as measured after the test. This loss of anisotropy would then be seen as stress activated sintering. There is further evidence of the density sensitivity of activated sintering. Take the following pairs of samples (C25, 75% dense, 21 min, and C41 70% dense, 10 min), (C26, 75% dense, 120 min and C39, 70% dense, 130 min), and

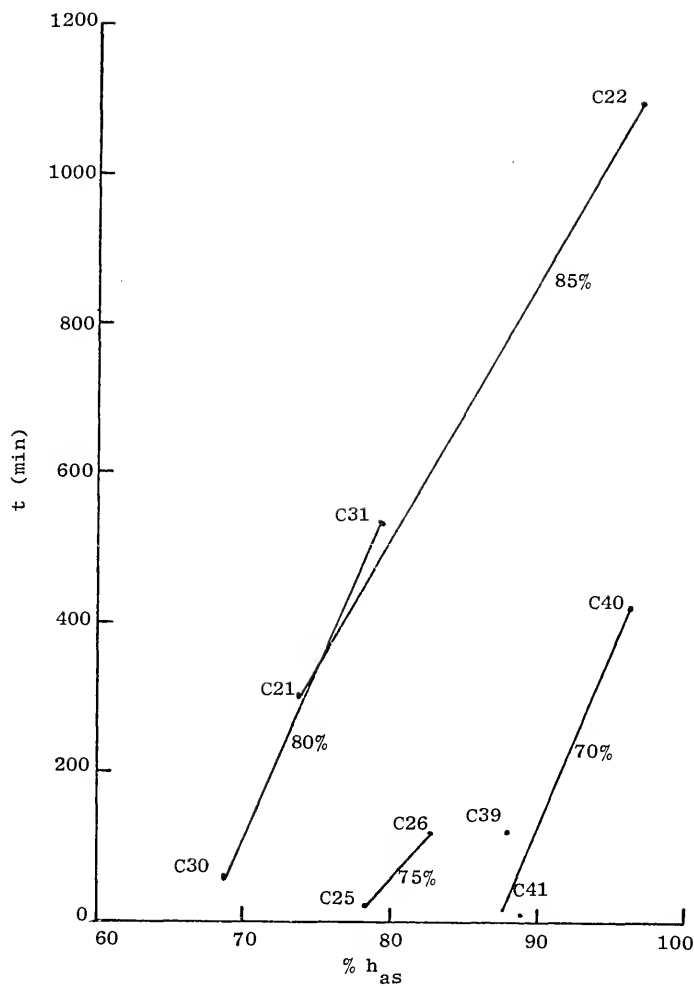


Figure 45. Total time of test versus $\% h_{as}$ as calculated from the model.

(C31, 80% dense, 534 min and C40, 70% dense, 420 min), Figure 45, and observe that in each case, the percentage of activated sintering is greater in the lower density sample, although the times involved are equal to or shorter than in the higher density samples.

4.6 Summary

All of the pertinent points of the research have been discussed separately in the previous sections of this chapter. The general principles learned from these observations will now be discussed.

High temperature creep of porous nickel has shown that sintering as a densification mechanism per se does not contribute significantly to the deformation found in these creep experiments. Sintering does, however, command a prominent position in maintaining the internal structure of a porous creep sample. As the creep load continuously deforms a specimen, local sintering forces continuously strive to return the structure to an isotropic, minimal, surface area state as is found in a loose stack sintered sample. The structure of a creep sample after a test is such that it appears to have had an extremely large surface tension in operation, causing the densification. Although the internal structure of a creep sample appears as though the creep load has been transformed into a triaxial compressive force, the nearness of the internal shape to isotropy is in fact due to local pore shape change. The significance of this maintenance of isotropy from the standpoint of creep deformation lies in the load bearing area of the sample. The local sintering effect strives to maintain the minimal load bearing cross section, A_{Af} , in a sample undergoing

creep. This means that to the extent to which the local sintering maintains the minimal cross-sectional area as a specimen densifies in creep, the creep load is resisted by the minimal amount of cross section possible at a given density.

As the starting density of a sample increases, the creep rate for a given temperature and load decreases. This follows from the fact that there is more cross-sectional area resisting the creep load resulting in a lower unit stress. Likewise, an increase in creep load increases the creep rate for a given temperature and density because the unit stress on the load bearing area is increased. The increase in creep with increase in temperature is consistent with a general weakening of material, making it less resistant to deformation. This weakening is from faster recovery and lower modulus. The amount of anisotropy of pore outline left in a creep sample after a creep test shows that the denser the sample is, the more anisotropy remains. The reason for this fact is that the deformation is not as confined to the A_{Af} cross section as in lower densities and thus the disruption of the pore shape is not as localized as in a low density sample. The local potential gradient for diffusion is not as large, making the process slower. The deformation is more widespread in a high density sample, a fact which increases diffusion distances. The distances involved in the redistribution of surface are also a factor in the rate at which the pore-solid interface approaches isotropy or keeps from being totally flattened in a test. This means that the shorter the distance over which diffusion must occur to change the shape, the faster the shape can change. As there is a factor of 10

difference in average particle size between the 115μ and the -20μ specimens, it is easily seen why a much smaller amount of anisotropy remains in a -20μ sample after a test than in a comparable sample of the 115μ size fraction. The increase in total load bearing cross section in 115μ samples of the various densities is proportional with creep for the small amounts of creep in the tests in which the dependence of creep on minimal load bearing area was checked. The apparent lack of dependence of creep on load bearing area in the -20μ samples of varying densities is due to two factors. First, the nature of the deformation (movement of dislocations) changes as density changes and second, the change in load bearing area with creep-induced densification is not as severe in the 60% to 80% density range as in the 115μ samples. That is, the slope of the A_{Af} plot versus density is not as large for the -20μ as for the 115μ particle size samples. Thus, one could have a larger creep and creep-induced densification in a -20μ sample than in a 115μ sample and not have decreased the load on the minimum cross section as much as on the minimum cross section of a 115μ sample.

The dependence of tensile strength on density has been found to be a function of A_{Af} which is itself dependent upon the particle shape and the original loose stack density from which sintering began (Figure 35). The reason for the particular dependence of strength on density in sinter bodies can now be understood in the light of this minimal cross section, A_{Af} .

In the density region from 80% to 100% density, all loose stack sinter bodies have the same A_{Af} . The change in A_{Af} with density in this region can also be considered to be linear with density.

That A_{Af} can be approximated by a straight line is not surprising in light of the knowledge that many other quantitative microscopic quantities are also linear in this region.

The path of the change of A_{Af} with density is surface tension controlled just as are the quantitative microscopic quantities of S_V , M_V , \bar{H} , and genus. An important aspect of this linearity of A_{Af} in this region is that A_{Af} is entirely independent of starting particle size or original stacking. This can be useful from an engineering standpoint in that one only needs to know the bulk tensile strength of a solid piece of like material to be able to predict the strength of a sinter body in this density region. Ultimate tensile strength has been shown to be directly related to A_{Af} for nickel [87], Figure 38, and copper [90,91]. Modulus data for a large variety of iron and steel sinter bodies [92] also follow the same curve.

The relationship obtained between amount of porosity and tensile strength can be formulated simply from the slope of the A_{Af} line in the 80% to 100% dense region. The strength of a sinter body at 80% is A_{Af} (bulk strength) or 0.33 times the bulk strength. The slope of the A_{Af} versus V_V line is therefore 3.35. The strength at any density in this linear region can then be expressed as:

$$\tau(A_A) = [1 - \pi A_{A_{por}}] \tau(\text{bulk})$$

where $\tau(A_A)$ is the strength of the compact in the density range, $.8 \leq A_A \leq 1.0$, and $\tau(\text{bulk})$ is the strength of the bulk (100% dense) material. Thus in this commercially important density range, one needs

only to know the bulk strength of a material and the relative density to know the strength of the sinter body.

The basic elements of the model of high temperature creep of porous, sintered nickel have been reviewed. Creep in the porous nickel samples by this research is seen to depend upon temperature and load in a fully rational manner. The intrinsic properties of the material used, such as chemistry, particle size, and grain size, are all seen as strong factors in determining creep of sintered nickel as well as the internal and external appearances after a test.

Hot pressing of metal powders into shapes is completely similar to high temperature compressive creep of porous metal samples and the same phenomena would be found in hot pressing as were found in compressive creep.

CHAPTER 5

CONCLUSIONS

The creep of porous sintered nickel and the structure resulting from a compressive creep test have been found to be the result of the interplay of short and long range stresses and the movement of material as a result of these stresses.

The long range stress, which is the applied compressive load, deforms the solid network on both a short range and a long range basis. The creep load induced deformation on the scale of the sample as a whole, is simply the sum of the local deformations on the scale of the particle size, less the densification. That is, the densification of the sample reduces the barreling from what would be required if their density remained the same.

The short range stresses are those produced by the surface tension forces that are present at the pore solid interface. These forces are responsible for the redistribution of the pore shape in a creep test. It was found that the faster the material could respond to these forces (increased temperature) or the larger amount of these forces available (lower density, smaller particle size) the less anisotropy would be found in a sample for a given total amount of creep. The distance over which these forces must act to move material was also important (particle size) with the smaller the distance involved, the faster the response to the surface tension.

The particle size effect on creep deformation rate has been found to be a result of the morphology of the particles rather than size alone, i.e., grain size relative to particle size. The ease with which a dislocation could reach a free surface was determined by the particle size.

The loose stack sintering rate was found to be negligible in all creep samples except those of the finest particle size ($\sim 20\mu$).

In general, the effects of surface tension and sintering phenomena were restricted to short range effects such as pore shape and load bearing area, whereas the external load had both short and long range effects on shape of the porosity as well as the sample as a whole.

The effective load bearing area was found to be represented by the area fraction of fracture surface, A_{Af} .

BIBLIOGRAPHY

1. F. Thummler and W. Tomma. "The Sintering Process," Metallurgical Reviews, The Metals and Metallurgy Trust, 1967, p. 69.
2. R. L. Coble and J. E. Burke. "Sintering in Ceramics," Progress in Ceramic Science, Vol. 3, Editor, J. E. Burke, Pergamon Press, New York, 1963, p. 197.
3. W. E. Kingston and G. F. Huettig. "Fundamental Problems of Sintering Processes," The Physics of Powder Metallurgy, Editor, W. E. Kingston, McGraw-Hill Book Co., New York, 1951, p. 1.
4. G. C. Kuczynski. "Theory of Solid State Sintering," Powder Metallurgy, Editor, W. Leszynski, Interscience Publishers, New York, 1961, p. 11.
5. R. A. Gregg. Analysis of the Sintering Force in Copper, Ph.D. Dissertation, University of Florida, 1968.
6. R. A. Gregg and F. N. Rhines. "Analysis of the Sintering Force in Copper," Metall. Trans., Vol. 4, 1973, p. 1365.
7. F. N. Rhines. "A New Viewpoint on Sintering," Plansee Proc., 1958, p. 38.
8. F. N. Rhines. "Seminar on the Theory of Sintering," T.A.I.M.E., Vol. 166, 1946, p. 474.
9. F. N. Rhines, C. E. Birchnall, and L. A. Hughes, T.A.I.M.E., Vol. 188, 1950, p. 378.
10. P. Schwartzkopf and R. Kieffer (Editors). "The Mechanism of Sintering (General Principles)," Cemented Carbides, Chap. III, p. 55.
11. G. C. Kuczynski. "Self-Diffusion in Sintering of Metallic Particles," T.A.I.M.E., Feb. 1949, p. 169, Vol. 185.
12. T. L. Wison and P. G. Shewmon. "The Role of Interfacial Diffusion in the Sintering of Copper," T.A.I.M.E., Vol. 236, 1966, p. 48.
13. G. C. Kuczynski. "Study of Sintering in Glass," J. Appl. Phys., Vol. 20, 1949, p. 1160.
14. J. White. Basic Phenomena in Sintering Science of Ceramics, Vol. 1, Academic Press, New York, 1962, p. 1.

15. W. D. Kingery and M. Berg. "Study of the Initial Stages of Sintering by Viscous Flow, Evaporation-Condition, and Self-Diffusion," J. Appl. Phys., Vol. 26, No. 10, 1955, p. 1205.
16. G. C. Kuczynski. "Discussion," T.A.I.M.E., Vol. 185, 1949, p. 796.
17. P. Schwed. "Surface Diffusion in Sintering of Spheres on Planes" (Technical Note), J. of Metals, Vol. 3, 1951, p. 245.
18. N. Cabrera. "Sintering of Metallic Particles" (Note on Surface Diffusion in), T.A.I.M.E., Vol. 188, p. 667.
19. G. Bockstiegel. "On the Rate of Sintering," J. of Metals, Vol. 8, 1956, p. 580.
20. F. N. Rhines and H. S. Cannon. "Rate of Sintering of Copper under Dead Load," J. of Metals, Vol. 3, 1951, p. 529.
21. D. L. Johnson. "New Method of Obtaining Volume, Grain Boundary, and Surface Diffusion Coefficients from Sintering Data," J. Appl. Phys., Vol. 40, 1969, p. 192.
22. J. K. Mackenzie and R. Shuttleworth. "A Phenomenological Theory of Sintering," Proc. Phys. Soc., Vol. 62, 1949, p. 55.
23. J. G. Early, F. V. Lenel, and G. S. Ansell. "The Material Transport Mechanism during Sintering of Copper-Powder Compacts at High Temperature," T.A.I.M.E., Vol. 230, 1964, p. 1641.
24. M. J. Salkind, F. V. Lenel and G. S. Ansell. "The Kinetics of Creep during Hot Pressing of Loose Powder Aggregates," T.A.I.M.E., Vol. 233, 1965, p. 39.
25. F. N. Rhines. Private Communication.
26. G. C. Kuczynski. "The Mechanism of Densification during Sintering of Metallic Particles," Acta Met., Vol. 4, 1956, p. 58.
27. R. L. Coble. "Sintering in crystalline Solids I. Intermediate and Final State Diffusion Models," J. Appl. Phys., Vol. 32, 1961, p. 787.
28. R. L. Coble. "Sintering in Crystalline Solids II. Experimental Test of Diffusion Models in Powder Compacts," J. Appl. Phys., Vol. 32, 1961, p. 793.
29. D. L. Johnson and T. M. Clark. "Grain Boundary and Volume Diffusion in the Sintering of Silver," Acta Met., Vol. 12, 1964, p. 1173.

30. R. L. Coble. "Ceramic and Metal Sintering: Mechanisms of Material Transport and Density Limiting Characteristics," Fundamental Phenomena in the Material Sciences, Vol. 1, Plenum Press, New York, 1964, p. 11.
31. D. L. Johnson and I. B. Cutler. "Diffusion Sintering I. Initial Stage Sintering Models and Their Application to Shrinkage of Powder Compacts," J. Am. Cer. Soc., Vol. 46, 1963, p. 541.
32. D. L. Johnson and I. B. Cutler. "Diffusion Sintering II. Initial Sintering Kinetics of Alumina," J. Am. Cer. Soc., 1963, p. 545.
33. F. N. Rhines. Unpublished data. (Eight pounds of copper powder sintered and sectioned. No density variation was found.)
34. A. H. Cottrell. "The Time Laws of Creep," J. of Mechanics and Physics of Solids, Vol. 1, 1952, p. 53.
35. A. K. Mukherjee, J. E. Bird, and J. E. Dorn. "Experimental Correlations for High Temperature Creep," Trans. A.S.M., Vol. 62, 1969, p. 155.
36. J. Weertman. "Dislocation Climb and High Temperature Creep Processes," Trans. A.S.M., Vol. 61, 1968, p. 680.
37. D. McLean. "The Physics of High Temperature Creep in Metals," Rep. Progress Physics, Vol. 29, 1966, p. 1.
38. O. D. Sherby and P. M. Burke. "Mechanical Behavior of Crystalline Solids at Elevated Temperatures," Progress in Materials Science, Vol. 13, 1964, p. 325.
39. R. E. Reed-Hill. Physical Metallurgy Principles, D. Van Nostrand Co., Inc., Princeton, New Jersey, 1964, p. 571.
40. H. Conrad. "Experimental Evaluation of Creep and Stress Rupture. Part 1. Experimental Evaluation of Creep," Scientific Paper 6-40104-1-P2, Sept. 29, 1959, Westinghouse Research Laboratories.
41. J. B. Conway and M. J. Mullikin. "An Evaluation of Various Equations for Expressing First Stage Creep Behavior," T.A.I.M.E., Vol. 236, 1966, p. 1496.
42. P. W. Davies and K. R. Williams. "The Tertiary Creep and Fracture of O.F.H.C. Copper over the Temperature Range 335-500°C," J. Inst. Metals, Vol. 97, 1969, p. 337.
43. S. K. Mitra and D. McLean. "Work Hardening and Recovery in Creep," Proc. Roy. Soc., Vol. 295A, 1966, p. 288.

44. A. S. Nemy and F. N. Rhines. "On the Origin of Tertiary Creep in an Aluminum Alloy," T.A.I.M.E., Vol. 215, 1959, p. 992.
45. A. E. B. Presland and R. I. Hutchinson. "The Effect of Substructure on the Nucleation of Grain-Boundary Cavities in Magnesium," J. Inst. Metals, Vol. 92, 1963-64, p. 264.
46. W. Rosenhain and S. L. Archbutt. "On the Intercrystalline Fracture of Metals under Prolonged Application" (Preliminary Paper), Proc. Roy. Soc., 1919, p. 55.
47. G. Brinson and B. B. Argent, "The Creep of Niobium," J. Inst. Metals, Vol. 91, 1962-63, p. 293.
48. J. E. Cannaday, R. J. Austin, and R. K. Sorer. "Activation Energies for Creep of Polycrystalline Wire," T.A.I.M.E., Vol. 236, 1966, p. 595.
49. F. R. N. Nabarro. Proceedings of Conference on Strength of Solids, Physical Society (London), 1948, p. 75.
50. C. Herring. "Diffusional Viscosity of a Polycrystalline Solid," J. Appl. Phys., Vol. 21, 1950, p. 437.
51. I. M. Bernstein. "Diffusion Creep in Zirconium and Certain Zirconium Alloys," T.A.I.M.E., Vol. 239, 1967, p. 1518.
52. R. L. Coble. "A Model for Boundary Diffusion Controlled Creep in Polycrystalline Materials," J. Appl. Phys., Vol. 34, 1963, p. 1679.
53. R. Lagneborg. "Dislocation Mechanisms in Creep," International Metallurgical Reviews, IMRVBH 17, June 1972, p. 130.
54. P. W. Davies, T. C. Finniear, and B. Wilshir. "A Comparison of Tensile and Compressive Creep Rates," J. Inst. Metals, Vol. 90, 1961-62, p. 368.
55. Y. Ishida, C.-Y. Cheng, and J. E. Dorn. "Creep Mechanisms in Alpha Iron," T.A.I.M.E., Vol. 236, 1966, p. 964.
56. E. R. Parker. "Modern Concepts of Flow and Fracture," Trans. A.S.M., Vol. 50, 1958, p. 52.
57. P. Feltham and J. D. Meakin. "Creep in Face-Centered Cubic Metals with Special Reference to Copper," Acta Met., Vol. 7, 1959, p. 614.
58. S. Bhattacharya, W. K. A. Congrieve, and F. C. Thompson. "The Creep/Time Relationship under Constant Tensile Stress," J. Inst. Metals, Vol. 81, 1952-53, p. 83.

59. J. B. Conway and M. J. Mullikin. "Techniques for Analyzing Combined First and Second Stage Creep Data," T.A.I.M.E., Vol. 236, 1966, p. 1629.
60. H. Conrad and W. D. Robertson. "Creep Characteristics of Magnesium Single Crystals from 78° to 361°K," T.A.I.M.E., 1958, p. 536.
61. E. N. da C. Andrade. "The Viscous Flow of Metals, and Allied Phenomena," Proc. Roy. Soc., Vol. 84A, 1910, p. 1.
62. E. N. da C. Andrade. "The Flow in Metals under Large Constant Stresses," Proc. Roy. Soc., Vol. 90, 1914, p. 329.
63. E. N. da C. Andrade and D. A. Aboav. "The Flow of Polycrystalline Cadmium under Simple Shear," Proc. Roy. Soc., 1964, p. 353.
64. E. N. da C. Andrade. "The Validity of the $t^{1/3}$ Law of Flow of Metals," Phil. Mag., Vol. 7, 1962, p. 2003.
65. T. H. Hazlett and Rosa D. Hansen. "Influence of Substructure on the Shape of the Creep Curve," Trans. A.S.M., Vol. 47, 1955, p. 508.
66. A. H. Cottrell and V. Aytakin. "The Flow of Zinc under Constant Stress," J. Inst. Metals, Vol. 77, 1950, p. 389.
67. W. J. Evans and B. Wilshir. "Transient and Steady State Creep Behavior of Nickel, Zinc, and Iron," T.A.I.M.E., Vol. 242, 1968, p. 1303.
68. T. H. Hazlett and E. R. Parker. "Nature of the Creep Curve," J. of Metals, 1953, p. 318.
69. P. Haasen. "Plastic Deformation of Nickel Single Crystals at Low Temperatures," Phil. Mag., Vol. 3, 1958, p. 384.
70. H. J. McQueen and J. E. Hockett. "Microstructures of Aluminum Compressed at Various Rates," Met. Trans., Vol. 1, 1970, p. 2997.
71. J. C. Fisher and J. H. Hollomon. "Wanted, Experimental Support for Theories of Plastic Flow. A Symposium on the Plastic Deformation of Crystalline Solids," Mellon Institute, Pittsburgh, May, 1950.
72. D. Hardwick, C. M. Sellars, and W. J. McG. Tegart. "The Occurrence of Recrystallization during High Temperature Creep," J. Inst. Metals, Vol. 90, 1961-62, p. 21.
73. C. S. Barrett and L. H. Levenson. "The Structure of Aluminum after Compression," T.A.I.M.E., 1939-40, p. 112.

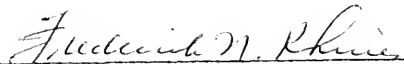
74. C. R. Barrett, A. J. Ardell, and O. D. Sherby. "Influence of Modulus on the Temperature Dependence of the Activation Energy for Creep at High Temperatures," T.A.I.M.E., Vol. 230, 1964, p. 200.
75. C. R. Barrett and O. D. Sherby. "Influence of Stacking Fault Energy on High-Temperature Creep of Pure Metals," T.A.I.M.E., Vol. 233, 1965, p. 1116.
76. J. Weertman. "Theory of the Influence of Stacking-Fault Width of Split Dislocations on High Temperature Creep Rate," T.A.I.M.E., Vol. 233, 1965, p. 2069.
77. C. K. L. Davies, P. W. Davies, and B. Wilshire. "The Effect of Variations in Stacking Fault Energy on the Creep of Nickel-Cobalt Alloys," Phil. Mag., Vol. 12, 1965, p. 827.
78. C. R. Barrett, J. L. Lytton, and O. D. Sherby. "Effect of Grain Size and Annealing Treatment on Steady-State Creep of Copper," T.A.I.M.E., Vol. 239, 1967, p. 170.
79. W. A. Wood, G. R. Wilms, and W. A. Rachinger. "Three Basic Stages in the Mechanism of Deformation of Metals at Different Temperatures and Strain Rates," J. Inst. Metals, Vol. 79, 1951, p. 159.
80. J. P. Dennison. "The Effect of Heat-Treatment on the Creep and Creep-Rupture Behavior of a High-Purity Alpha Copper-Aluminum Alloy at 300° and 500°C," J. Inst. Metals, Vol. 91, 1962-63, p. 293.
81. F. N. Rhines, W. E. Bond, and M. A. Kissel. "Grain Boundary Creep in Aluminum Bicrystals," Trans. A.S.M., Vol. 48, 1956, p. 918.
82. R. G. Connell, Jr., The Microstructural Evolution of Aluminum During the Course of High Temperature Creep, Ph.D. Dissertation, University of Florida, 1973.
83. R. D. Gifkins. "A Mechanism for the Formation of Intergranular Cracks when Boundary Sliding Occurs," Acta Met., Vol. 4, 1956, p. 98.
84. D. Kramer and E. S. Machlin. "High Temperature Intercrystalline Cracking," Acta Met., Vol. 6, 1958, p. 454.
85. R. C. Gifkins. Mechanisms of Intergranular Fracture at Elevated Temperatures, J. Wiley and Sons, New York, 1959, Chap. 27, p. 579.
86. N. J. Grant. "Intercrystalline Failure at High Temperatures," Ibid., 1959, Chap. 26, p. 562.

87. S. Gehl. Private Communication, 1973.
88. A. Seeger. "Defects in Crystalline Solids," London: Physical Society, Vol. 49, 1955, p. 337.
89. C. R. Smeal. Structural Evolution in Nickel during Annealing Subsequent to Hot Deformation, Ph.D. Dissertation, University of Florida, 1965.
90. J. P. Gillard. Particle Size Dependence of the Mechanical Properties of Sintered Copper, Master's Thesis, University of Florida, 1964.
91. R. T. DeHoff and J. P. Gillard. "Relationship Between Microstructure and Mechanical Properties in Sintered Copper," Modern Developments in Powder Metallurgy, Vol. 4, Processes, Plenum Press, New York-London, 1971.
92. G. D. McAdam. "Some Relations of Powder Characteristics to the Elastic Modulus and Shrinkage of Sintered Ferrous Compacts," J. Iron-Steel Inst., Vol. 168, 1951, p. 346.


BIOGRAPHICAL SKETCH

Walter Ralph Tarr was born September 17, 1945, in Philadelphia, Pennsylvania. He moved to Orange Park, Florida, in 1946, and received primary schooling in the Jacksonville, Florida, school system. He attended high school at Darlington preparatory school in Rome, Georgia, from which he graduated in June, 1963. He entered the University of Florida in June, 1966, and received the Bachelor of Science in Metallurgical Engineering in April, 1967. In September, 1967, he entered the University of Florida Graduate School and received the Master of Metallurgical Engineering in August, 1969. The time from August, 1969, to the present has been spent in doctoral research at the University of Florida.

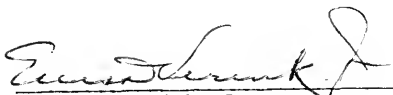
I certify that I have read this study and that in my opinion it conforms to acceptable standards of scholarly presentation and is fully adequate, in scope and quality, as a dissertation for the degree of Doctor of Philosophy.


Frederick N. Rhines, Chairman
Professor of Materials Science
and Engineering

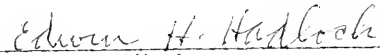
I certify that I have read this study and that in my opinion it conforms to acceptable standards of scholarly presentation and is fully adequate, in scope and quality, as a dissertation for the degree of Doctor of Philosophy.


Robert T. DeHoff
Professor of Materials Science
and Engineering

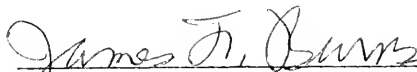
I certify that I have read this study and that in my opinion it conforms to acceptable standards of scholarly presentation and is fully adequate, in scope and quality, as a dissertation for the degree of Doctor of Philosophy.


Ellis D. Verink, Jr.
Chairman of Department of Materials
Science and Engineering

I certify that I have read this study and that in my opinion it conforms to acceptable standards of scholarly presentation and is fully adequate, in scope and quality, as a dissertation for the degree of Doctor of Philosophy.


Edwin H. Hadlock
Professor of Mathematics

I certify that I have read this study and that in my opinion it conforms to acceptable standards of scholarly presentation and is fully adequate, in scope and quality, as a dissertation for the degree of Doctor of Philosophy.

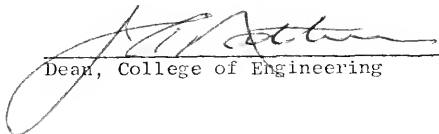


James F. Burns

Associate Director of Planning Analysis

This dissertation was submitted to the Dean of the College of Engineering and to the Graduate Council, and was accepted as partial fulfillment of the requirements for the degree of Doctor of Philosophy.

August, 1973



Dean, College of Engineering

Dean, Graduate School



UNIVERSITY OF FLORIDA



3 1262 08553 0185